MASTER THESIS

Thesis submitted in partial fulfillment of the requirements for the degree of Master of Science in Engineering at the University of Applied Sciences Technikum Wien - Degree Program Tissue Engineering and Regenerative Medicine

Elucidating the Transcriptional Program Specifying Endothelial Cells in the Zebrafish Blood Stem Cell Niche

By: Inés Fernández Maestre, BSc
Student Number: 1610692030

Supervisor 1: Mag. Daniela Praher, PhD
Supervisors 2: Dr. Leonard I. Zon and Dr. Elliott J. Hagedorn

Boston (MA, USA), Sunday, September 30, 2018

Declaration of Authenticity

"As author and creator of this work to hand, I confirm with my signature knowledge of the relevant copyright regulations governed by higher education acts (for example see §§ 21, 42f and 57 UrhG (Austrian copyright law) as amended as well as § 14 of the Statute on Studies Act Provisions / Examination Regulations of the UAS Technikum Wien).

In particular, I declare that I have made use of third-party content correctly, regardless what form it may have, and I am aware of any consequences I may face on the part of the degree program director if there should be evidence of missing autonomy and independence or evidence of any intent to fraudulently achieve a pass mark for this work (see § 14 para. 1 Statute on Studies Act Provisions / Examination Regulations of the UAS Technikum Wien).

I further declare that up to this date I have not published the work to hand nor have I presented it to another examination board in the same or similar form. I affirm that the version submitted matches the version in the upload tool."

Boston, MA, USA, September 30, 2018

| Place, Date | Signature |

Kurzfassung

Die Transplantation von hämatopoetischen Stamm- und Progenitorzellen (HSPZ) ist eine potenziell kurative Therapieoption für zahlreiche hämatologische Krankheiten, einschließlich Krebs. Obwohl die HSPZ-Transplantation derzeit als die effektivste medizinische Anwendung von Stammzellen beschrieben wird, bleibt sie dennoch eine riskante, gefährliche Prozedur mit ungewissem Ausgang. Um das volle Potenzial dieser Therapie ausschöpfen zu können, muss es das Ziel zukünftiger Untersuchungen sein, die HSPZ-Nische – die physiologische Umgebung von Stammzellen – besser zu erforschen.

Perivaskulären Endothelzellen (EZ) sind eine Kernkomponente der HSPZ-Nische, da sie innerhalb dieser die Stammzellfunktion und -homöostase fördern können. In der vorliegenden Arbeit definieren wir in Zebrafish einen Transkriptionsfaktor (TF)-Code, der aus Mitgliedern der Ets-, Sox F- und Nuclear Hormon- (NH-, konkret RXRA / RORA / NR2F2) Rezeptorfamilien besteht. Wir zeigen, dass ein solcher TF-Code die sinusoidalen EZ der embryonalen HSPZ-Nische in Zebrafisch spezifiziert, die auf Englisch „*Caudal Hematopoietic Tissue*" (CHT) genannt wird.

Mittels Injektion von Konstrukten mit modifizierten Enhancersequenzen für zwei Gene, *mrc1a* und *selectin-e*, die weitgehend selektiv in CHT EZ exprimiert werden, zeigten wir, dass TF-Bindungsstellen für Ets, Sox F und NH-Rezeptor nötig für die Expression dieser Gene in CHT EZ sind. In weiteren Experimenten überexprimierten wir mehrere TF-Gene (mit mindestens einem Vertreter aus jeder der drei TF Familien) in Zebrafisch-Embryonen und fanden heraus, dass die Überexpression von erstaunlicherweise nur drei verschiedenen TF-Genen – *ETV2*, *SOX7* und *nr2f2* – ausreichend ist, um ektopische *CHT*-ähnliche vaskuläre Stellen außerhalb der CHT zu induzieren. Bemerkenswerterweise konnten diese Bereiche *runx1* positive HSPZ rekrutieren und direkt mit ihnen interagieren. Um den relativen Beitrag jedes TFs zu bestimmen, injizierten wir DNA-Konstrukte für jedes TF Gen einzeln. Während die Überexpression von *SOX7* oder *nr2f2* allein keine ektopische Expression ergab, induzierte die Injektion des *ETV2*-Konstrukts eine deutliche ektopische CHT-EZ-Genexpression. Die Häufigkeit war allerdings geringer als bei der „*ETV2, SOX7* und *nr2f2*"-Kombination. Weiters konnten wir zeigen, dass die einzelne Überexpression von *ETV2* die Expression einiger anderer TF vom CHT-EZ TF-Code induzierte, sodass es ziemlich wahrscheinlich ist, dass nur *ETV2* allein das genetische Programm der EZ teilweise induzieren kann. Aus den Resultaten dieser Versuchsreihe ging hervor, dass eine Kombination von TF aus den Ets-, Sox- und NH-Rezeptorfamilien sowohl notwendig als auch ausreichend für das CHT-EZ-genetische Programm ist.

Weiters untersuchten wir die extrinsischen Faktoren, die das CHT-EZ-Genprogramm regulieren könnten und fanden heraus, dass Blutfluss für die Expression der CHT-spezifizierenden Gene erforderlich ist. Die Inhibierung des Blutflusses in Zebrafisch-Embryonen führte zu einer Herunterregulierung oder einem Verlust der Expression von CHT-EZ Genen, einschließlich *gpr182* und *selectin-e*, sowie des TF-Gens *sox7*. Schließlich charakterisierten wir die morphologischen Veränderungen der CHT-EZ sowie die Dynamik der HSPZ Population, die im Laufe der Entwicklung auftraten. Wir beobachteten, dass der CHT-Venenplexus während der ersten zwei Wochen der Entwicklung in eine einzelne Schwanzvene umgebaut wurde. Diese Remodellierung stimmte genau mit der Zeit, währenddessen sich HSPZ in der CHT-Nische befanden, überein. In einem Zeitraum von acht bis 14 Tagen nach der Befruchtung verringerte sich die Anzahl der HSPZ deutlich, sodass 14 Tage nach der Befruchtung keine HSPZ mehr in der CHT-Region nachgewiesen werden konnten. Wir konnten dann zeigen, dass diese zeitliche Dynamik mit der Herunterregulation der CHT-spezifischen endothelialen Gene, einschließlich *gpr182*, *mrc1a* und *lgmn*, zusammenfiel. Diese Ergebnisse stellen eine korrelative Beziehung zwischen der Dynamik der hämatopoetischen Zellpopulation innerhalb der CHT, der Morphologie des CHT-EZ-Plexuss und der Expression des endothelialen Nischenprogramms in den CHT-EZ her.

Zusammenfassend fördern diese Studien unser grundlegendes Verständnis der regulatorischen Programme, die EZ-Identität in der HSPZ-Nische kontrollieren. Daraus ergeben sich wichtige Implikationen für die Entwicklung von synthetischen Nischen zur *in-vitro* und *in-vivo*-Expansion von HSPZ sowie für die Modulation der Stammzellnische. Beide stellen verschiedene Ansätze zur Verbesserung der HSPZ-Transplantationseffizienz dar.

Schlagwörter: „HSPZ-Nische", „Endothelzell", „Transkriptionsfaktor-Code", „Ektopische Nische", „Zebrafisch".

Abstract

Hematopoietic stem and progenitor cell (HSPC) transplantation is a potentially curative therapy for multiple hematological disorders including cancer. Despite being reported as the most effective medical application of stem cells, HSPC transplantation remains an inherently risky procedure with uncertain outcomes. Realizing the full potential of this therapy will require further investigation into the biology of HSPCs, and in particular the HSPC niche, which is the essential natural environment that supports the function and maintenance of these cells.

Perivascular niche endothelial cells (ECs) are a core component of the HSPC niche, where they promote stem cell function and homeostasis. Here, we defined a transcription factor (TF) code, composed of members of the Ets, Sox F, and Nuclear Hormone (NH, specifically RXRA/RORA/NR2F2) receptor families, that specifies sinusoidal ECs in the caudal hematopoietic tissue (CHT) – the embryonic HSPC niche in zebrafish. Using sequence variants of enhancers for two genes that are selectively expressed by CHT ECs, *mrc1a* and *selectin-e,* we demonstrated that Ets, Sox F and NH (RXRA/RORA/NR2F2) receptor binding sites are required for expression in these cells. We next overexpressed pools of transcription factor (TF) genes, containing at least one member from each of the three families, in zebrafish embryos. Strikingly, we found that overexpression of just three TF genes – *ETV2*, *SOX7* and *Nr2f2* – is sufficient to give rise to ectopic patches of niche endothelial gene expression outside the CHT. Remarkably, such vascular sites were able to recruit and directly interact with *runx1* positive HSPCs. To assess the relative contribution of each TF, we injected the constructs of the individual TF genes on their own. While overexpression of *SOX7* or *Nr2f2* alone gave no ectopic expression, injection of the *ETV2* alone construct induced noticeable ectopic CHT EC gene expression, although the frequency was less than the *ETV2*, *SOX7* and *Nr2f2* combination. With additional experiments we were able to demonstrate that overexpression of *ETV2* alone induced the expression of some of the other TFs that we had implicated in CHT EC specification, suggesting that *ETV2* alone is able to partially induce the CHT EC program. These results indicate that a combination of TFs from the Ets, Sox and NH receptor families are both necessary and sufficient for CHT EC gene expression.

We next investigated extrinsic factors that might regulate the CHT EC gene program and found that blood flow was required for CHT EC gene expression. Blockage of blood flow in zebrafish embryos led to downregulation or loss of expression of CHT endothelial genes, including *gpr182 and selectine-e*, as well as the TF gene *sox7*. Lastly, we characterized the

morphological changes of the CHT ECs, as well as the dynamics of the HSPC population, that occur over the course of development. We observed that the CHT venous plexus remodels down into a single caudal vein during the first two weeks of development and that this remodelling precisely aligns with the time during which HSPCs reside in the CHT niche. After eight days post fertilization (dpf), the number of HSPCs notably decreased until 14 dpf, at which point essentially no HSPCs were detected in the CHT region. We were able to show that these temporal dynamics coincided with downregulation of the CHT-specific endothelial genes from our previous studies, including *gpr182*, *mrc1a* and *lgmn*. These results establish a correlative link between the dynamics of the hematopoietic cell population within the CHT, the morphology of the CHT EC plexus, and the expression of the niche endothelial program within the CHT ECs.

Collectively, these studies advance our basic understanding of the regulatory programs that control EC identity within the HSPC niche, which has important implications for designing synthetic niches to expand HSPCs *in vitro* or *in vivo,* or for modulating the niche as a means to improve transplantation efficiency during the treatment of hematopoietic disorders.

Acknowledgements

I would like to thank my P.I, the Dr. Zon for believing in me and giving me the fantastic opportunity to work in his lab during this period of time. While here, I have grown significantly as a scientist and I am really grateful to him to make it possible and for all his excellent pieces of advice about scientific research and career in general.

I am especially indebted to Elliott, my direct supervisor in the lab. As my mentor, he has taught me how a real good scientist should be. I want to thank him for his patience, his understanding and his marvelous mentorship. It is been great working under his supervision!

I want to thank all the inspiring members of the Zon lab, especially I gratefully acknowledge Yi and Song for their bioinformatics support; Serine for a fantastic lecture about Flow Cytometry analysis; Alicia for help with the RNA-sequencing protocol; Shane for his help with the rotifers' culture; Sam, Sara and TX, my brilliant bay mates, for being such awesome co-workers; and of course, Maddie and Rebecca, the talented technicians I had the pleasure to work with.

I am also grateful to all of those I have met in Boston, and made my stay here so incredible.

I also want to thank the Austrian Marshall Plan Institution, since my stay here would not have been possible without their financial support.

Last but not least, I would like to thank my family, whose love, guidance and support mean everything to me. For that, I dedicate this thesis to my mother and my sister, my ultimate role models and my best friends. *Mamá, Marina, me es imposible describir con palabras lo mucho que os estimo. ¡Gracias por todo!*

Table of Contents

1 Introduction

1.1 Preface

Hematopoietic stem and progenitor cell (HSPC) transplantation is a potentially curative therapy used to treat a myriad of congenital and acquired conditions of the hematopoietic system, including hematological malignancies and immunological disorders [1], [2]. Since the first HSPC transplantations in the 1950s, a multitude of patients have benefitted from this therapy, which is currently the most commonly used stem cell-based treatment. Despite being reported as the most effective medical application of stem cells, HSPC transplantation remains an inherently risky procedure with uncertain outcomes, and more research is needed to improve these lifesaving therapies [3], [4].

Hematopoietic stem cells (HSCs) are a multipotent cell population that is able to self-renew and yield lineage-restricted progenitor cells that will differentiate into all mature blood lineages throughout life [2],[5]. Following ablation of diseased hematopoietic stem and progenitor cells (HSPCs), healthy HSPCs collected from a donor's bone marrow (BM), peripheral blood or the umbilical cord can reconstitute the hematopoietic system once transplanted into a patient [6]. The number of cells infused, however, is a key determinant of transplant success, and a relatively high number of HSPCs must be delivered to ensure a favorable outcome. Despite their great potential in the clinic, HSPCs are a rare cell population in the body [2], and their limited availability, especially from immunologically matched donors, still curtails their application in transplantation therapies. Thus, there remains a dire need to better understand the behaviour of these cells *in vivo*, and the endogenous regulatory mechanisms that control HSPC specification, maintenance and expansion so as to learn of new ways to expand HSPC numbers *in vitro* or to enhance HSPC transplantation in the clinic [1], [2], [7], [8].

HSPCs reside in defined local microenvironments dubbed "hematopoietic niches", where they are in immediate contact or in close proximity to other cell types [9]. Neighboring cells within the niche are thought to contribute to HSPC maintenance and regulation through direct interaction with the HSPCs or indirectly via secreted or cell surface-bound signaling or adhesion molecules [9],[10]. One of the essential cell types comprising the HSPC niche are endothelial cells (ECs). ECs are necessary for the emergence of definitive HSCs and play critical roles in regulating HSPC function and homeostasis within the perivascular niche [9], [11]. Although a number of secreted and cell surface molecules have described functions within niche ECs, much less is known about the transcriptional programs that specify

endothelial subtypes within the HSPC niche. Unveiling the regulatory programs that control the identity of these cells will be of fundamental importance for designing new strategies to expand HSPCs *in vitro* or to modulate the niche as a means to improve transplantation efficiency during the treatment of hematopoietic disorders [9]. The work presented here is focused on defining the regulatory program that specifies sinusoidal ECs within the HSPC niche. In addition, it also aims to shed light to the dynamics of the perivascular HSPC niche using the zebrafish as a model organism.

1.2 Emergence of Hematopoietic Stem Cells

Approximately 100 billion blood cells are required each day to replace the short-lived mature blood cells in an adult human. HSPCs, a rare population of cells residing in the BM, sustain blood cell production throughout the lifetime of an individual. HSCs lie at the top of the blood cell lineage hierarchy and give rise to specific progenitor cells that will in turn produce all blood lineages [9].

Hematopoiesis – the formation of the entire repertoire of the cellular components of the blood – initially commences within the early embryo, when the supply of oxygen and nutrients by passive diffusion becomes limiting to support continued growth [12]. In vertebrates, this process takes place in two sequential waves of development referred to as primitive and definitive hematopoiesis (**Figure 1**). Each phase occurs in a temporally and spatially controlled manner [1], [13]. During the primitive wave, blood cells arise from the blood islands within the extra-embryonic yolk sac [14]. These include erythroid progenitors that subsequently differentiate into both primitive myeloid cells and erythrocytes, necessary cell types for commencing the innate immune response and facilitating the tissue oxygenation of the developing organism, respectively [1], [15]. The resulting progenitor cells cannot, however, self-renew. The primitive hematopoietic wave is hence transitory, and eventually gives way to the definitive wave of hematopoiesis [14].

The switch to definitive hematopoiesis begins when HSPCs emerge from specialized hemogenic ECs in the ventral dorsal aorta or aorta-gonad mesonephros (AGM) region of the embryo in a process known as endothelial-to-hematopoietic cell transition (EHT) [9], [16]. Blood stem cells born in the AGM are already endowed with long-term repopulation potential [17]; they are multipotent and capable of self-renewal. These are the first HSPC formed in the organism that are able to completely reconstitute the entire hematopoietic system upon transplantation [18]. AGM-derived HSPC subsequently enter the primitive blood circulation and migrate to colonize successive sites of embryonic and fetal hematopoiesis before

eventually lodging in the BM microenvironment and the thymus. Although extramedullary sites can be observed under different pathological or stress conditions, life-long hematopoiesis is largely confined to the BM in mammals (**Figure 1**) [19].

During fetal development the main hematopoietic organ for HSPC expansion and differentiation is the liver (**Figure 1**). Additional hematopoietic sites are found in the placenta, thymus, spleen and umbilical arteries where hematopoietic and ECs are observed to co-localize [15]. While transient sites of intra-embryonic hematopoiesis, especially the fetal liver, are characterized by rapid HSPC expansion, stem cells residing in the BM are predominantly quiescent and divide only to replenish mature blood cells, and to maintain the size of the stem cell pool. HSPCs in extra-embryonic tissues similarly divide at a slower rate than those within intra-embryonic tissues. Thus, the properties of HSPCs appear to vary throughout development, and are likely to be influenced by differences within distinct stem cell microenvironments [15], [20],[21].
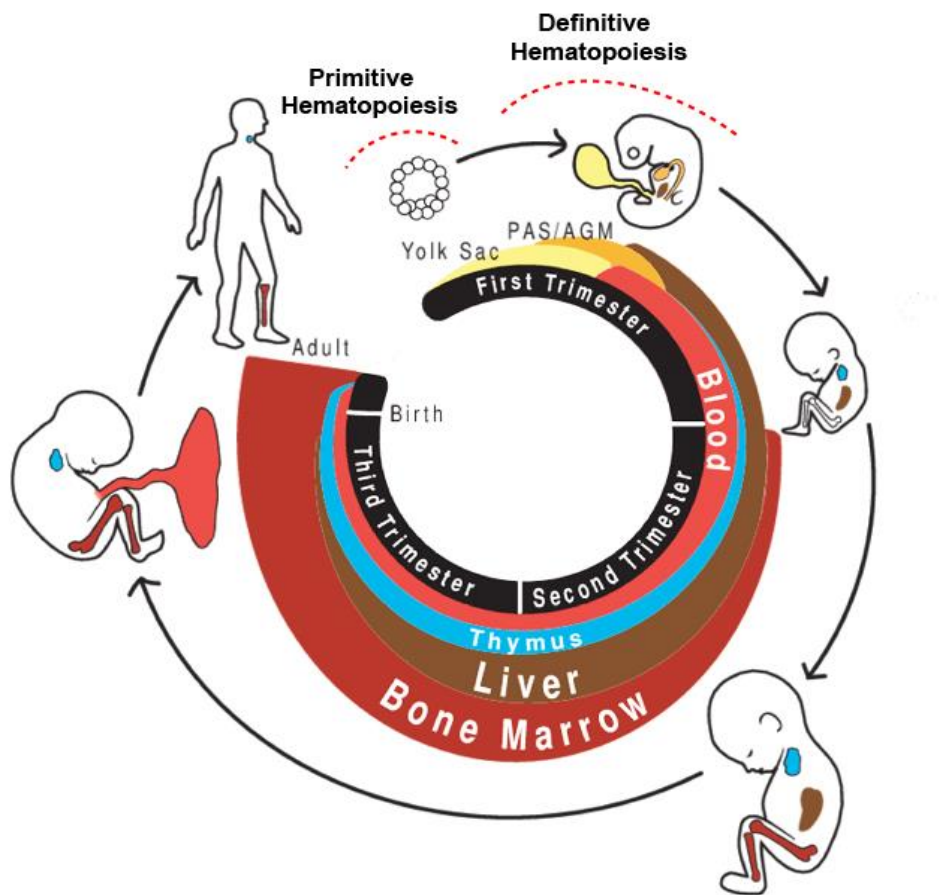
Figure 1. The site of hematopoiesis changes during vertebrate development. During primitive hematopoiesis, blood cells arise from the blood islands within the extra-embryonic yolk sac. The switch to definitive hematopoiesis begins when HSPCs emerge from specialized hemogenic ECs in the AGM region of the embryo. Thereafter, AGM-derived HSCs enter the blood circulation and migrate to the liver – the most relevant embryonic/fetal site of hematopoiesis. After expansion there, HSPCs colonize the BM and thymus, with the former being the primary site of hematopoiesis in the adult (PAS, para-aortic splanchnopleura; AGM, aorta-gonad-mesonephros). Adapted from [21].

1.3 The Adult Hematopoietic Stem Cell Niche

The HSPC niche is a specialized, local tissue microenvironment where HSPCs reside and self-renew. The adult HSPC niche, which is situated in the BM in mammals, provides a complex milieu that ensures HSPC homeostasis throughout life [19], [22]. Multiple distinct cell types, in combination with non-cellular components, such as extracellular matrix (ECM) proteins, are thought to comprise the adult HSPC niche. Together the different elements of the niche work in concert to regulate HSPC differentiation and self-renewal [9], [19].

The first use of the term "stem cell niche" can be traced back to 1978, when R. Schoefield first proposed the concept. He surmised that HSCs reside within a specialized location in the BM, where they co-existed with other tissue-resident cell populations that were critical for the sustainability and function of HSCs. This was inferred from the comparison between splenic HSCs (spleen colony-forming cells, CFU-S) and HSCs from the BM, where reconstitution of the hematopoietic system in irradiated animals was less efficacious using CFU-S- *versus* BM-derived HSCs. It was postulated that the reduced proliferative potential of the splenic cells was the result of these cells no longer being in close proximity to supportive cells within the BM. Schoefield's theory thus implied that there had to be a specific environment within the BM that was crucial for proper HSC activity and that removal of stem cells from their natural habitat leads to loss of their self-renewal ability and the onset of differentiation [23].

Since Schoefield's initial theory was put forth, numerous subsequent studies have confirmed that the HSPC niche is indeed a complex microenvironment that orchestrates the maintenance and function of HSPCs, including their differentiation into progenitor cells that maintain blood cell homeostasis [23],[24]. The niche is comprised of not only diverse cell types, but also the interplay of a large number of factors, such as ECM molecules (secreted by niche cells), various extracellular cues like hypoxia, and a broad, intrinsic genetic program that specifies HSPC behavior [25],[26].

The primary adult hematopoietic niche is contained within the BM, which is a complex multifunctional organ located within the shaft of spongy bones. It consists of a medullary cavity, harboring hematopoietic tissue islands and adipose cells, surrounded by a shell of trabecular bone [24]. The interior surface of the bone, which is in contact with the BM, is covered by a thin, soft connective tissue, termed "endosteum", through which the nutrient arteries penetrate and branch off, thereby forming arterioles, transition zone vessels and venous sinusoids that uniformly occupy the BM [27], [28]. For many years, HSPCs have been thought to reside along the endosteal surface. They are, however, not only in close proximity to the bone, but most HSPCs are also contiguous to the sinusoidal blood vessels throughout the BM. Hence, multiple cell types, including osteoblasts, vascular ECs and reticular stromal cells, constitute the HSPC niche (**Figure 2**) [9], [24]. Although a large number of studies have been conducted to determine which heterologous cell type contributes the most to HSPC niche function, the specific roles of the distinct cell types within the niche, and how these cells function in concert, remain incompletely understood. As the number of cell types with implicated functions in the niche continues to increase, uncovering

the precise function of each cell type, and the crosstalk between these cells and HSPCs becomes more and more challenging [22], [29], [30].
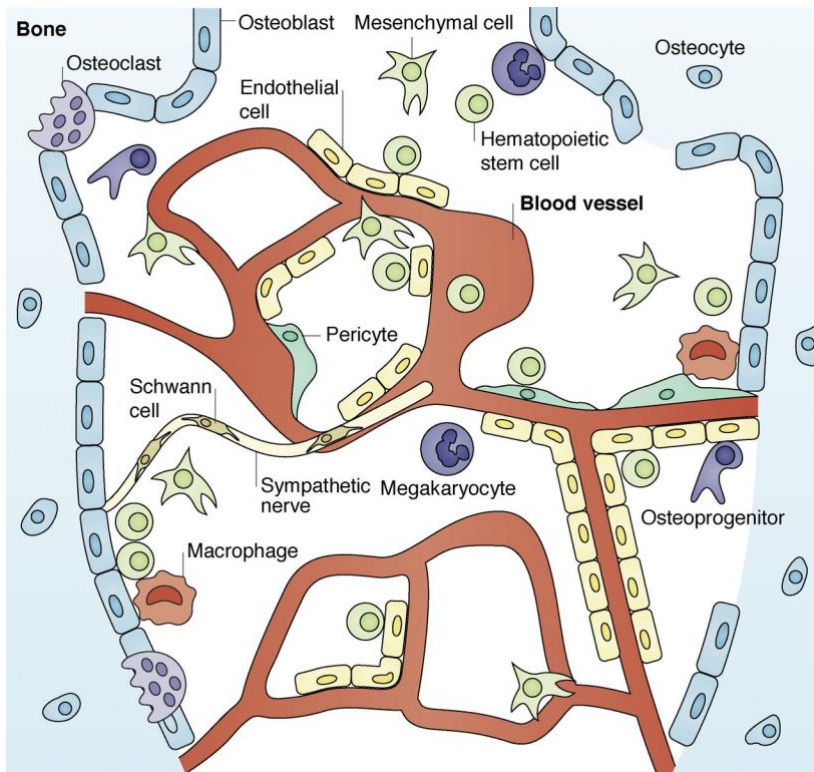

Figure 2. The cellular makeup of the mammalian bone marrow niche. The mammalian BM environment consists of a plethora of cell types, such as osteoblasts, vascular ECs, reticular stromal cells, pericytes, megakaryocytes, Schwann cells and immune cells. These cells are thought to support HSPC fuction and homeostasis. Extracted from [30].

1.3.1 Endosteal Niche *Versus* Perivascular Niche

In general, it has been thought that the adult BM contains two singular niches, organized by different stromal cell types that sustain the dynamics of the hematopoietic system. These niches, located at distinct anatomical locations within the BM, are commonly referred to as (I) the endosteal niche, which is along the inner bone shell surface, and (II) the perivascular niche, which is associated with the sinusoidal endothelium [31].

The endosteal niche, which includes osteoblasts and their progenitors, was initially thought to be the preferential site of residence for most HSPCs, and therefore investigation in HSPC biology was originally geared towards the study of this microenvironment. The importance of osteoblasts in regulating the HSPC niche was supported by two different research groups that published their reports in the same October issue of *Nature*, in 2003

[32]. Both papers showed that alteration in murine models of essential signaling pathways governing osteoblast proliferation and function (i.e., bone morphogenic protein (BMP) signaling in one paper [33], and parathyroid hormone (PTH)/PTH related peptide (PTHrP) signaling in the other [34]), in a way that the osteoblast population was increased, also led to larger HSPC numbers. Taken together, their results suggested that osteoblastic cells were key players in the *in vivo* regulation of the HSPC niche. However, a more recent study published in the journal *Blood* in 2009, demonstrated that mice suffering from chronic inflammatory arthritis, which leads to defective osteoblast activity, exhibited paradoxically normal HSPC function. This result suggested that additional cells residing in the HSPC niche (e.g., endothelial or reticular cells) could likely play a pivotal role in maintaining HSPC integrity and are able to compensate for the osteoblast defects [35]. Also, in the same year, Chan *et al.* presented an *in vivo* assay that they had developed in order to assess adult HSPC niche formation. Their model showed that transplantation of fetal bone implants under the mouse kidney capsule, a region known to be devoid of resident HSPCs, was sufficient to drive ectopic HSPC niche formation. While this discovery reinforced the concept of the osteoblastic niche, the same study showed that Vascular Endothelial Growth Factor (VEGF) activity, which drives vascular recruitment, was required for ectopic niche formation and that VEGF promoted the differentiation of HSPCs into other blood lineage [36]. Consequently, these results, along with the fact that HSPCs were also anatomically in close proximity to the BM blood vessels [37], turned the spotlight on the perivascular niche within the BM and its relationship to the endosteal niche.

At the present time there seems to be a consensus of opinion that both osteoblasts and vascular ECs – critical components of the endosteal and perivascular niches, respectively – contribute, along with other cell types, to the function of the HSPC niche. Currently, one proposed theory suggests that osteoblastic cells support an environment where stem cells are kept in the G_0 phase of the cell cycle. The perivascular niche, on the other hand, is thought to provide a transitional niche in which the HSPCs are in a more activated state where they are committed either to differentiate into progenitor cells or return to dormancy. In this way, the endosteal and perivascular niches would provide not only distinct anatomical, but also functional environments. In this scenario, HSPCs would need to traffic from one niche to another depending on the body's demands for blood cell production (**Figure 3**) [29], [38], [39]. In contrast, an alternative model suggests that the HSPC niche likely consists of a unique multicellular niche, given the close proximity between the different cell types, especially in flat bones like the calvaria, where the BM is so thin that the vast majority of osteoblasts are themselves perivascular [32], [39]. Even in larger bones the endosteal region

is highly vascularized, which supports the idea of a single, common HSPC niche [28]. Several studies have supported this hypothesis with data indicating that both endosteal and perivascular niches produce common chemical mediators that altogether orchestrate HSPC regulation [40],[41]. For example, CXCL12-CXCR4 chemokine signaling is relevant in stromal cells associated with both endosteal and perivascular cells in the adult BM, as demonstrated by the presence of CXCL12-abundant reticular (CAR) cells as key components of the two niches [41].

In view of the above, endosteal and perivascular niches are likely to have in common certain structural elements, as well as to carry out, to some extent, redundant roles in HSPC regulation [32]. Nonetheless, more research is needed in order to further characterize these niches and clarify whether they represent two distinct entities or, on the contrary, constitute a single niche. Something that is currently clear, however, is that the HSPC niche as a whole is comprised of multiple distinct cell types that engage in highly dynamic interactions. It may be, in part, this variety of niche cell types that contributes to the great heterogeneity observed within the HSPC compartment, ranging from differences in the metabolic state of the HSPCs to the various lineage commitment programs [42].[1]

---

[1] Note to the reader: the endosteal and perivascular niches will be hereinafter considered two distinct structures throughout the present thesis.
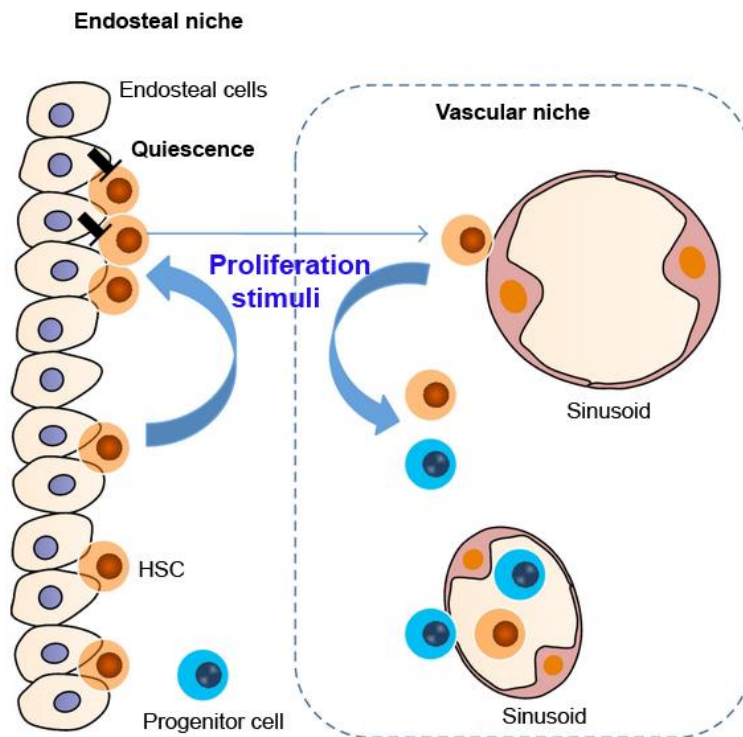
Figure 3. **The bone marrow microenvironment.** The endosteal cells support an environment where most HSCs are kept in the G_0 phase of the cell cycle. The perivascular niche, on the other hand, is thought to provide a transitional niche in which HSCs are rather in a more activated state where they are committed to differentiate into progenitor cells and different kinds of mature blood cells, that will subsequently enter the bloodstream. Upon proliferation stimuli, HSCs can shuffle from the endosteal to the vascular niche to respond to the body's demands for blood cell production. Arrows and "T" indicate induction of proliferation and induction of quiescence (G_0), respectively (HSC, Hematopoietic Stem Cell). Adapted from [38].

1.3.2 Intrinsic and Extrinsic Regulation of Hematopoietic Stem Cells

Over the last few years, it has been established that the heterogeneity observed within the HSPC population rely on both intrinsic and extrinsic regulators. The former involve, among others, an array of transcription factors (TFs), signaling pathways and chromatin and epigenetic modifiers that altogether comprise the genetic programs within the HSPC [43]. Extrinsic elements include different cell types and their products (e.g., cytokines and ECM molecules) [44], as well as other extracellular cues like hypoxia or hemodynamics [45], [46]. This plethora of extrinsic regulators within the HSPC microenvironment interface with the intrinsic regulation within the cell. Therefore, HSPC behaviour and fate are ultimately the

result of the combined, intricate influences of intrinsic and extrinsic factors, that integrate and counter the fluctuating physiological needs of the body [43].

1.3.2.1 Intrinsic factors for HSPC specification and maintenance

Ontogeny of the hematopoietic system is based upon the temporal and spatial regulation of different cellular processes, including cellular differentiation, migration, homing, self-renewal and survival of HSPCs [47]. The expression of the different TFs that regulate these distinct processes will therefore vary throughout the life of HSPCs, from their emergence to the establishment of the adult niche. There is a large number of TFs that play a central role in developmental hematopoiesis. Among these, we can cite Stem Cell Leukemia (Scl), LIM domain Only 2 (Lmo2), and Runt-related transcription factor 1 (Runx1), with the latter being considered the master TF in definitive hematopoiesis across species. These factors have been shown to be essential for the establishment of hematopoiesis. For example, Runx1 is indispensable for the generation of definitive HSPCs and mice lacking this protein die during embryonic development between days 11.5 and 12.5 due to the absence of definitive hematopoiesis [1], [47].

Once the adult HSPC niche has been established, genetic programs ensuring the maintenance of the HSPC pool are of the utmost importance. A tightly balanced control of self-renewal and differentiation of HSPCs is required for continuous blood cell production throughout life. Several intrinsic mechanisms regulate these processes in order to sustain HSPCs within the niche, while giving rise to daughter cells with more restricted differentiation potential. The balance between self-renewal and differentiation is regulated by (I) a combination of specific TFs, including Runx1, GATA binding factor 2 (GATA-2) and Scl; (II) the crosstalk between distinct signaling pathways, such as Wnt/β-catenin, Notch and sonic Hedgehog (SHH) signaling; and (III) a number of epigenetic and chromatin modifiers, like the Polycomb Group (PcG) member, B Lymphoma Mo-MLV Insertion Region 1 homolog (Bmi-1) [48], [49]. While some of these factors seem to simply enhance HSPC maintenance, others are indispensable. For example, mice lacking Bmi-1 do not possess self-renewing HSCs [50].

The mechanisms by which the aforementioned intrinsic factors modulate HSPC self-renewal and differentiation rely on the regulation of target genes that are crucial for HSPC fate and survival, such as the *erythropoietin* (*Epo*) gene (Epo is the major growth factor for erythroid cells), cell cycle core components and proliferation-related genes (e.g., *Cyclin D2*) and apoptosis regulator genes (e.g., *B-cell lymphoma-extra large* (*Bcl-xL*)) [51],[52].

Due to their complexity, most of these mechanisms are not well understood yet. Still, it

has become clear that the cell-intrinsic programs do not stand alone, but are heavily integrated with extrinsic regulators [26].

1.3.2.2 Extrinsic factors affecting HSPCs in the niche

Within the HSPC niche there are a plethora of extrinsic regulators that affect genetic programs within the HSPC, ultimately preserving a functional HSPC pool for lifelong hematopoiesis [53]. For example, local oxygen concentrations and reactive oxygen species (ROS) levels are two variable extrinsic factors that impact the expression of a series of genes involved in stem cell proliferation, homing, survival and metabolism [45], [54], [55].

Despite the presence of a large number of blood vessels, the BM constitutes a physiologically hypoxic environment compared to other tissues [45], [53]. According to the dichotomous view of the HSPC niche, the endosteal niche serves to maintain stem cells in a quiescent state, whereas the perivascular niche allows the cells to actively proliferate and differentiate into multipotent progenitors (MPPs). Supporting this hypothesis, it has been shown that the two niches differ in their oxygen availability. The endosteal niche, which is thought to be important for stem cell dormancy, has lower concentrations of oxygen; whereas the perivascular niche, which is intimately associated with the blood circulation, provides a higher oxygen concentration, and is thought to contribute to self-renewal, proliferation and differentiation of HSPCs [18]. Furthermore, the low-oxygen endosteal milieu is thought to attenuate the intracellular formation of ROS, thus protecting HSPCs from the oxidative stress that can lead to loss of their "stemness". Consequently, when HSPCs are exposed to the perivascular niche, intracellular production of ROS is triggered, thereby promoting stem cells to lose their long-term (LT) repopulation capacity, and to migrate and differentiate into MPPs [56], [57]. Consistent with this, the low ROS HSPC population has a higher reconstitution capacity following BM transplantation than high ROS HSPCs [11], [58].

As the heart beats, it pumps blood throughout the circulatory system. The flow of blood, in turn, generates shear stress forces that act as an extrinsic regulator of the development and maintenance of HSPCs. Different studies have looked at HSPC gene expression patterns in response to changes in blood flow during embryonic development. These studies, using zebrafish and mouse as model organisms, revealed that alterations in blood flow have an effect on the nitric oxid (NO) signaling. Consequently, as NO is a conserved regulator of vertebrate HSPC development, variations of NO production, in both zebrafish and mice, lead to changes in the expression of genes involved in HSPC development and homeostasis, such as *Runx1* and *c-myb* [59], [60]. Together, these studies demonstrated that the blood circulation itself, through NO induction, plays a vital role in the establishment of definitive

hematopoiesis and HSPC maintenance, processes that are highly conserved across vertebrates. This makes sense in the context of embryonic development, where definitive HSPCs emerge from the hemogenic endothelium in the AGM region and then traffic to subsequent niches through the systemic circulation. In the adult niche, however, most HSPCs are outside of circulation and would thus not be exposed directly to blood flow. In this context, other niche cells, such as vascular ECs and pericytes, may experience shear stress and indirectly influence HSPCs via paracrine signaling [61].

Work from numerous research groups suggests that the HSPC niche is comprised of multiple cell types, including the vascular ECs and pericytes mentioned above. As previously outlined, two parallel mouse genetic models, each one described in a report published in the journal *Nature* in October of 2003, served to established a positive correlation between the numbers of osteoblasts and HSPCs [33], [34]. This suggested that osteoblasts were important regulators of hematopoiesis. Subsequent studies then focused on the exact mechanisms by which these cells are able to regulate HSPCs. Diverse cell adhesion molecules and soluble factors have been proposed to mediate osteoblast-HSPC interactions. Key among these are stromal-derived factor-1 (SDF-1; also known as CXCL12), granulocyte colony stimulating factor (G-CSF), Angiopoietin-1 (ANGPT1), TPO, N-cadherin-mediated cell adhesion, Osteopontin (OPN) and the Notch and Wnt signaling pathways [33], [34], [62],[63]. These studies, however, have been challenged by more recent work. In 2007, Kiel *et al*. demonstrated that total ablation of osteoblasts in the BM had no effect on the number of HSPCs [64]. Additionally, it was shown in separate studies that changes in the number of osteoblasts did not affect the number of HSPCs [65], [66]. Moreover, imaging studies of the BM did not reveal a significant association between osteoblasts and HSPCs either [67], [57]. In fact, these imaging techniques revealed that the sinusoidal vasculature is the only BM marrow structure that is consistently observed in close proximity to HSPCs [68]. Collectively, these studies demonstrated that the role of osteoblasts in modulating HSPCs was not as important as initially proposed, and suggested that other cell types might play essential roles in the regulation and maintenance of HSPCs [63]. Consequently, research over the past few years has focused attention on the different cell populations that dwell in the HSPC perivascular niche.

The perivascular niche is comprised of multiple cell types, including vascular ECs, various types of mesenchymal stromal cells, sympathetic nerves, megakararyocytes and macrophages. ECs constitute a core component of this niche. Apart from assisting the transmigration of HSPCs into and out of circulation, these cells secrete soluble factors and express cell surface adhesion molecules that support HSPC recruitment, maintenance and

function [9]. While ECs in the perivascular niche appear to be indispensable for hematopoiesis (discussed in more detail in the following section), multiple other cell types (e.g., CAR cells, Nestin-expressing cells, leptin receptor (LepR) positive cells, megakarayocytes, macrophages and Schwann cells) have also been implicated to function within the perivascular HSPC niche, supporting HSPCs and promoting their maintenance (**Figure 4**) [69],[70].
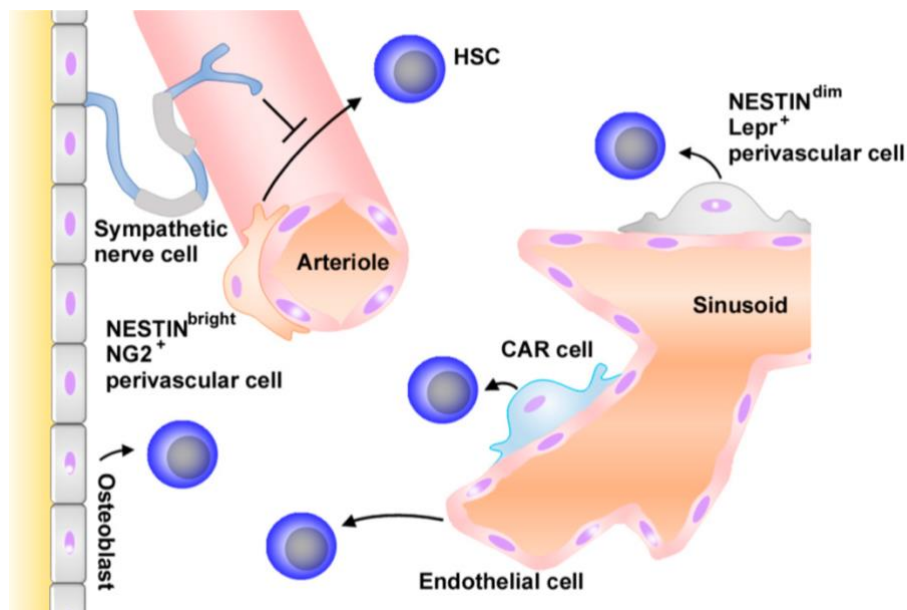

Figure 4. Multiple cell types contribute to maintenance of hematopoietic stem and progenitor cells in the perivascular niche. Cell types other than ECs, such as CAR cells, Nestin-expressing cells, LepR positive cells, nerve and perivascular cells, contribute to HSPC maintenance. Arrows and "T" indicate stimulating and suppresive activities, respectively (NG2, neuron-glial antigen 2; CAR, CXCL12-abundant reticular, Lepr, leptin receptor). Extracted from [70].

1.4 Endothelial Cells in the Perivascular HSPC Niche

In the human body, the vascular system is composed of a multitude of vessels (e.g., arteries, capillaries, sinusoids and veins) that allow the circulation of the blood throughout the entire circulatory system. The vascular system is thus essential, since it permits the supply of oxygen and nutrients to distinct tissues of the body, as well as removal of carbon dioxide and other waste products from them [71], [72].

Vascular ECs comprise the most inner constituent layer of blood vessels and perform a critical role in a variety of homeostatic functions, including delivery of oxygen and nutrients, regulation of coagulation and transit of immune cells into the vascularized tissues. Moreover,

ECs exhibit a regenerative capability. This is due to their interaction with corresponding tissue-resident stem cells in order to coordinate organ regeneration and eventually reestablish homeostasis in the context of an injury. Therefore, given the fact that ECs can carry out a great variety of functions, it is not surprising that they represent a highly heterogenous population of cells, thus showing unique, organ-specific signatures. Moreover, even within the same organ, these cells can be exceptionally diverse, and differ in their vascular characteristics and functions. This is for instance, the case of the ECs that reside in the BM, which have proven to be essential for hematopoiesis [73], [74], [75].

In the BM, there are distinct blood vessels, and each type is comprised of a different subset of ECs. Two different blood vessel types are mainly integrated into the HSPC niche: (I) the arterioles and (II) the sinusoids, which are in turn connected to each other. Arterioles, that emerge from larger arteries, are responsible for blood flow regulation in the BM microvascular compartment [76]. They are, however, scarce, and are mostly confined to the endosteal zone. Arterioles branch into sinusoids – vessels with a wider lumen – and thus arborize ultimately in a highly interspersed network of sinusoidal capillaries, that occupy around the 30% of the BM volume [9], [77]. Sinusoids represent a special type of capillaries. Their walls are incomplete due to the presence of a discontinuous basement membrane plus large fenestrations [78]. This way, sinusoids are leaky and extraordinarily permeable, as opposed to arterioles, which highly express junctional proteins such as vascular endothelial (VE)-Cadherin. These characteristics make sinusoidal ECs perfect conduits for hematopoietic cells to shuffle between the bloodstream and the BM, as well as for the transport of soluble factors between these two compartments [9]. This might be the reason why the majority of HSPCs are located near sinusoidal blood vessels. However, rather than merely regulating transmigration, sinusoidal ECs play indispensable roles for HSPC maintenance. It is known that these cells contribute to HSPC biology, primarily through expression of a series of angiocrine factors, including growth factors, chemokines and ECM components. Via these molecules, ECs are capable of stimulating, within the perivascular niche, both self-renewal and differentiation of HSPCs. The proliferative niche is thus believed to be mostly made up of sinusoids. Consistent with this, sinusoidal ECs are associated with high ROS levels in their surroundings. Clearly, this is coupled with increased intracellular production of ROS within the HSPCs, that, as previously explained in this thesis, seems to correlate with their migration and subsequent multi-lineage differentiation. In contrast, arteriolar ECs, as they are less permeable, provide less oxygen concentration and a ROS low environment, thereby sustaining quiescence of LT repopulating HSCs – the most undifferentiated cells at the top of the hematopoietic hierarchy (**Figure 5**) [9], [76], [79], [80].
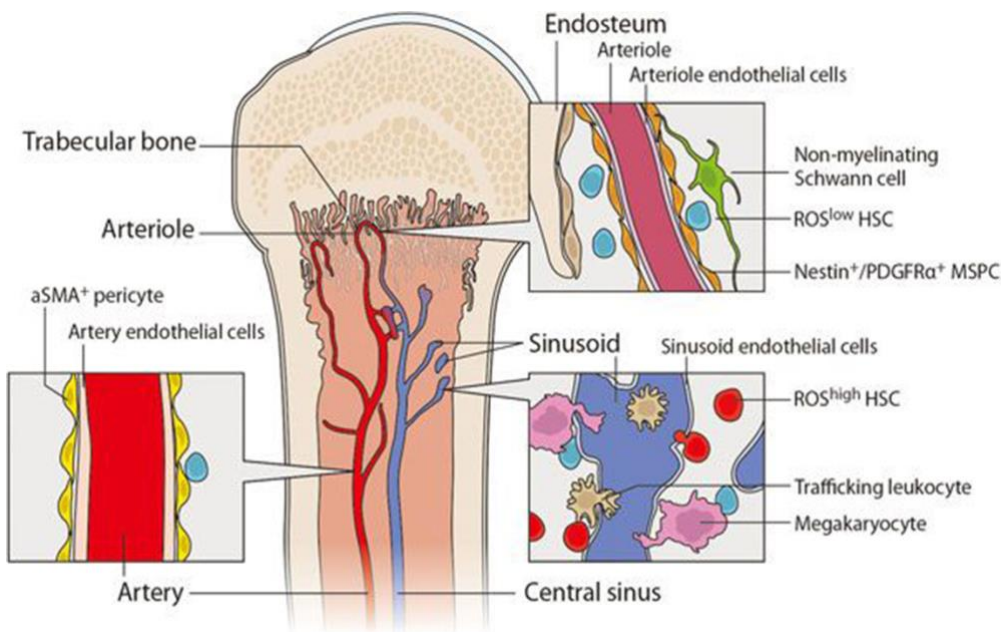
Figure 5. The distinct blood vessels in the bone marrow associate with different cell cycle status of hematopoietic stem cells. Sinusoidal ECs are associated with high ROS levels in their surroundings, thus representing a proliferative niche, whereas arteriolar ECs provide a ROS low environment where HSC are mostly maintained quiescent (α-SMA, alpha-smooth muscle actin; ROS, Reactive Oxygen Species; PDGFRα, Platelet-derived Growth Factor Receptor alpha). Extracted from [80].

Besides showing distinct metabolic signatures, arteriolar and sinusoidal vessels also differ in their hemodynamics. While arterioles exhibit high blood flow velocities and shear stress, sinusoids show low blood flow rate and shear stress (**Figure 6**) [46]. Different studies have demonstrated that marrow sinusoidal vessels display significantly lower flow velocities and shear stress than those seen in capillaries in other locations, while marrow arterioles do not differ much from arterioles elsewhere. It is thus logical to think that the distinction between marrow sinusoidal vessels and the rest of sinusoids may be ascribed to the importance of low shear forces in HSPC biology in a sense that these could facilitate the transit of HSPCs into and out of the BM [9], [46], [81].
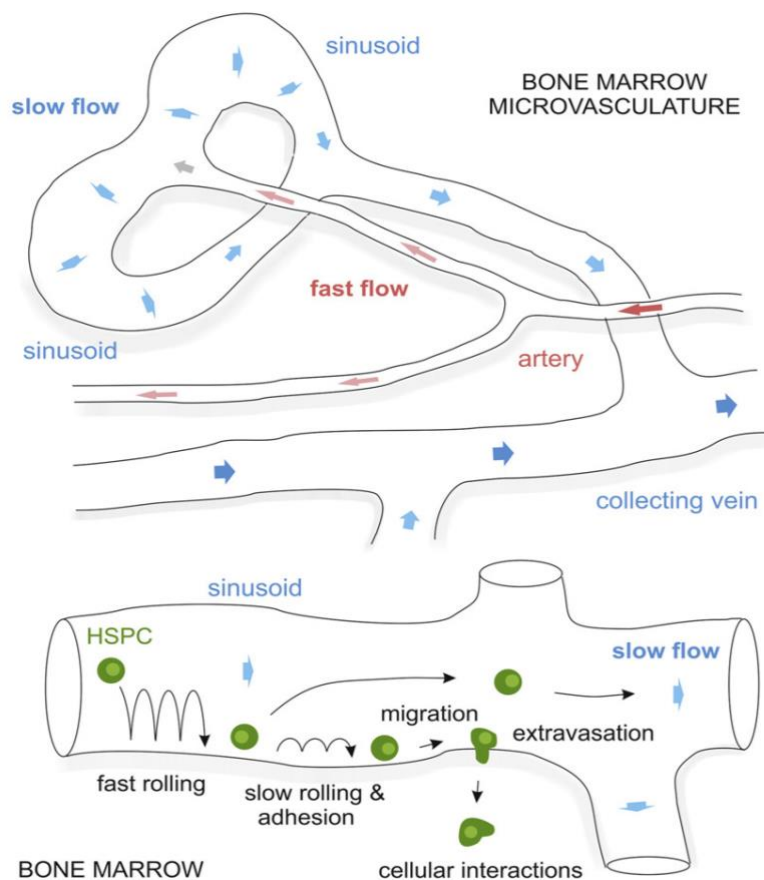
Figure 6. Sinusoids show low blood flow rate and shear stress to facilitate the transit of hematopoietic stem and progenitor cells into and out of the bone marrow. While arterioles exhibit high blood flow velocities and shear stress, sinusoids show low blood flow rate and shear stress. Besides, sinusoids in the BM display significantly lower flow velocities and shear stress than other sinusoids located elsewhere. This eases the role of sinusoidal ECs as conduits for HSPCs. Extracted from [46].

Yet it has become clear that sinusoidal ECs are essential for HSPC homing and proliferation. Supporting this, there is strong evidence that, when compared to arteriolar ECs, sinusoidal ECs express significantly higher levels of E-selectin (sele), an adhesion molecule that is constitutively expressed in marrow ECs [9]. It has been demonstrated that sele, along with P-selectin, interact with the glycoprotein ligand-1 (PSGL1-1) – their counter-receptor expressed on HSPCs – in response to CXCL12/CXCR4 signaling. As a result of this interaction, marrow ECs can mediate the transmigration of HSPCs [82], [83]. The fact that sele is highly expressed by sinusoidal ECs, but not by the arteriolar endothelial subtype, indicate that sinusoids are fundamentally involved in HSPCs homing. It is therefore conceivable that sinusoidal ECs could also induce the homeostatic proliferation and

26

differentiation of HSPCs, processes that take place prior or in parallel to HSPC homing [9], [76]. This idea is consistent with studies showing that sele promotes HSPC proliferation, as inferred from *Sele* kockout mice (*Sele -/-*), where the HSC cycle is significantly slower than that in their wild type counterparts. Moreover, this explains why blockade of sele has proven to protect HSPCs against chemotherapy or irradiation. Since restriction of sele activity renders a low-proliferative state, HSPCs develop resistance to such treatments, that are known to preferentially target fast-proliferating cells [84].

Both in arterioles and sinusoids, ECs are thought to work in concert with their surrounding stromal cells in order to ensure homeostasis of HSPCs in the perivascular niche. In general terms, it has been established that both ECs and their associated stromal cells produce two major niche factors: stem cell factor (SCF) and as SDF-1. Expression of these by both stromal cells and ECs is believed to promote HSPC maintenance [9]. In this trifling particular, future research is, however, necessary in order to explicate the exact roles of the aforementioned cell types, and clarify whether the endothelial subtypes really make up different environments within the perivascular BM niche. Still, something that we know for certain, is that the presence of ECs, along with their interactions with the stromal cells, are crucial for healthy hematopoiesis, as demonstrated by *in vivo* studies, in which deletion of genes encoding important niche factors expressed by these cells, such as CXCL12, glycoprotein 130 (gp130) cytokine receptor and SCF, leads to little-to-no numbers of HSPCs and overall hypocellularity in the BM [85], [86], [87].

1.4.1 Endothelial Cell Development

ECs are not only intimately associated with HSPCs in the adult niche, but also during embryonic development, since both cells types simultaneously emerge from the extra-embryonic mesoderm, specifically within the bloods islands of the yolk sac [14]. The concurrent births of hematopoietic and endothelial cells, as well as the expression of common cell-surface markers, including the Cluster of Differentiation 34 antigen (CD34) and Stem cell antigen-1 (Sca-1), and key transcription regulators, such as Scl and members of the GATA TF family, in both cell types suggest that these cells derive from a common mesodermal progenitor, widely known as hemangioblast [9], [75]. In line with this notion, two distinct populations of cells can be distinguished within the blood islands: the central and the peripheral hemangioblasts. On the one hand, the former give rise to the embryo's first blood cells during the primitive wave of hematopoiesis. On the other hand, the latter differentiate into the precursors of mature ECs, the so-called angioblasts. Individual angioblasts

subsequently fuse with each other and remodel into tubular structures, thereby forming vessels *de novo* in a process known as vasculogenesis (**Figure 7**) [88].
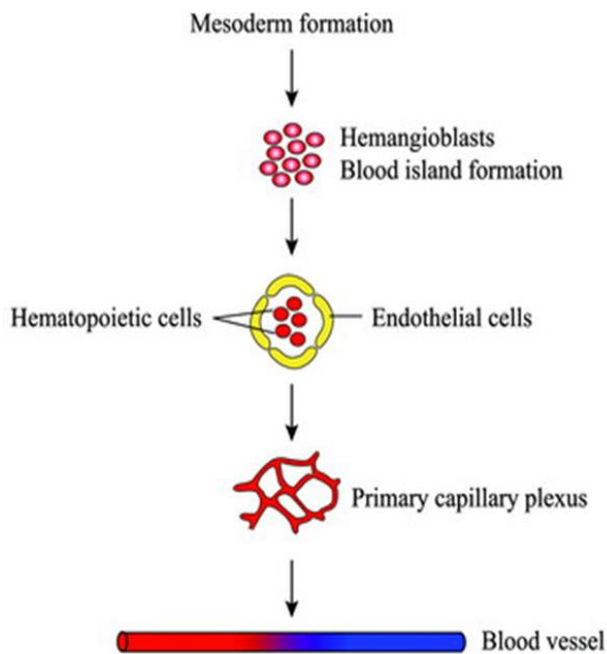

Figure 7. Hematopoietic and endothelial cell lineages emerge from the same precursors. Both hematopoietic and endothelial cell lineages emerge from the mesodermal cells that make up the primitive blood islands of the yolk sac. Within the blood islands, there are central and peripheral hemangioblasts. While the former give rise to the hematopoietic cells, the latter differentiate into the angioblasts – the precursors of mature ECs. Individual angioblasts subsequently fuse with each other and remodel into tubular structures, giving rise to the primary capillary plexus. Later in development, this plexus remodels into larger vessels via vasculogenesis. Adapted from [88].

In contrast to the concept of the common ancestor, definitive HSPCs, the first blood cells with LT repopulation capacity, arise later in development, during definitive hematopoiesis, from a specified hemogenic subset of ECs lining the ventral luminal surface of the dorsal aorta, in the AGM region. This process is referred to as "endothelial-to-hematopoietic (ETH) transition" (**Figure 8**) [16], [89].
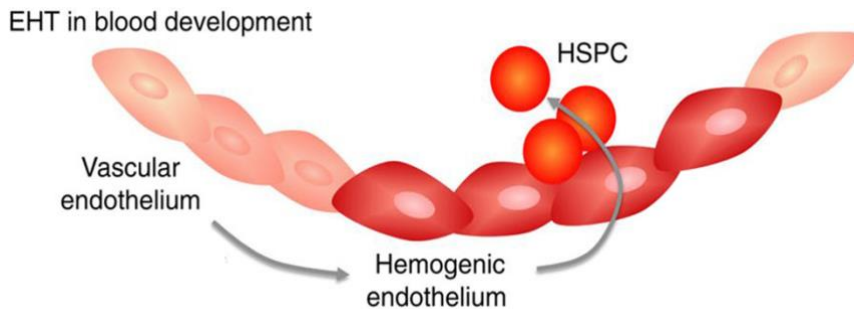
Figure 8. The endothelial-to-hematopoietic transition. The first blood stem cells with LT repopulation capacity arise during definitive hematopoiesis from the AGM region (EHT, endothelial-to-hematopoietic; HSPC, hematopoietic stem and progenitor cell). Adapted from [16].

Although the mechanisms underlying the simultaneous emergence of hematopoietic and endothelial cells remain poorly understood, their close developmental association is, in either way, unequivocal. The first genetic evidence that both cell types are related came from deletion in mice of the *Fetal Liver Kinase 1* (*Flk1*) gene, also known *Kinase Insert Domain Receptor* (*KDR*) gene. This gene encodes a tyrosine-protein kinase that functions as a cell-surface receptor for VEGFA, VEGFC and VEGFD (VEGF receptor 2), and its expression is widely used as a pan-endothelial marker. Global deletion of the *Flk1* gene results not only in aberrant vessel formation, but also in total absence of HSPCs, thus causing lethality between E8.5 and E9.5 of mouse embryos [90], [91].

During vascular development, the distinction between arteries and veins is a required process that occur even prior to the onset of blood circulation [9]. A myriad of factors and signaling pathways are implicated in the arteriovenous (AV) specification. Among others, these include Notch, SHH, and VEGF signaling pathways; members of the GATA and SRY-box (SOX) TF families; E26 transformation-specific (ETS) factors; Forkhead box (Fox) TFs; and COUP2 TF (COUP-TFII), also known as nuclear receptor subfamily 2, group F, member 2 (Nr2f2). Extensive work in animal models, like the zebrafish, have revealed that the Notch signaling, along with the SHH and VEGF signaling pathways, are essential for arterial specification, as well as endothelial cell sprouting during angiogenesis – the process following vasculogenesis, in which new vessels are formed from existing ones. On the contrary, COUP-TFII antagonizes pro-artery Notch signaling to promote venous EC identity [9], [92]. More than dozen ETS factors have been broadly detected in the endothelium during vascular development. Notably, these factors show functional redundancy, a fact that suggests they carry out a combinatorial action. This is supported by the fact that deletion of both *Ets1* and *Ets2* genes leads to vascular branching defects during mouse development; however, loss of function of the individual genes has not shown any negative effects [93]. Among the ETS factors, special attention has been recently

drawn to the protein known as ETS translocation variant 2 (ETV2). ETV2 has demonstrated to be indispensable not only for vascular development, but also for formation of hematopoietic cells, since it has the ability to bind promoters or enhancer regions of genes that are essential for both endothelial and hematopoietic cells lineages, such as *Scl*, *Flk1*, *Friend leukemia virus integration 1* (*Fli-1*) Proto-Oncogene and the myeloid marker *PU.1*. By inducing the expression of these genes, ETV2 promotes the differentiation of primitive mesoderm into vascular mesoderm and endothelial and hematopoietic lineages [92]–[94]. Supporting this, previous work in the zebrafish and frog have shown that overexpression of *Etv2* alone is sufficient to induce ectopic endothelial and myeloid marker expression [95], [96]. Members of the Sox and FOX TF families (i.e., Sox7, Sox17, and Sox18; and Foxc1 and Foxc1, respectively) are likewise thought to be necessary for correct AV specification, as zebrafish and murine models lacking these proteins show serious vascular defects [92], [97], [98]. Lastly, GATA members also play a role in vascular development. GATA2, the most abundantly expressed GATA factor in ECs, is believed to act in the early embryo, particularly in the specification of the hemangioblast progenitors from the mesoderm. Thus, as long as the hemangioblast is truly considered the common ancestor of endothelial and hematopoietic cells, it is not surprising that GATA2 acts as a common regulator of both cell lineages [98], [99].

Although the exact hierarchical EC signaling program remains incompletely understood, there is a scientific consensus that vascular development is closely associated with development of the hematopoietic system, and that the ontogeny and specification of both systems rely on the spatial and temporal regulation of gene expression, as well as the coordinated action of a great variety of molecular players [9].

1.4.2 Co-Culture of Hematopoietic Stem and Progenitor Cells with Endothelial Cells

As the main limitation of HSPC transplantation is the low numbers of cells available to support engraftment in adult patients, several strategies to expand HSPCs have been devised and subjected to exhaustive examination. The procedures to expand HSPCs *ex vivo* deal with (I) the usage of extrinsic factors (e.g., cytokines, growth factors, or a combination thereof), (II) the exploiting of the own HSPC intrinsic factors (e.g., overexpression of TFs involved in self-renewal), and/or (III) the co-culture of HSPCs with supportive cell types from the BM niche. The main goal is, however, the same for all of them: increase the numbers of cells without attrition of the stem cell identity [3], [100], [101].

Focusing on the co-culture strategy, different research groups have investigated the supportive effects of sinusoidal ECs on HSPC homeostasis. The regulatory effect of ECs on HSPCs has already been validated by data showing that co-culturing HSPCs with ECs (e.g., Human Umbilical Vein Endothelial Cells, HUVECs) can enhance expansion of HSPCs *in vitro*, as well as facilitate engraftment and reconstitution of the hematopoietic system *in vivo* upon transplantation [102]. The first evidence that BM sinusoidal ECs play a crucial role in the regulation of hematopoiesis came from the results of a study carried out by Avecilla *et al.* There, they demonstrated that revascularization of the BM following myelosuppresive therapy could completely reestablish thrombopoiesis in TPO-deficient mice. This finding indicated that lineage-specific differentiation of hematopoietic progenitors was driven by the sole regeneration of functional sinusoidal ECs, thus highlighting the role of these cells in HSPC regulation and differentiation [103]. Subsequent co-culture studies indicated that the effects of ECs were likely dependent of the secretion of distinct angiocrine factors, such as SCF (also known as Kit-ligand; KITL) and Notch ligands, essential factors for self-renewal; or interleukin (IL)-1 and IL-6, cytokines involved in lineage-specific differentiation [9]. Backing the notion that ECs predominantly act via their paracrine effects, it was observed that a molecular cocktail, including KITL, TPO, Flk-2, and angiopoietin-like factors could robustly support HSPC expansion under serum-free conditions [104], [105]. Although the action of these molecules seems to be of the utmost importance, direct contact between ECs and HSPCs has also proven to be required for HSPC self-renewal and differentiation in culture. This points out that the physical forces, exerted by ECs, might be importantly involved in HSPC regulation as well [9], [106], [107]. Therefore, co-culturing HSPCs with ECs is expected to have better outcomes than the mere addition of relevant angiocrine factors in the medium when culturing HSPCs alone. In addition, co-culture studies have also shown that modulation of certain signaling pathways in ECs indirectly contributes to expansion of HSPCs. For instance, this was demonstrated by a study, where HUVECs were transformed with an AKT serine/threonine kinase 1 (*Akt1*) activating-adenoviral gene, thereby expressing *Akt1* constitutively. This led to activation of the phosphatidylinositol-3-kinase (PI3K)/Akt and the mammalian target of rapamycin (mTOR) signaling pathways, which are known to be involved in EC proliferation, survival and apoptosis. As an important player of these pathways, it has become clear that Akt1 particularly induces survival of ECs and expression of angiocrine factors [108], [109]. This explains why overexpression of *Akt* enhanced indirectly the expansion of HSPCs.

All the striking results derived from these co-culture studies serve to foster our understanding of the interactions between endothelial and hematopoietic cells. Dissecting

the crosstalk between these two cell types represents a significant focus of the regenerative medicine community, since this knowledge will be necessary in order to improve HSPC transplantation therapies.

1.5 Generation of Ectopic Stem Cell Niches

Kai and Spradling published a report in 2003 where they highlighted the importance of the niche environment in *Drosophila* ovarioles. There, they showed that the niche can preserve its ability to support proliferation and maintenance of ectopic cells even after loss of endogenous stem cells. To show that, they ablated the normal stem cells of the niches in the ovarioles. Surprisingly, they found that even so, the niches were themselves able to trigger within incoming ectopic somatic cells signaling pathways controlling germ-line stem cell function, such as the decapentaplegic (Dpp) pathway, and thus change the fate and the growth properties of the ectopic cells [110]. This indicated that the niche and the signals occurring in this microenvironment are *per se* key to converting susceptible cells into stem cells, as well as controlling stem cell function. In this sense, it was revealed that there is a distinctive molecular program characterizing the stem cell niche that is able to modify residing cells. In view of the significance of this microenvironment, the goal later on was to establish new niches at ectopic sites and see whether endogenous stem cells could migrate there and be sustained as efficiently as in their natural niches. In order to accomplish this, some studies have tried to artificially induce signaling pathways and molecules that play a pivotal role within the niche [111],[112]. For example, Silva-Vargas *et al.* showed that when Wnt signaling is artificially activated in the basal layer of the epidermis, it causes new dermal papillae to emerge, as well as ectopic development of hair follicles, with new stem cell niches being induced [112].

Particularly, in the field of hematopoiesis, different studies have aimed to drive ectopic formation of HSPC niches as well. As previously outlined in this thesis, Chan et al. managed to induce an ectopic hematopoietic niche in the mouse kidney after *in situ* transplantation of fetal bone implants. Importantly, with these experiments, they found that in the new generated HSPC niche, certain molecules, such as osterix (Osx) and VEGF, were indeed specifically required for its generation, as well as maintenance [36]. This finding further highlighted the role of specific sets of molecules in the induction of a concrete stem cell niche. Building on this study, the Osx−/− mutants generated by Coşkun *et al.* demonstrated that the Osx factor is indeed indispensable for the establishment of a healthy BM microenvironment, since in its absence, the BM is not capable of supporting the development

or maintenance of LT-HSCs [113]. Therefore, it is logical to think that those factors that are required for correct function of the normal HSPC niche are also necessary for induction of functional blood cell formation elsewhere. Recent work has indeed confirmed the contribution of specific factors in the induction and maintenance of hematopoiesis at ectopic sites. For instance, overexpression of T Cell Leukemia Homeobox 1 (Tlx1) has been shown to lead to extramedullary hematopoiesis in the spleen and that high levels of Tlx1 are in fact specifically required for HSPC recruitment to that organ [114]. Although more research is clearly needed to define the niche-specific molecular programs, all these previous reports indicate that the stem cell niches function as signaling platforms and that it is the artificial expression of the specific niche factors what determines the induction of new stem cell niches outside the normal locations.

1.6 Zebrafish as a Model for Hematopoiesis

The teleost zebrafish (*Danio rerio*) has emerged as a versatile model organism to study vertebrate hematopoiesis. There are many reasons why it represents an ideal system for this work. In general, easy breeding, low maintenance cost and short generation times (2-3 months) are key aspects for the convenience of zebrafish models. In addition, they present the advantage that their externally fertilized eggs develop fast, progressing to larvae in three days, and if desired, the developmental rate can also be tailored by simply changing the incubation temperature. Moreover, zebrafish embryos pose, withal, no difficulties for mechanical manipulations, like injection or transplantation, and are thus amenable to different genetic modifications, allowing for the generation of many informative mutants. In addition, as the embryos are transparent, the introduction of fluorescent reporter genes fused to the genes of study permits the straightforward visualization of detailed morphogenetic movements, as well as changes in gene expression either during normal development or upon genetic alterations or exposure to chemicals of interest [1], [115],[116].

Hematopoiesis in zebrafish is very similar to that in mammals, given the fact that this process is evolutionarily conserved across vertebrates. Besides having the same all major blood cell types (derived from common lineages of HSPCs), most of the TFs and signaling pathways involved in zebrafish hematopoiesis are conserved with mammals [117]. Akin to the mammalian process of blood formation, zebrafish hematopoiesis takes place in the form of sequential waves. HSPCs traffic among distinct niches, situated in various anatomical locations throughout development. As previously explained, in mammals, definitive HSPCs are born in the AGM and subsequently migrate to the fetal liver and other intermediate

niches, before lodging in the BM and thymus – the adult HSPC niches. In zebrafish, definitive HSPCs also bud off from the AGM, but then migrate to the analogue intermediate niche, known as caudal hematopoietic tissue (CHT), a vascular plexus in the ventral region of the tail. Eventually, HSPCs migrate to, and colonize the adult HSPC niches: the kidney marrow (the equivalent to the BM in mammals) and the thymus (**Figure 9**) [1]. As outlined above, the fast, embryonic development of zebrafish represents a clear benefit of this model organism. Particularly, in hematopoiesis, this offers a more rapid and facile course of investigation when compared to mammals. In zebrafish, nascent HSPCs emerge from the AGM around 30 hours post fertilization (hpf), and are thought to commence seeding the adult niches by 5-6 days post fertilization (dpf). In contrast, this process generally takes longer in mammals [15], [20], [118]. For example, in mouse, the EHT occurs at day 10 of gestation (E10), whereas colonization of the adult niche starts shortly before birth, around E17.5 [1].
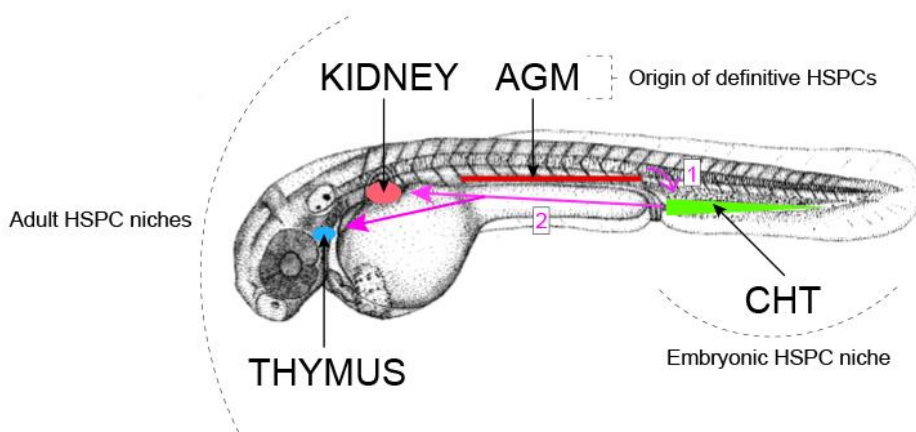
Figure 9. Changes in the anatomical location of hematopoiesis in the zebrafish. HSPCs emerge from the AGM around 30 hpf and therafter colonize the CHT – the embryonic HSPC niche (1). By 5-6 dpf, HSPCs start migrating to the kidney marrow and the thymus (2), which are the definitive niches (AGM, aorta-gonad mesonephros; CHT, caudal hematopoietic tissue; HSPC, hematopoietic stem and progenitor cell). Adapted from [116].

The study of the blood stem cells, from their origin to their residency in the definitive niches, has been possible thanks to different transgenic zebrafish lines, in which the gene of interest is fused to a fluorescent protein cassette (e.g., green fluorescent protein (GFP), or mCherry fluorescent protein), which serves as a reporter of gene expression. In this sense, the generation of transgenic zebrafish expressing fluorescent proteins allows for lineage tracing experiments, in which discrete cell populations can be distinguished and subsequently analyzed. Transgenic reporter lines with fluorescently labeled HSPCs, such as *runx:GFP* and *cmyb:GFP*, along with the pan-endothelial marker *flk:mCherry*, have

permitted the easy observation of HSPCs as they first emerge from the hemogenic endothelium in the AGM. In addition, tracking endogenous HSPCs in the live embryo allows for the study of the dynamic cellular interactions within the HSPC niche [1], [119]. Particularly, this kind of studies has highlighted the importance of ECs in the perivascular HSPC niche. For instance, a group in our laboratory recently discovered in this way a novel perivascular EC behavior that is thought to be triggered upon arrival of HSPCs in the CHT microenvironment. They observed that ECs remodelled around HSPCs to form different "stem cell pockets" following the colonization of the niche by HSPCs. This phenomenon, termed "endothelial cell cuddling" [22], highly suggested that ECs create these distinct compartments in order to harbor and protect HSPCs within the hematopoietic niche.

1.7 Previous Work

Since different studies have heretofore shown that vascular ECs function as fundamental components of the HSPC niche, our research group has focused on dissecting the differential genetic regulation of this exceptional subset of ECs, using zebrafish as an animal model. Our current research project focuses on ECs from the CHT. As previously outlined, the CHT environment serves as the intermediate niche for HSPCs, and it is in a manner equivalent to the mammalian fetal liver [1]. Shortly before I joined the group, a set of around 20 genes that are selectively expressed by CHT ECs was identified using a combination of RNA tomography (a technique that involves cryosectioning and RNA-sequencing (RNA-seq) to examine spatial patterns of gene expression) and tissue-specific RNA-seq [120]. Two of the genes that were most strongly expressed by CHT ECs are *sele* and *mannose receptor, C type 1a* (*mrc1a*). The selective expression of these genes in the CHT was validated using whole-mount *in situ* hybridization (WISH) (**Figure 10 I A**). Strikingly, the group found that many of these CHT endothelial genes are similarly expressed in the adult zebrafish kidney — the adult HSPC niche, analogous to the BM in mammals [1]. In addition, it was found that many of the same genes were expressed by ECs in the mammalian fetal liver niche and BM, suggesting these genes represented a conserved niche EC signature. Subsequently, GFP reporter transgenes were generated using large upstream regulatory sequences for the *sele* and *mrc1a* genes. Analysis of the GFP expression in the *sele:GFP* and *mrc1a*:*GFP* lines revealed that the GFP expression patterns matched the endogenous expression of the genes (based on WISH) (**Figure 10 I B**). These transgenes thus allowed for the *in vivo* visualization of the CHT EC compartment by fluorescence microscopy. Subsequently, either the *sele*:*GFP* or the *mrc1a*:*GFP* reporter line was out-crossed to the pan-endothelial

flk:mCherry reporter line. Offspring of these crosses was screened for both GFP and mCherry expression and double positive embryos were processed for fluorescence-activated cell sorting (FACS). Four different cell populations, including the double positive CHT ECs, were isolated by FACS (**Figure 10** I **C**).
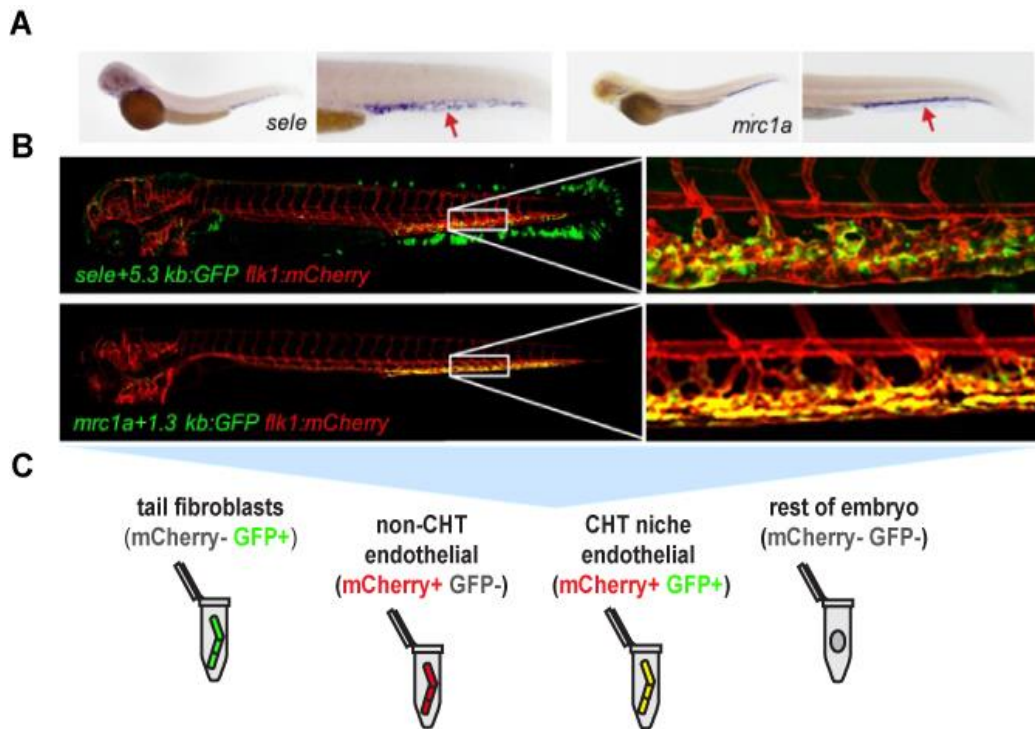
Figure 10. Reporter transgenes for *sele* and *mrc1a* drive GFP expression in endothelial cells in the CHT niche (A) WISH shows the endogenous expression of *sele* and *mrc1a*, two of the genes selectively expressed by ECs in the CHT niche (red arrows). **(B)** Analysis of the GFP reporter transgenes showed that GFP fluorescence matched the endogenous expression patterns of the genes. Subsequent out-crossing of these transgenics to the pan-endothelial *flk:mCherry* marker confirmed that both transgenes labeled ECs in the CHT niche — ECs are labeled in yellow as a result of the overlap between the red (*flk:mCherry*) and green (*sele:GFP* or *mrc1a:GFP*) colors. **(C)** Four different cell populations were isolated by FACS: tail fibroblasts (mCherry-, GFP+), non-CHT ECs (mCherry+, GFP), CHT niche ECs (mCherry+, GFP), and transgene negative rest of the embryo (mCherry-, GFP-).

The assay for transposase-accessible chromatin (ATAC-seq) – a technique for mapping chromatin accessibility genome-wide [121] – was subsequently performed on the four FACS-isolated cell populations. This analysis revealed that 6,848 regions of open chromatin were uniquely present in the CHT EC population, but not the other three populations, including ECs located elsewhere (mCherry +, GFP -). Of note, several of the 20 genes identified by tomo-seq had unique ATAC-seq peaks associated with them. To test whether these unique sequences of open chromatin were tissue-specific enhancers, several of these regions were

cloned and fused to a minimal beta-globin promoter coupled to a GFP reporter gene. The resulting DNA constructs were injected into one cell-stage zebrafish embryos and then screened for GFP expression. For 12/15 injected constructs, significant GFP expression was observed in CHT ECs in 60-72 hpf-embryos, suggesting these regions of open chromatin represented indeed tissue-specific enhancers.

Based on the data outlined in the two paragraphs above, it was postulated there might be a specific transcriptional program regulating the niche-specific expression of these endothelial genes. In order to determine the TFs that might bind the CHT EC enhancers, a motif enrichment program, known as "Hypergeometric Optimization of Motif EnRichment (HOMER)" [122], was utilized. HOMER analysis of the 6,848 CHT EC peaks revealed that Ets, Sox (Sox F factors, specifically) and Nuclear Hormone (NH) receptor factors (RXRA/RORA/NR2F2, specifically) binding motifs were most enriched. In addition, promoter truncation studies were performed for a few of the enhancers. These experiments allowed for the identification of regions located upstream of *mrc1a* and *sele* that were as small as 125 bp and 158 bp, respectively. These regions, which perfectly aligned with the apex of an ATAC-seq peak at the same locations and contained Ets, Sox and NH sites, were sufficient to drive GFP expression when fused to GFP and injected into one cell-stage zebrafish embryos. To test whether the TF binding sites, identified by the HOMER analysis, were required for the observed GFP expression of the *sele 158 bp*:*GFP* and *mrc1a 125 bp*:*GFP* transgenes, sequences variants for these small regions were generated, in which each of the three different classes of motifs was disrupted by mutation. In either case, a significant reduction or complete loss of GFP expression was observed, thus suggesting that Ets, Sox and NH receptor binding sites are independently required for expression of niche-specific endothelial genes. These results indicated that a transcriptional code, involving members of the TF families, determines the genetic signature of niche ECs.

Uncovering the genes that make niche ECs unique will enable their genetic manipulation. In so doing, HSPC transplantation therapies can be enhanced by improving HSPC engraftment and maintenance in the niche. The present work provides insight into the genes that are relevant for the identity of the ECs that reside in the CHT niche of the zebrafish, as well as the intrinsic and extrinsic regulators that control the expression of such genes and the temporal dynamics of the CHT microenvironment. We expect our work to be significant for *in vitro* co-cultures of HSPCs with ECs, or for the modulation of the HSPC niche upon disease or transplantation. Given the similarities between the zebrafish and human hematopoiesis, we anticipate that our findings in the zebrafish model will be also applicable to the human hematopoietic system.

1.8 Specific Aims

Leveraging strengths of the zebrafish system, our investigation aimed to 1) elucidate the transcriptional network that controls the expression of the niche-specific genes expressed by ECs, 2) investigate the extrinsic regulation that mediates the expression of such genes, and 3) resolve the temporal dynamics of the morphology of the CHT niche, as well as the hematopoietic population and the differential niche endothelial gene expression over the course of development. We therefore dissected the differential molecular regulation of the subset of ECs that dwell in the hematopoietic niche, supporting HSPCs. The main objectives of our research included:

1. To determine which TFs are sufficient to drive niche EC identity by overexpressing different combinations of TFs from the Ets, Sox and NH receptor family. This allowed us to determine specific combinations of factors that are optimal for inducing ectopic niche EC gene expression.
2. To investigate the regulation of niche endothelial gene expression by blood flow. For these studies, *SOX7* was overexpressed in an effort to rescue the loss of niche endothelial gene expression in the absence of blood flow.
3. To characterize the temporal dynamics of the HSPC niche, including morphological, cellular and molecular changes over the course of development, using different approaches such as a quantitative analysis of the CHT vascular network, and WISH and RNA-seq for time-course analysis of gene expression.

2 Material and Methods

A detailed list of relevant reagents, materials and equipment utilized for the experiments described in this thesis work can be found in **Appendix B: Materials, Reagents and Equipment.** Throughout the manuscript, the supplier is only specified for kits and software, as well as for enzymes or other key solutions.

2.1 Zebrafish Husbandry and Maintenance

Both wild type (WT) and GFP and mCherry transgenics zebrafish (*Danio rerio*) of EKK strain were used in this study (**Appendix A: Supplementary Information; SI.1. Generation of Transgenic Zebrafish**). Adults were reared using standard husbandry techniques, at 28.5° C under a 14-h light–10-h dark cycle.

Embryos used for all the experiments were rinsed and collected in system water (deionized, reverse osmosis water), and transferred to Zebrafish E3 medium (5 mM NaCl, 0.17 mM KCl, 0.33 mM $CaCl_2$, 0.33 mM $MgSO_4$) shortly thereafter. Embryos were stored in a 28.5°C incubator in round Petri dishes (145 x 20 mm) at a density of approximately 50 embryos per dish, and daily checked for mortality and any morphological abnormality. Dead and dying embryos were immediately removed when detected, and medium was replaced every 1-2 days. Starting at 5 dpf, zebrafish, belonging already to the larval stage, were fed every 1-2 days with fresh saltwater rotifers (*Brachionus plicatilis*) and algae feed mixture diluted with saline water to a final salinity of 3–5 ppt. The water change included removal of diseased and dead larvae and any other debris. Embryos and larvae were staged by hpf or dpf according to standard criteria [116], and grown until the desired stage. All animals were housed at the facilities of the Zon laboratory at Boston Children's Hospital, and maintained and euthanized according to Institutional Animal Care and Use Committee of Boston Children's Hospital.

2.2 Zebrafish Microinjection

2.2.1 Breeding of Adults and Egg Collection

For the purposes of breeding, one or two adult males and one female were placed in mating cages separated by a plastic divider either in the early morning (for afternoon injections) or the evening (for injections in the next morning). After removal of the divider, spawning was allowed to occur undisturbed until sufficient number of embryos were laid at the bottom of

the cage. Subsequently, embryos were carefully collected using a fine-mesh tea strainer, washed thoroughly with system water and placed in Petri dishes. Embryos were next used for the injection experiment. If not injected immediately, embryos were collected and stored at 4ºC until needed in an effort to slow down development and be able to inject them at the one cell-stage.

2.2.2 Fabrication of Microinjection Molds

In order to ensure the correct orientation of the embryos during microinjection, agarose molds were made to hold embryos in place during the procedure. For casting the agarose molds, a 1.5% agarose solution was first prepared by dissolving agarose powder in distilled water (ddH$_2$O) in an Erlenmeyer flask, and subsequently heating up the solution in the microwave until boiling. When heating, the solution was agitated by gently swirling the flask so as to reduce foaming and prevent formation of clumps and bubbles. Approximately 50 mL of hot agarose were then poured into a Petri dish (100 x 15 mm) on a level surface. Immediately thereafter, a plastic mold with furrows was placed into the liquid agarose and the gel was then allowed to cool down to room temperature for 15-20 minutes. Once set, the plastic mold was carefully removed. The microinjection plate was then wetted with E3 medium and sealed with parafilm to be stored at 4ºC until use.

2.2.3 Needle Loading and Calibration

0.5 mm borosilicate OD glass microcapillary needles with inner filament were used for microinjection. With a needle puller, each needle was pulled into two. The resulting needles were stored in a Petri dish by laying therein over two strips of reversed tapes. To backload a needle with the desired DNA solution, the needle was filled using an extra-long tip and a p20 pipette. Generally, 2.5-3 µL of the injection solution were loaded, avoiding the formation of air bubbles. The loaded needle was then placed on the reversed tapes for a couple of minutes, so that the liquid went down to the needle tip by capillary action. In addition, the inner filament within the needle facilitated that the solution was pulled to the end of the needle.

The microinjection set-up included a micromanipulator, which was attached to a magnetic clamp stand, a pneumatic microinjector connected to a pressure source, and a stereoscope (**Figure 11**). Once the pressure source and the microinjector were turned on, the needle was placed in the holder of the micromanipulator. After that, the microscope was focused on the tip of the needle, which was subsequently broken using fine watchmaker forceps to give the

end of the needle an opening. A microscope micrometer was then used to calibrate the injection volume. To that end, a glass cover slip was placed over the ruler of the micrometer slide and a drop of mineral oil was added on it. When injected into the oil, the diameter of the droplet was calibrated to 100 μm, thus containing 0.5 nL of injection material (**Figure 12 | B**). The size of the droplet was adjusted by trimming the needle and modifying the injection pressure and duration of the pressure pulse, two parameters controlled by the microinjector itself.
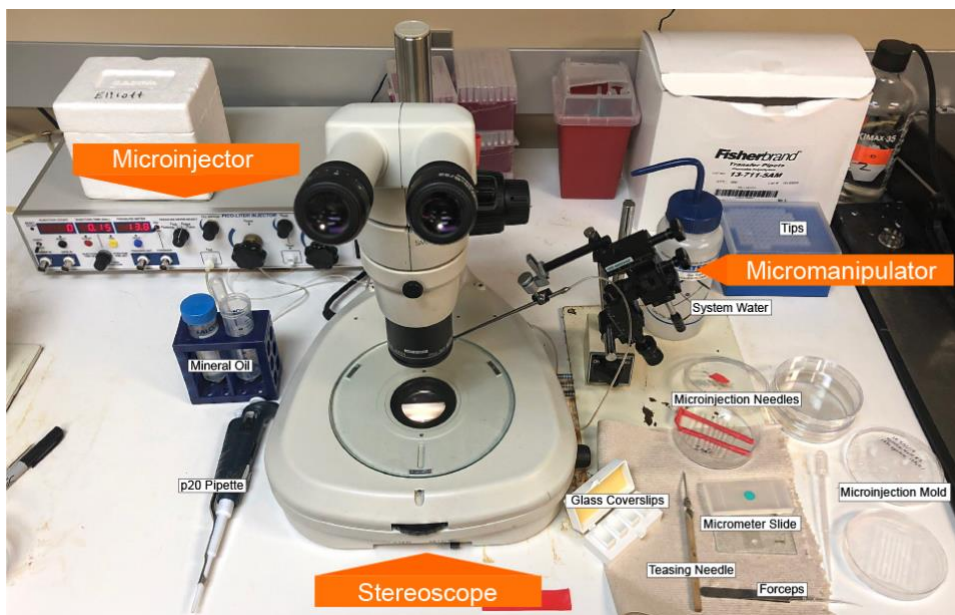
Figure 11. Typical microinjection set-up. Annotated image showing the typical microinjection set-up, composed of a micromanipulator, a pneumatic microinjector and a stereoscope. Other tools used for microinjection are also herein depicted. These include a p20 pipette, tips, the microinjection needles and the mold, the micrometer slide, the mineral oil, the glass coverslips, the fine watchmaker forceps, the teasing needle and system water to dislodge the embryos from the mold after injections.

2.2.4 Microinjection

Before microinjection, recently collected fertilized eggs were aligned in the grooves of the microinjection plate with a wood handled teasing needle with a plastic gel-loading pipette tip (**Figure 12 | A**). After that, they were orientated so that the embryonic cell of each embryo was facing the needle. To inject the desired DNA solution, the embryo's chorion was pierced carefully with the tip of the microinjection needle so as to penetrate the embryonic cell, into which the solution was then injected. All embryos were injected at one cell-stage to increase

the chances of targeting the nucleus and ensure a high rate of transgenesis and minimize mosaicism. Each injection delivered between 0.5–1 nL injection material into the embryonic cell (**Figure 12 | B**). Embryos that were difficult to inject or had passed the one cell-stage at the moment of microinjection were sacrificed. Those successfully injected were collected by flooding the microinjection plate with system water and dislodging them by gentle swirling. Embryos were then transferred to a Petri dish with a disposable plastic Pasteur pipette. Thereafter, system water was replaced with E3 medium, and embryos were raised, as previously described above in section 2.1.
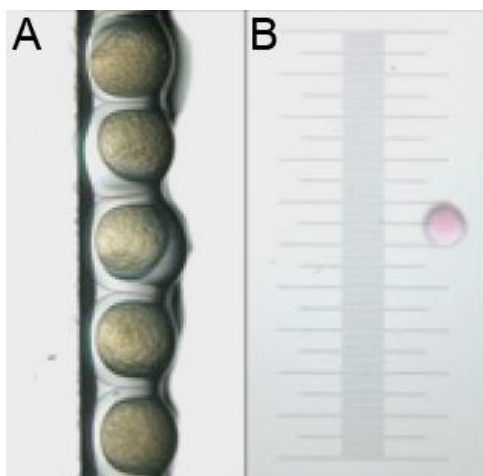
Figure 12. The DNA solution is injected into one cell-stage Zebrafish embryos. (A) Embryos to be injected are lined up in the grooves of the microinjection mold. **(B)** When injected into mineral oil, the diameter of the droplet is calibrated to a diameter of 100 µm, thus containing 0.5 nL of injection material. In order to inject 1 nL instead, the user should simply inject twice. Adapted from [122].

2.3 Zebrafish Transgenesis

2.3.1 DNA Constructs

In order to overexpress TFs in zebrafish embryos, DNA constructs for the human (*Homo sapiens*) genes *FLI1A*, *ETV2*, *ETS1*, *SOX7 and RXRAA*, the xe*nopus (Xenopus laevis) gene sox18*, and the zebrafish gene *nr2f2* driven by a ubiquitous (*ubi*) promoter were injected into one cell-stage embryos. These DNA constructs, including the open reading frame (ORF) sequence of the TF gene, were originally generated by Gateway cloning and readily available in our laboratory from previous work by other colleagues. When needed, the gateway vectors were propagated. Separate reactions for each plasmid were set up. In each case, 10 pg – 100 ng of the plasmid stock were transformed into 50 µL of One Shot TOP10

chemically component cells (Invitrogen™; Thermo Fisher Scientific, Waltham, MA, USA) using the heat shock method. After a 30 minutes' incubation on ice, the mixture of chemically competent bacteria and DNA was heat-shocked at 37 ⁰C for 30 seconds, and then placed back in ice for 2 minutes. Thereafter, 250 µL S.O.C. media were added. The transformed cells were subsequently incubated at 42 ⁰C for 1 hour at 225 rpm in a shaking incubator. Following incubation, 20-200 µL from each transformation vial were plated onto a separate, labeled Luria-Bertani (LB) agar plate supplemented with the antibiotic prescribed by the vector of interest (i.e., ampicillin, chloramphenicol), and subsequently incubated overnight at 37 ⁰C. The next morning, at least three single colonies were selected and again separately cultured overnight at 37 ⁰C, in LB medium supplemented with antibiotic (e.g., ampicillin) diluted 1:1000 (stock solution at a concentration of 100 mg/mL). The following day, the pellet of each bacterial culture was obtained by centrifugation at maximum speed for 10 minutes. The DNA from the plasmids was subsequently extracted from each culture using Qiaprep Spin Miniprep kit (Qiagen, Hilden, Germany), following manufacturer's instructions. Finally, the DNA was eluted with 50 µL elution buffer. DNA concentrations were analyzed using a NanoDrop and the purified plasmids were next verified by DNA sequencing.

2.3.2 Synthesis of Transposase mRNA *In Vitro*

Tol2 mRNA was synthesized *in vitro* using the vector pCS-TP, which carries the Tol2 transposase cDNA. First, the pCS-TP plasmid was linearized by digestion with *NotI* enzyme overnight at 37⁰C in a thermocycler. The next day, a 1% agarose gel prepared in 1x Tris-acetate–EDTA (TAE) buffer, containing 0.5 µg/ml ethidium bromide, was electrophoresed to determine whether the plasmid was completely linearized. After confirming plasmid linearization, the obtained Tol2 fragment was purified using the Qiagen PCR Purification Kit (Qiagen, Hilden, Germany) according to manufacturer's instructions. mRNA was next synthesized *in vitro* using the mMESSAGE mMACHINE SP6 kit (Ambion™; Thermo Fisher Scientific, Waltham, MA, USA) following manufacturer's instructions. Following mRNA synthesis, DNAse treatment with DNase I (Sigma-Aldrich, St. Louis, MO, USA; stock solution at a concentration of 100 U/µL) was performed for 15 minutes at 37⁰C in a thermocycler. Thereafter, Tol2 mRNA was purified using RNeasy MinElute kit (Qiagen, Hilden, Germany), following manufacturer's instructions. A 1% agarose gel prepared in 1xTAE buffer and containing 0.5 µg/ml ethidium bromide, was electrophoresed for 30-45 minutes at 120 V to check for mRNA integrity. Previously, 0.5 µL RNase inhibitor was added to each lane of the gel to help prevent RNA degradation. In addition, both the casting tray and the combs were

thoroughly wiped with a Kimwipe wetted in RNase AWAY reagent to eliminate unwanted RNase contamination. Once mRNA integrity was confirmed, mRNA was finally diluted to a concentration of 125 ng/uL and dispensed into 2 uL aliquots for long-term storage at – 20°C.

2.3.3 Preparation of Injection Solutions

Before the injection experiment, the DNA solutions to be injected were prepared. To that end, different combinations of the DNA constructs were made and adjusted to reach a total DNA concentration of 25 ng/μL. The injected DNA mixtures contained diverse TF genes, as follows: the seven-factor mix (*FLI1A*, *ETV2*, *ETS1*, *sox18*, *SOX7*, *nr2f2* and *RXRAA)* (**Table 1**)*,* the three-factor mix (either *ETV2* or *ETS1* in combination with *SOX7* and *nr2f2)* (**Table 2**) and the single TF solution (i.e., *ETV2*, *ETS1*, *SOX7* and *nr2f2* alone*)* (**Table 3**). Besides the DNA, 2 uL Tol2 mRNA were also added to the injection mix at a concentration of 25 ng/μL. In addition, 1 uL 0.5% phenol red serving as an injection tracer, as well as nuclease-free water were added to adjust the final volume of the injection mixture to 10 uL. Later, 0.5-1 nL of each solution was injected into one cell-stage zebrafish embryos, as previously outlined in section 2.2. Uninjected embryos or embryos injected with the Gateway destination vector (*pDest394*; also, at a concentration of 25 ng/μL) served as a negative control. Both TF-injected embryos and their control counterparts were examined for ectopic expression of niche endothelial genes by WISH and/or by assessment of fluorescent transgene expression using spinning disk confocal microscopy, as described more fully in later sections.

Table 1: Components of the seven TF mix. The total volume of the solution is 10 μL, with a final DNA concentration of 25 ng/μL ([], concentration).

Component	Volume (μl)	Initial [ ]	Final [ ]
ubi:ETV2	0.43		
ubi:ETS1	0.43		
ubi:FLI1a	0.43		
ubi:SOX7	0.43	50 ng/μl each	25 ng/μl total
ubi:sox18	0.43		
ubi:nr2f2	0.43		
ubi:RXRAA	0.43		
Phenol Red	1	0.5%	0.05%
Tol2 mRNA	2	125 ng/μl	25 ng/μl
Nuclease-free H_2O	3.99	-	-
Total	10		

Table 2: Components of the three TF mix. The total volume of the solution is 10 µL, with a final DNA concentration of 25 ng/µL ([], concentration).

Component	Volume (µl)	Initial [ ]	Final [ ]
ubi:ETV2 or *ubi:ETS1*	1		
ubi:SOX7	1	50 ng/µl each	25 ng/µl total
ubi:nr2f2	1		
Phenol Red	1	0.5%	0.05%
Tol2 mRNA	2	125 ng/µl	25 ng/µl
Nuclease-free H_2O	4	-	-
Total	**10**		

Table 3: Components of the single TF mix. The total volume of the solution is 10 µL, with a final DNA concentration of 25 ng/µL ([], concentration).

Component	Volume (µl)	Initial [ ]	Final [ ]
ubi:TF	1	50 ng/µl each	25 ng/µl total
pDest394	2		
Phenol Red	1	0.5%	0.05%
Tol2 mRNA	2	125 ng/µl	25 ng/µl
Nuclease-free H_2O	4	-	-
Total	**10**		

2.4 Generation of Mutant Enhancer Constructs

In order to test whether the Ets, Sox and NH receptor TF binding sites were indeed required for *mrc1a* and *sele* transgene expression, mutant enhancer constructs containing mutations targeted to intervening sequences between these motifs were generated. To that end, overlapping oligonucleotides (forward and reverse) were first designed to feature unnatural bases by substitution of pyrimidine with purine in the core motifs located within the enhancer sequences of the *mrc1a* and *sele* genes. Constructs containing unaltered full enhancer sequences served as a control. All oligonucleotides were ordered from IDT, and once received, their stock solutions were prepared with nuclease-free water to the final concentration of 100 µM and stored at – 20°C. The nucleotide sequences are listed in **Table 4.**

Table 4: Nucleotide sequences of the wild type and mutant enhancers of the *sele* and *mrc1a* genes. Overlap between all the primer pairs is 24 bp. Modified base pairs are written in lowercase.

Construct	Forward Oligonucleotide	Reverse Oligonucleotide
***sele* gene**		
Wild Type	CCATGAAACTGGGAAGATGAAAGCATTAGTTGAA TTGTTACTGGCAACATCTTCTCTGTAATGCCCCCT GTGACCCATATTGTCTCGCTCTTTCCTTTATAAAC AGAGCTGTAGATATCCACAGGAAATGGGGGTGT TTTTGCCATTATTTCTTCCTG	CAGGAAGAAATAATGGCAAAAACACCC CCATTTCCTGTGGATATCTACAGCTCTG TTTATAAAGGAAAGAGCGAGACAATATG GGTCACAG
Mutant	CCATGAAACTGGGAAtcTGAAAGCATTAGTTGAAG TTACTGGCAACATCTTCTCTGTAATTGCCCCCTGT GACCCATATTGTCTCGCTCTTTCCTTTATAAACAG AGagGTAGATATCCACAGGAAATGGGGGacTTTTT GCCATTATTTCTTCCTG	CAGGAAGAAATAATGGCAAAAAgtCCCCC ATTTCCTGTGGATATCTACCtCTCTGTTTA TAAAGGAAAGAGCGAGACAATATGGGTC ACAG
***mrc1a* gene**		
Wild Type	TGAAGCTTGTACCTTTCATTTCCTTTTTGCTGAGC TTTATTTTCTCTAGAATTGCCATTGTGTTTCCATTC TAGCAAATCAGCATTTTTTTTTCAGCTGAAAGAAA AATACCAGGAACTGAGAGC	GCTCTCAGTTCCTGGTATTTTTCTTTCAG CTGAAAAAAAAATGCTGATTTGCTAGAAT GGAAACACAATGGCAAT
Mutant	TGAAGCTTGTACCTTTCATTTCCTTTTTGCTGAGC TTTATTTTCTCTAGAATTGCCATTGTGTTTCCATT CcgGCAAATCAGCATTTTTTTTTTCAGCTGAccGAA AAATACCAGGAACTGAGAGC	GCTCTCAGTTCCTGGTATTTTTCggTCAG CTGAAAAAAAAATGCTGATTTGCcgGAAT GGAAACACAATGGCAAT

Later, T4 DNA ligase was employed to carry out an annealing and T4-fill-in reaction. Each reaction had a total volume of 20 µL and contained 0,5 uL T4 DNA Ligase (NEB; New England Biolabs, Ipswich, MA, USA; stock solution at a concentration of 400,000 U/mL), 2 uL 10X NEB buffer 2, 0.2 µL 100X Bovine Serum Albumin (BSA), the corresponding forward and reverse oligonucleotides (1 µL each), and 12.8 nuclease-free water. Ligations were carried out at 12°C for 20 minutes. The reaction products were next analyzed on a 2% agarose gel prepared with ultrapure agarose powder dissolved in 1X TAE buffer, containing 0.5 µg/ml ethidium bromide. The gel was electrophoresed for 30-45 minutes at 140 V. The resulting bands were then extracted from the gel and weighted before purification using the QIAquick Gel Extraction Kit (Qiagen, Hilden, Germany). As the last step of the purification procedure, 45 µL nuclease-free water were used to elute the purified DNA extracted from the bands. Approximately, 43 µL DNA product were obtained per each reaction. Next, in order to allow for A-tailing, incorporation of deoxynucleotide triphosphates (dNTPs) by the Klenow fragment was carried out. Reactions were assembled in 8-strip Polymerase Chain Reaction (PCR) tubes using a thermocycler at 37 °C for 30 minutes. Each reaction mixture

contained, in a total volume of 50 µL, 43 µL DNA, 5 µL 10X NEB buffer 2, 1 µL 10 mM dNTP and 1 µL Klenow fragment. Klenow reaction products were next subjected to phenol-chloroform extraction and ethanol precipitation. To that end, the reaction mixtures were first transferred to 1.7 mL microcentrifuge tubes. Then, 50 µL nuclease-free water were added to each tube to make up a final volume of 100 µL. After that, 100 µL phenol chloroform were added to each tube. Samples were subsequently spun down at 14,000 rpm for 5 minutes using a microcentrifuge. Following centrifugation, the aqueous DNA phase was transferred to a new tube (approximately, 90 µL per tube). Thereafter, 270 µL 100% ethanol were added along with 9 µL of sodium acetate (3 M, pH 5.2). Samples were then placed at − 20°C for 15-20 minutes until the solution became viscous, in order to allow precipitation to occur. Afterwards, samples were centrifuged at 14,000 rpm for 15 minutes and washed with 1 mL 70% ethanol. Thereafter, the tubes were flicked gently a few times, and then centrifuged at 14,000 rpm for 5 minutes. Following centrifugation, samples were resuspended in 20 µL nuclease-free water. Later, the DNA concentration of each sample was measured using a nanodrop spectrophotometer.

The sequence variants were fused to a minimal β-globin promoter and GFP using the Gateway technology. In order to generate the enhancer plasmids (p5E; middle entry vectors), the purified Klenow reaction products were cloned into pENTRE5'-TOPO-TA vectors by TOPO cloning, using the TOPO TA Cloning kit (Invitrogen™; Thermo Fisher Scientific, Waltham, MA, USA) according to manufacturer's instructions. After cloning, the ligated DNA of each sample was transformed into One Shot Top10 Competent Cells by the heat shock method (performed as already explained in section 2.3.1) and subsequently spread on LB-agar added with kanamycin. After overnight culture at 37ºC, three single colonies (i.e., the middle entry clones) were picked and separately cultured again overnight at 37 ºC, in LB medium supplemented with antibiotic (in a similar way to the procedure described in section 2.3.1). The following day, the DNA from the middle entry clones was extracted from each culture using the Qiaprep Spin Miniprep kit according to manufacturer's specifications, and the DNA was finally eluted with 50 µL elution buffer. DNA concentrations, analyzed using a NanoDrop, ranged from 161.4 ng/µL and 280.6 ng/µL, with a A260/A280 ratio above 1.8. The resulting p5E-enhancer plasmids, including either the WT or the mutated enhancer sequence of the *sele* or *mrc1a* gene, were then assembled together with the minimal β-globin promoter and GFP (pME), the Tol2 Gateway destination vector (#394; pDestTol2A2) and the globin intron SV40 polyA (#143 p3E_SV40polyA) in Gateway LR reactions, catalyzed by the LR Clonase II enzyme (1 µL; Invitrogen™, Thermo Fisher Scientific, Waltham, MA, USA). Prior to the LR reaction, the p5E-enhancer constructs were

diluted to a concentration of 20 ng/μL with nuclease-free water. The resulting Gateway products were sequence-verified.

In order to prepare the constructs for injection, the Gateway products were diluted to a concentration of 50 ng/μL with nuclease-free water and stored at – 20°C until use. These constructs were injected at a final DNA concentration of 25 ng/μL into one cell-stage embryos to assess whether mutations targeted to intervening sequences between the Ets, Sox and NH receptor TF binding sites would result in reduction or loss of GFP expression, as compared to control embryos, into which the constructs containing the full WT enhancer were injected. For these experiments, injected embryos were observed at 48 to 72 hpf to detect and analyze GFP expression. For the *sele* gene, 5-7 clutches were examined per injected construct, with 65.6 embryos on average, per clutch, whereas for the *mrc1a* gene, 4 clutches were analyzed per injected construct, with 40.3 embryos on average, per clutch.

2.5 Whole-Mount In Situ Hybridization

2.5.1 Embryo Fixation and Storage

Embryos were grown until the selected time point. After proper staging was confirmed, fixation was performed. Viable embryos were first dechorionated either mechanically by manual removal of the chorion using fine forceps, or with addition of 2-3 μL pronase solution (Roche, Sigma-Aldrich, St. Louis, MO, USA) overnight. Thereafter, dechorionated embryos were euthanized by tricaine overdose and subsequently transferred into 1.7 mL microcentrifuge tubes, whereas dead embryos were discarded. E3 medium was removed and replaced with 1 mL ice cold 4% paraformaldehyde (PFA) diluted in 1X phosphate buffered saline (PBS) for overnight fixation at 4°C. The following day, embryos were dehydrated through three washes with 100% methanol. After the last wash, methanol was replaced with fresh 100% methanol, and the embryos were subsequently stored at − 20°C until WISH analysis was performed.

2.5.2 Anti-Sense RNA Probe Synthesis

2.5.2.1 RNA Extraction and cDNA Synthesis

EKK WT embryos from different developmental stages (24 hpf – 5 dpf; 40 embryos for each stage) were transferred to 1.7 mL microcentrifuge tubes, snap-frozen in dry ice and stored at − 80 °C until RNA isolation was performed. For RNA isolation, the whole embryos samples were first thawed, and carefully resuspended in 350 μL lysis buffer (RLT buffer; provided by

the RNeasy Mini kit (Qiagen, Hilden, Germany) supplemented with 1% β-mercaptoethanol. Embryos were subsequently homogenized on ice using mechanical shredders for at least 20 seconds per sample. Each sample was thereafter centrifuged through a QIAshredder homogenizer (Qiagen, Hilden, Germany) for 2 minutes at maximum speed. Afterwards, for removal of genomic DNA (gDNA), the obtained supernatants were transferred to gDNA Eliminator spin columns (provided by the RNeasy Mini kit) and centrifuged at 10,000 × g for 30 seconds. Next, total RNA was extracted using RNeasy Mini Kit according to manufacturer's specifications. Finally, RNA was eluted in 30 µL RNase-free water (provided by the RNeasy Mini kit). RNA concentration and quality were then determined using a nanodrop spectrophotometer. RNA concentration ranged from 50 to 300 ng/µL, and only samples with an A260/280 nm ratio of 1.8-2.0 were considered acceptable to proceed with to reverse transcription. Up to 5 µg RNA was used for cDNA synthesis using the SuperScript III First-Strand Synthesis Super Mix Kit (Invitrogen™; Thermo Fisher Scientific, Waltham, MA, USA) according to manufacturer's instructions. A reaction with nuclease-free water in lieu of enzyme mix served as the "no reverse transcriptase" control (NRT control). After transcription, cDNA samples from different stages were pooled together and further diluted with nuclease-free water if necessary. cDNA was then stored at − 20 ºC until PCR was performed.

2.5.2.2 PCR-Amplification and *in Vitro* Transcription

Specific anti-sense RNA probes were synthesized from *in vitro* transcription of PCR products carrying the T7 RNA polymerase recognition sequence at one end, using cDNA from pooled embryos as a template. Primer sequences, spanning exon-exon junctions, were either designed using NCBI Primer Blast or obtained from the available literature. In addition, T3 and T7 promoter sequences were added to the 5' ends of the forward and reverse primers, respectively. Primers used for amplification are listed in **Table 5**.

Table 5. Primer sequences for *in situ* hybridization probes. All genes listed in this table are zebrafish genes.

Gene	Forward (5′-3′)	Reverse (5′-3′)	Expected amplicon size (bp)	Reference
mrc1a	GTGTCCCCTCATCAATGCCA	ACGGCATTCCACAAACCAGA	946	Designed
gpr182	CTTCCCACAGCAGCACAAAC	GAAAGTTGTTGTTGAAGTGAACG	938	Designed
sele	ATGCTTCCATTGGGAAGTAGAA	CCATCAAACAATAAAAGGGGGCA	1918	Designed
lgmn	AACTTGAGCCACCGAGGATTT	CCCTAACTCCAGCACACACT	817	Designed
ets1	ACAGACTCTGTACGTTTGAATGCGT	GTCCAGACTTTACTCGTCCGTGTC	1333	[124]
sox18	TCCTTGGACGCTGTGGACCAAC	TCAAAGCGCTGCTTTCCTCGC	139	[126]
sox7	TATAGCCCTTCGTTCCCCCA	ACCGAAACCGGCTAAACTGA	999	Designed
fli1a	CAGACCCGTCTCTGTGGTC	CCAGTATGGGGTTGTGGGAC	887	Designed
nr2f2	ACCCCCGAACAACAATAACA	AGAGGGCAAGCGCAGTAATA	964	Designed
etv2	TATGACTGCAGTGGTGAAGACC	CTTTCCCGCCGTTTTGTGAA	864	Designed
T3 and T7 sequences				
T3	CATTAACCCTCATAAAGGGAA (added to the 5' end of forward primers)			
T7	TAATACGACTCACTATAGGG (added to the 5' end of reverse primers)			

Primers were ordered from Invitrogen. Once received, they were resuspended accordingly in nuclease-free water to a concentration of 100 µM. From these stock solutions, 10 µM working solutions were prepared by diluting with nuclease-free water. Primer solutions were kept at − 20 ºC until subjected to PCR. For probe making, a touch-down PCR-amplification (with a reduction of the annealing temperature of 0.5°C each cycle) was first performed, following the thermal cycling conditions listed in **Table 6**.

Table 6: Thermocycler conditions for PCR amplification of cDNA and re-amplification of PCR products (n/a, not applicable).

Step	Temperature [°C]	Time [sec]	Cycles
1	94	60	n/a
2	94	20	
3	*65 (* - 0.5 °C/cycle)	30	30x
4	72	60	
5	94	20	
6	58	30	10x
7	72	60	
8	72	360	n/a
9	4	∞	

Re-amplification of PCR products followed the first PCR, using the same set of primers and conditions as in the first round (**Table 5** and **Table 6**). For both PCR rounds, reaction mixes (50 µl) were assembled in 8-strip PCR tubes as follows: 25 µl REDTaq DNA polymerase (Sigma-Aldrich, St. Louis, MO, USA), 1 µl 10 µM forward primer, 1 µl 10 µM reverse primer, 1-5 µl cDNA template (for the first PCR round; 1 µg cDNA required) or 5 µl PCR product (for the second round), and 18-22 µl ddH$_2$O. A blank reaction containing no template cDNA served as a negative control. Following the second PCR, products were purified using the PCR Purification Qiagen kit according to manufacturer's instructions. To analyze the purified reaction products, a 1% agarose gel prepared with ultrapure agarose powder dissolved in 1X TAE buffer, containing 0.5 µg/ml ethidium bromide, was electrophoresed for 30-45 minutes at 120 V. Thereafter, the gel was photographed on a UV gel imager (405 nm) with a digital camera. If the resulted PCR products coincided in length with the expected amplicons, *in vitro* transcription of the PCR products using T7 RNA polymerase (Roche, Sigma-Aldrich, St. Louis, MO, USA; stock solution of 5,000 U) was next performed. In addition, the NRT control, previously prepared during the cDNA synthesis protocol, as well as the negative control were analyzed on the gel in order to ensure that there was no gDNA contamination. For *in vitro* transcription, each reaction (20 µL) contained 14.5 µL PCR product as a template, 2 µl 10X Transcription Buffer, 2 µl 10X DIG NTP mix, 1 µl RNAse inhibitor and 1 µl of T7 RNA polymerase. After 2-3 hours of incubation at 37 °C in the thermocycler, 1 µl DNase was added to each reaction followed by a 20 minutes' incubation at 37 °C in order to remove the DNA probe template. Immediately

thereafter, 10 μl RNAse-free water were added to make up a final volume of 22 μl. RNA probes were then purified through size-fractionation columns using the Illustra ProbeQuant G-50 Micro Columns (GE Healthcare, Sigma-Aldrich, St. Louis, MO, USA) according to manufacturer's instructions. Next, a 1% agarose gel was electrophoresed for 30-45 minutes at 120 V. 0.5 μL RNase inhibitor was previously added to each lane of the gel to help prevent RNA degradation. In addition, both the casting tray and the combs were thoroughly wiped with a Kimwipe wetted in RNase AWAY reagent to eliminate unwanted RNase contamination. After confirming the integrity of the RNA probes (detected as one or two discrete bands on the gel), probes were diluted with 100 μL hybridization (Hyb+) solution (50% formamide, 5x Saline Sodium Citrate (SSC), pH 5, 0.1% Tween20, 50 μg/ml heparin, 250 μg/mL Torula RNA and 9 mM Citric Acid, pH 6) and stored at − 20 ºC for short-term use. Prior to use and depending on the probe and the strength of the band observed on the gel, the probe was further diluted 1:10-1:200 to a final concentration of 50-100 ng/μL using more Hyb+ solution.

2.5.3 Whole-Mount In Situ Hybridization Analysis

Fixed embryos were rehydrated in a reverse methanol series in PBTw (PBS-Tween20; 0.1% Tween20 in 1X PBS) – 75% (vol/vol), 50% (vol/vol) and 25% (vol/vol) methanol/PBTw. In each dilution series, the samples were sit on shaker for 5 minutes at room temperature. Following rehydration, samples were washed four times with PBTw for 5 minutes each on shaker. To remove pigmentation, embryos were next bleached. To that end, embryos were transferred to and kept in bleach solution (10% KOH, 30% H2O2, 100% Tween20 and ddH2O) until pigmentation disappeared completely except for the eyes. The duration of the bleaching process varied from 8 to 25 minutes depending on the embryo's developmental stage, as noted in **Table 7**.

Table 7: Duration of the bleaching treatment at different stages of development.

Developmental stage (hpf)	Approximate bleaching times [min]
24	No bleaching required
36	8
48	10
56-60	11
72	12
96	14
5	15
8	17
10	20
14	25

After bleaching, embryos were rinsed twice with PBTw for 5 minutes and subsequently digested with proteinase K (Roche, Sigma-Aldrich, St. Louis, MO, USA; stock solution at a concentration of 19 mg/mL) to render them permeable, at room temperature and without agitation. For each developmental stage, the duration of the proteinase K treatment, as well as the proteinase K concentration were different as listed in **Table 8**.

Table 8: Proteinase K treatment for different stages of development.

Developmental stage (hpf)	Time [min]	Proteinase K dilution
24	7	1:2000
36	8-9	
48	10	
56-60	11	
72	12	
96	12	1:1000
5	15	
8	25-30	
10	35	
14	28-30	1:500

Following permeabilization, embryos were rinsed twice with PBTw to stop the digestion and post-fixed in 4% PFA / 2% glutaraldehyde diluted in PBTw for 20 minutes at room temperature on shaker. Embryos were subsequently rinsed five times with PBTw for 5

minutes each wash on shaker and pre-hybridized at 70°C in Hyb+ solution for at least 1.5 hours. After pre-hybridization, embryos were incubated overnight at 70 ºC in 500 µL diluted RNA anti-sense probe per tube.

On the second day, embryos were consecutively washed with different solutions, including Hybridization negative (Hyb-) solution (50% Formamide, 5X SSC, 0.1% Tween20 and 9 mM Citric Acid, pH6); 2X SSCTw (SSC-Tween20; 0.1% Tween20 in 2X SSC); 0,2X SSCTw (0.1% Tween20 in 0.2X SSC) and PBTw, following the order and conditions listed in **Table 9**.

Table 9: Washes performed on the second day of the WISH protocol.

Step	Solution	Time [min]	Temperature [°C]	Agitation on shaker
1	75% Hyb- / 25% 2X SSCTw	15	70	NO
2	50% Hyb- / 50% 2X SSCTw	25	70	NO
3	25% Hyb- / 75% 2X SSCTw	15	70	NO
4	2X SSCTw	15	70	NO
5	0.2X SSCTw	≥ 30	70	NO
6	0.2X SSCTw	≥ 30	70	NO
7	75% 0.2X SSCTw / 25% PBTw	10	RT	YES
8	50% 0.2X SSCTw / 50% PBTw	10	RT	YES
9	25% 0.2x SSCTw / 75% PBTw	10	RT	YES
10	PBTw	≥ 10	RT	YES

After the last wash with PBTw, embryos were blocked for 2 hours at room temperature with blocking solution containing 2 mg/mL BSA and 2 % lamb serum diluted in PBTw, for at least 1.5 hours on shaker. Following blocking, embryos were incubated overnight at 4°C in 500 µL blocking solution per tube with 1:5000 anti-Digoxigenin-AP, Fab Fragments (Roche, Sigma-Aldrich, St. Louis, MO, USA; stock solution of 150 U).

On the third day, embryos were washed with PBTw six times for 15 minutes each wash on shaker, followed by three quick consecutive washes with alkaline phosphatase (AP) buffer (100 mM Tris HCl, 50 mM $MgCl_2$, 100 mM NaCl, 0,1 % Tween20 and ddH_2O). In the last wash with AP buffer, the embryos were transferred to a 24 well-plate and then incubated in staining buffer, consisting of 0.5 mL AP Buffer each well, containing nitroblue tetrazolium chloride (NBT) and 5-bromo-4-chloro-3-indolyl-phosphate (BCIP). The staining buffer was prepared by adding 4.5 µL NBT (Promega, Madison, WI, USA; stock solution at a

concentration of 18.75 mg/mL) and 3,5µL BCIP (Promega, Madison, WI, USA; stock solution at a concentration of 9.4 mg/mL) to each mL AP buffer. The 24 well-plate was subsequently wrapped with aluminum foil to light-tight, so the staining reaction occurred in the dark. Staining reactions were generally carried out for 24-72 h at room temperature on shaker until the specific signal became visible. Staining was checked under a dissecting stereoscope with a fiber optic illuminator with articulated arms, and when appropriate, reactions were permanently stopped by washing the samples with three quick washes with PBTw. Immediately thereafter, stained embryos were fixed overnight in 4% PFA. After fixation, embryos were washed again with PBTw and subsequently transferred to 50% glycerol diluted in PBTw. After WISH, embryos were visualized and photographed using a fluorescence Nikon SMZ18 stereomicroscope.[2]

2.6 Blood Flow Experiments

SOX7 DNA coding sequence (*SOX7* ORF) was cloned under the control of an inducible heat shock promoter (*heat shock cognate 70-kd protein, like*; *hsp70l*) into Tol2-based expression vectors using the Gateway technology, similarly following the protocol previously described in section 2.4. For injections, casper EKK zebrafish lines were in-crossed and embryos were collected. A 25 ng/µL-DNA injection mixture containing the Tol2 expression vector plus 25 ng/µL Tol2 mRNA were microinjected into one cell-stage embryos. Uninjected embryos served as a negative control.

To block blood flow, embryos were treated with pimozide [125]. For that, the drug was dissolved in dimethyl sulfoxide (DMSO) to a final concentration of 25 µM in 1% DMSO, and embryos were then incubated in 25 µM pimozide solution, in six-well plates at 28.5ºC. Embryos exposed to 1% DMSO in E3 medium or in E3 media alone served as negative control. Each of the three groups (pimozide group, DMSO group and E3 medium control) consisted of n ≥ 20 embryos, from at least three different clutches. Embryos were treated from approximately 18 hpf to 48 hpf, stage at which they were euthanized by tricaine overdose and fixed in 4% PFA overnight.

In addition, heat shock induction was carried out in *hsp70l: SOX7* transgenic embryos at different time points: 24 hpf (prior to the establishment of the CHT) and 36-48 hpf (coincident with the initial wave of HSPC colonization of the CHT) [118]. Furthermore, uninjected embryos treated with pimozide were equally subjected to heat shock so as to ensure that

---

[2] Note to the reader: The WISH protocol described here was adapted from [126]. All washes were with 1 mL unless stated otherwise.

that the heat stress itself did not have any effect on niche endothelial gene expression. For purposes of heat shock, viable embryos were transferred to 1.7 mL microcentrifuge tubes at the mentioned time points, followed by heat shock treatment at 40°C for 30 minutes in a dry block incubator. After that, embryos were returned to the standard incubation temperature of 28.5° C **(Figure 13**). Fixed embryos were analyzed by WISH to determine whether overexpression of SOX7 the expression of the G protein-coupled receptor 182 gen (*gpr182*), a niche endothelial gene whose expression is lost in the absence of blood flow.
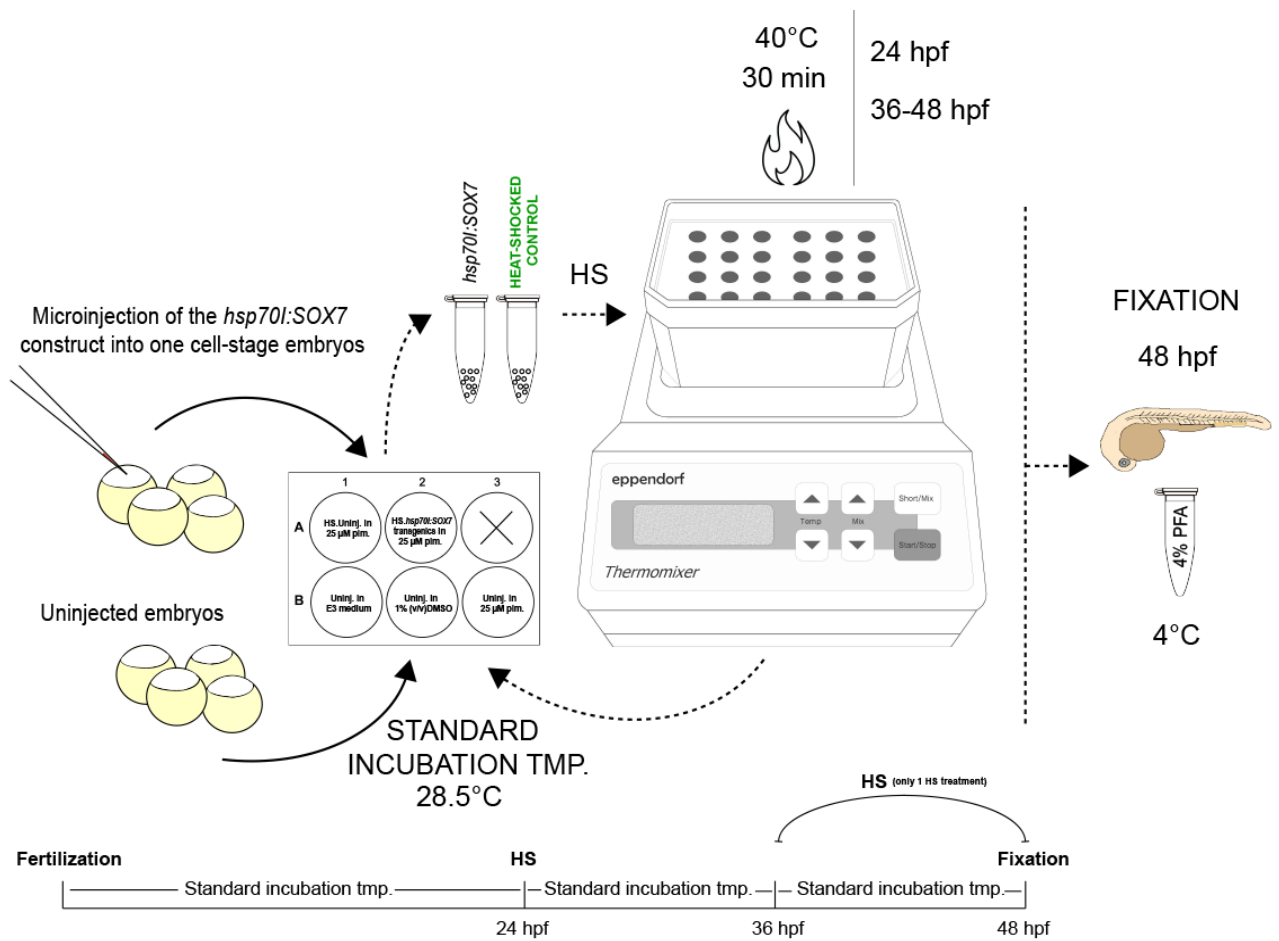
Figure 13. Experimental set-up for the blood flow experiments. One cell-stage zebrafish embryos were injected with the *hsp70I:SOX7* construct, whereas others were kept as uninjected. Embryos were distributed in different groups as follows: Negative control groups (uninjected in E3 medium and uninjected in 1% (v/v) DMSO); uninjected in 25 µM pimozide; heat-shocked control (heat-shocked uninjected in 25 µM pimozide) and heat-shocked *hsp70I:SOX7* transgenics in 25 µM pimozide (injected embryos). Embryos were incubated in the appropriate solution at the standard incubation temperature (28.5 ºC) until 48 hpf, time point at which they were fixed in 4% PFA at 4ºC overnight. Both injected and heat-shocked control embryos were subjected to heat shock at 40ºC during 30 minutes in a dry block incubator at two different time points: 24 hpf and 36-48 hpf. After heat shock, embryos were returned to the standard incubation temperature of 28.5° C. (HS, Heat Shock; PFA, Paraformaldehyde; Pim., Pimozide; TMP., Temperature; Uninj., Uninjected).

2.7 Spinning Disk Confocal Microscopy

Embryos were collected and raised until the appropriate stage. Embryos were mounted in glass bottom multi-well plates with 0.8% low melting point agarose, covered with E3 medium with tricaine and imaged by spinning disk confocal microscopy (SDCM). Multiple embryos were imaged at the same time using a motorized XY stage and z-drive, thereby photographing the entire CHT in an automated fashion, using a Yokogawa spinning disk and a Nikon Eclipse Ti inverted microscope. Z-stacks images were collected for multiple channels, including green (i.e., GFP signal) and red (i.e., mCherry signal) and Differential Interference Contrast (DIC), with a temperature-controlled stage set to 28.5°C throughout imaging. Images were taken with the 10X and 20X objectives. For comparison between different images, the settings for image acquisition and post-acquisition processing (e.g., exposure time, magnification) were kept constant.

2.8 RNA-sequencing Analysis

2.8.1 FACS Analysis of Zebrafish Embryos

Transgenic *mrc1a 125 bp:GFP* were out-crossed to *flk:mCherry* adults and the offspring was raised to 4 dpf, 7 dpf and 14 dpf, as described above in section 2.1. Between 2 and 3 dpf, embryos were screened for GFP and mCherry expression, and only double positive embryos were selected for subsequent FACS analysis.

For each developmental stage, between 50 and 70 double positive embryos were selected. At the appropriate stage, these embryos were pooled together in a Petri dish, and euthanized by tricaine overdose. After removal of E3 medium, they were thoroughly minced in the plate lid using a blade. Chopped embryos were collected in 1 mL solution of 1X PBS, and enzymatically digested with 1:65 liberase (Roche, Sigma-Aldrich, St. Louis, MO, USA; stock solution at a concentration of 2.5 mg/mL collagenase). Embryonic homogenate was filtered through a 40 µm cell strainer cap into a 5 mL polystyrene round-bottom tube to ensure a single cell suspension, which was subsequently centrifuged for 4 minutes at 800 rpm. Immediately thereafter, the supernatant was discarded and the pellet was resuspended in 800 µL - 1mL 1X PBS with 2% fetal bovine serum (FBS). The cell suspension was again filtered through 40 µm cell strainer caps into 5 mL polystyrene round-bottom tubes, and subsequently processed by FACS using a BD Biosystems Aria 2 FACS machine (BD Biosciences, Billerica, MA, USA).

Sytox blue was used as a marker to exclude dead cells and debris and gates were set with reference to non-fluorescent controls. Cells were fractioned into different populations in terms of their relative fluorescence: tail fibroblasts (mCherry-, GFP+), non-CHT ECs (mCherry+, GFP-), CHT niche ECs (mCherry+, GFP +), and transgene negative rest of the embryo (mCherry-, GFP-). After FACS, cells were spun down for 10 minutes at 2,000 rpm. For each sample, liquid was removed from the top of the supernatant to leave approximately 200 uL liquid left, and 600 uL Trizol LS reagent was then added to each tube to make an approximate final volume of 800 uL. After briefly vortexing, samples were stored at − 80°C until RNA isolation was performed. FACS data were visualized using FlowJo software, version 10 (FlowJo, LLC, Ashland, OR, USA). Only viable cells, gated from the dead cells and debris, were counted (**Appendix A: Supplementary Information**; **SI.2. FACS Analysis of Whole Zebrafish Embryos**).

2.8.2 RNA Extraction

Total RNA from the FACS-isolated cells was extracted using Trizol and GenElute LPA (Linear Polyacrylamide) carrier. First, samples were thawed and equilibrated at room temperature for approximately 10 minutes. Next, 160 μL pure chloroform were added to each tube. Samples were then vortexed for 30 seconds and incubated for 2 minutes at room temperature. After incubation, samples were centrifuged at 12,000 x g for 15 minutes at 4ºC. For each sample, the upper aqueous phase, containing the RNA, was carefully transferred to a new collection tube. Immediately thereafter, 1 μL GenElute LPA (stock solution at a concentration of 25 mg/mL) was added to each sample to aid RNA precipitation. After vortexing, 160 μL isopropanol were added to each tube and samples were incubated for 10 minutes at room temperature. Thereafter, samples were centrifuged at 12,000 x g for 10 minutes at 4ºC. Following centrifugation, supernatant was carefully removed from each sample, thus leaving the pellet – visible as a tiny flake – untouched. Then, 1 mL ice cold 75% ethanol diluted in diethylpyrocarbonate (DEPC)-treated water was added to wash each sample. This wash was repeated two more times and after each time, samples were centrifuged at 7,500 x g for 10 minutes at 4ºC. Following the last wash, residual ethanol was removed as much as possible, carefully with the aid of a 200 μL pipette. Next, the pellet was air-dried for 2-5 minutes and subsequently resuspended in 5.5 μL RNAase-free water. Concentration of RNA samples, as well as RNA integrity number (RIN) were determined using the Fragment Analyzer. Concentration values ranged from 0.41 ng/uL to 36.24 ng/uL and the average RIN was 7. RNA samples were stored at − 80°C until cDNA synthesis was performed.

2.8.3 cDNA Synthesis and cDNA Library Preparation

cDNA libraries were prepared using the SMART-Seq v4 Ultra Low Input RNA Kit for Sequencing (Takara Bio Inc., Kusatsu, Japan) and Nextera XT DNA Library Preparation Kit (Illumina, San Diego, CA, USA) according to manufacturer's specifications. Briefly, RNA samples were first thawed on ice. From each sample, 3.9 ng total RNA were used for the cDNA synthesis reaction. After cDNA synthesis, cDNA was amplified through PCR, following the cycling conditions listed in **Table 10**.

Table 10: Thermocycler conditions for cDNA synthesis (n/a, not applicable).

Step	Temperature [°C]	Time [sec]	Cycles
1	95	60	n/a
2	98	20	
3	65	30	10 x
4	68	360	
5	72	1200	n/a
6	4	∞	

Purification of amplified cDNA was subsequently performed using the Agencourt AMPure XP Kit (Beckman Coulter, Inc., Brea, CA, USA) according to manufacturer's instructions. For each sample, cDNA was finally eluted with 10 uL elution buffer. We then used the Fragment Analyzer for qualification of cDNA by smear analysis. After confirming good cDNA quality, we quantified cDNA concentrations using a fluorometric Qubit RNA HS assay. From each cDNA sample, we used 1 ng input cDNA for the library preparation. The index tags were later added by dual-indexing PCR amplification, following the cycling conditions listed in **Table 11**.

Table 11: Thermocycler conditions for PCR amplification of cDNA (n/a, not applicable).

Step	Temperature [°C]	Time [sec]	Cycles
1	72	360	n/a
2	95	30	
2	95	10	
3	55	30	12 x
4	72	30	
5	72	600	n/a
6	10	∞	

Next, PCR clean-up was performed using again the Agencourt AMPure XP Kit according to manufacturer's specifications. PCR products were resuspended with 20 uL resuspension buffer. cDNA concentrations were then quantified using a fluorometric Qubit RNA HS assay Invitrogen™; Thermo Fisher Scientific, Waltham, MA, USA., while cDNA quality was determined using the Fragment Analyzer (**Appendix A: Supplementary Information**; **SI.3. Evaluating Quality of a Prepared cDNA Library)**. Finally, we pooled the libraries to equalize index concentration before sequencing. The final volume and concentration of the pooled sample were 34.5 µL and 2 nM, respectively.

2.8.4 Mapping and Quantification

Library sequencing was performed at the Boston Children's Hospital HHMI NGS sequencing core, using an Illumina Hiseq 2500 (Illumina, San Diego, CA, USA). FastQC and Cutadapt were next used to examine the quality of the library and trim off the remaining adapter sequences, respectively. Reads were mapped to the zebrafish genome using Bowtie. Only the samples of CHT niche ECs (mCherry+, GFP +) were subjected to a genome-wide differential analysis.

2.9 Image and Statistical Analyses

Image processing was done using different software, such as NIS-elements (Nikon, Tokyo, Japan), Imaris (Bitplane, Belfast, Ireland) and Adobe Photoshop CS6 (Adobe Systems, San Jose, CA, USA). In order to study the CHT differences in terms of plexus morphology, the AngioTool software, a specialized package in Fiji, was used for vessel network analysis. Initally, the original Z-stack images (obtained by SDCM, as explained above in section 2.7)

were converted into 8-bit color and then analyzed using the AngioTool software. However, the images as such proved to be an inadequate input for the software, since the dimmest vessels could not be detected even after enhancing the image contrast, making it difficult for the CHT plexus topology parameters to be analyzed. Therefore, images were processed using Adobe Photoshop, where an additional layer was created in which the vessel structures were manually retraced with red color. Below, a black background layer was created. The posterior caudal vein (PCV) was excluded from this analysis. The obtained red and black images were converted into 8-bit color and analyzed with the AngioTool software software in order to measure the total number of branch points, the vessel length (µm) and the total number of endpoints within the CHT plexus (**Figure 14**). AngioTool values were analyzed using Microsoft Excel (Microsoft Corp., Redmond, WA, USA). The average value of each parameter and the standard error of the mean (SEM) were calculated for each developmental stage (n=10-15 embryos). As a part of an unbiased approach, analyzed embryos were randomly chosen from three different clutches.
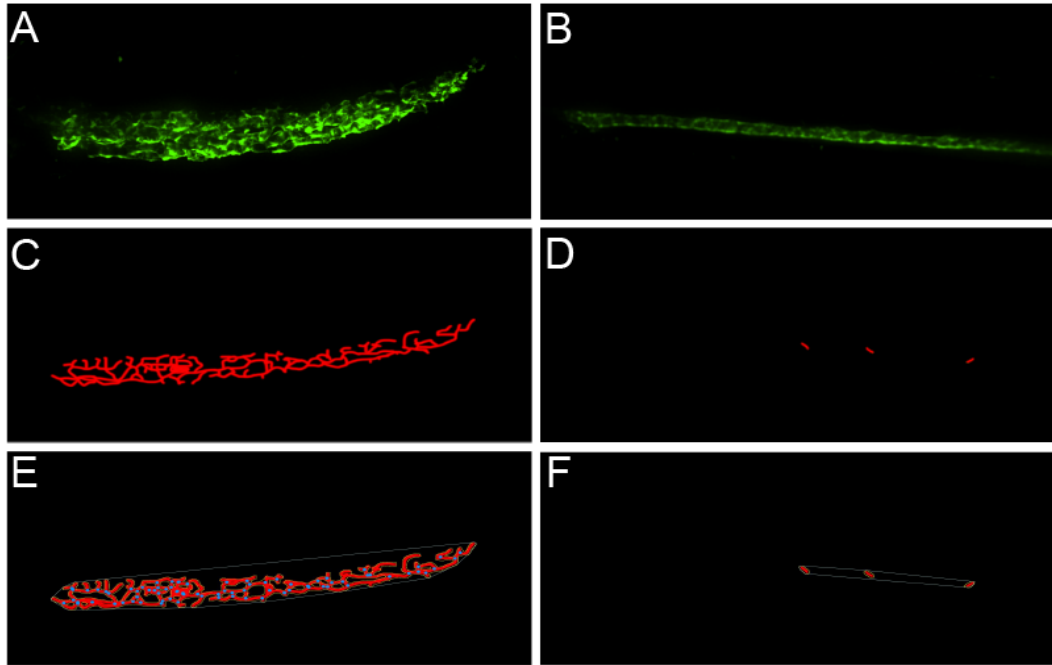
Figure 14. Analysis of the CHT plexus topology parameters using the Angiotool Software. Given the fact that the Angiotool software underestimated the network topology parameters to be analyzed using the 8-bit color Z-stack images (**A** and **B**), new input images were created on Adobe Photoshop. Using this last software, an additional layer was created in which the vessel structures were manually retraced with red color. Below, a black background layer was created. These red and black images served as an input for the Angiotool Software (**C** and **D**). After the Angiotool analysis, the output images displayed the outline of the vasculature shown in yellow, the vessels in red and the junctions in blue (**E** and **F**). Exemplary images are here shown. The left images are the sequential images employed in the quantification procedure of the CHT vascular plexus at 2 dpf, whereas the right images were used to quantify the topology parameters of the CHT plexus at 14 dpf.

Furthermore, both the maximum height and width of the intervascular structures, observed within the CHT plexus at early stages, were measured in µm using the Imaris software. For simplification purposes, given the irregular shape of these structures, a 2D sagittal section was analyzed. On an embryo basis, twenty spaces were inspected and the average values were then calculated. In total, five embryos were examined per developmental stage (n=5 both at 2 and 3 dpf). The mean of the average values and the SEM for both properties – maximum height and width – were calculated.

Additionally, to quantify HSPCs within the CHT region, *runx1:mCherry* positive cells were counted. The *runx1* marker was chosen for these experiments based on previous work in our laboratory, where it was estimated that the stem cell frequency of the *runx1* positive

population in the 3 dpf-embryo is approximately 1/2.88 cells [22]. Circulating *runx1* positive cells, as well as cells within the lumen of the PCV were excluded from this quantification. The average number of HSPCs and the SEM were calculated for each developmental stage (n= 8-10), using Microsoft Excel. As with the CHT vessel network analysis, photographed embryos were randomly chosen from three different clutches. For these analyses, data are presented as the mean ± SEM in the graphs.

Regarding statistical analyses, Chi-square non-parametric tests were used to test for the significance of the WISH scoring data and the percentages of ectopic niche endothelial gene expression between the different groups. Specifically, a pairwise comparison was performed between negative control and TF gene-injected embryos and also between two groups of embryos injected with different DNA mixes. The outcomes of the WISH analysis, performed after the blood flow experiments, were also compared using a Chi-square non-parametric test. On the other hand, in the mutant enhancer experiments and in the analysis of the CHT intervascular structures, comparison between the two groups ("WT *versus* mutant" in the former and "2 dpf *versus* 3 dpf" in the latter) was performed using unpaired Student's t-tests. For all the analyses, p values < 0.05 were considered to be statistically significant. The software package GraphPad Prism version 7 (GraphPad Software, San Diego, California) and Microsoft Excel were used to carry out these analyses and make the graphs. In the graphs, p values are denoted by asterisks: ∗∗ p<.01, ∗∗∗ p<.001 and ∗∗∗∗ p<.0001. All images were prepared for figures using Adobe Photoshop CS6 and Adobe Illustrator CC 2018 (Adobe Systems, San Jose, CA, USA).

3 Results

3.1 Disruption of the Ets, Sox and NH Receptor Motifs is Specific for Expression of Niche Endothelial Genes

As previously outlined, before I joined the group, sequence variants for the *sele 158 bp* and *mrc1a 125 bp* regions (enhancer sequences of the *sele* and *mrc1a* genes, respectively) were generated and fused to a minimal beta-globin promoter and GFP. These sequence variants contained mutations targeting Ets, Sox and NH receptor TF binding sites and the objective was to determine whether these sites were required for transgenic expression of GFP. A significant reduction or complete loss of GFP expression was observed upon injection of these constructs into one cell-stage zebrafish embryos compared to control experiments using the full WT sequence for each enhancer (data not shown). These results supported the hypothesis that a transcriptional code, involving members of the Ets, Sox and NH receptor families, is required for the expression of the CHT-specific endothelial genes.

To confirm whether the loss of GFP expression was due to the disruption of the specific TF motifs as opposed to a non-specific effect of disrupting the sequence *per se*, we generated additional sequence variants in which mutations were targeted to intervening sequences between the Ets, Sox and NH receptor motifs. These sequences were also fused to a beta-globin promoter and GFP and then injected into one cell-stage zebrafish embryos to see whether mutations elsewhere in the *sele 158 bp* and *mrc1a 125 bp* regions would lead to loss or reduction of GFP expression as it was observed with the mutations targeting the Ets, Sox and NH receptor motifs. As controls for these experiments, we re-injected the full WT sequences for these constructs where no mutations were introduced. Analysis of the injected embryos revealed that GFP expression was maintained in the mutant constructs targeting the intervening regions. On average, for the *sele* gene, 46,0% of the embryos injected with the mutant construct showed GFP positive CHT ECs, while 48,1% of those injected with the WT enhancer construct had GFP positive ECs in the CHT. On the other hand, for the *mrc1a* gene, 63,8% of the embryos injected with the mutant construct presented GFP positive CHT ECs, while 67,8% of the embryos injected with the WT enhancer construct showed GFP positive ECs in the CHT. In both cases, expression levels in the mutant constructs were not significantly different from the WT enhancer control constructs (**Figure 15** and **Figure 16**). Thus, these experiments suggested that the effects of the mutations targeting the Ets, Sox and NH receptor motifs are indeed specific, and not the result of indirect effects from simply modifying the original enhancer sequences.
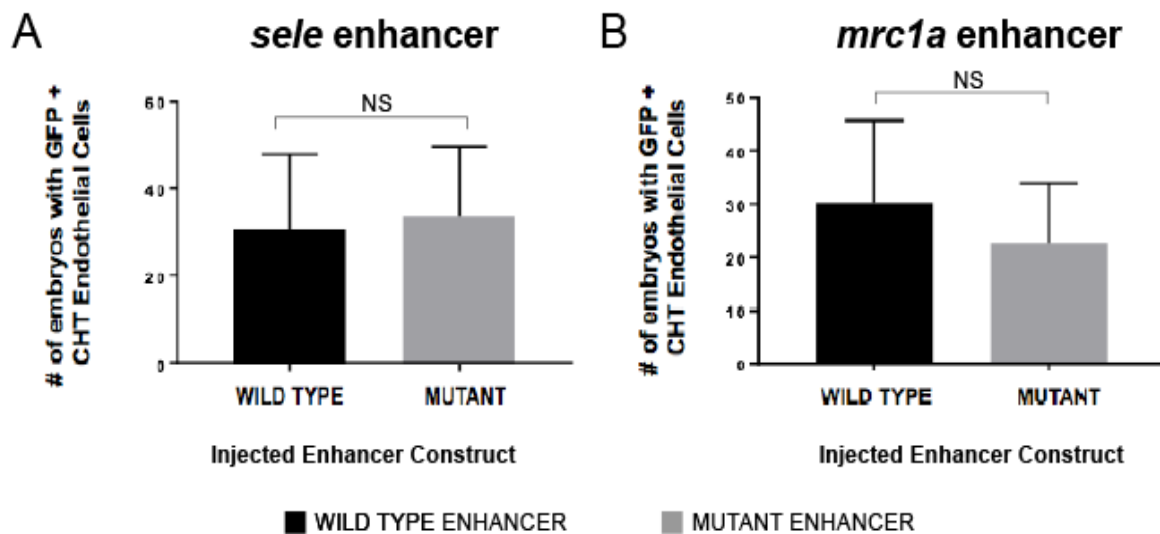
Figure 15. Injection of wild type and mutant enhancers for both *sele and mrc1a* genes. GFP expression was retained in the embryos injected with the mutant constructs where mutations were targeted to intervening sequences between the Ets, Sox and NH motifs. Expression was not significantly different from their control counterparts, injected with the full WT construct for the enhancer sequences of both (**A**) *sele* and (**B**) *mrc1a* genes. For each gene, comparison between the two groups (WT *versus* mutant) was performed using an unpaired Student's t-test. All data are presented as average values ± SEM (for *sele*, n= 5-7 clutches analyzed per injected construct, with 65.6 embryos on average, per clutch; and for *mrc1a*, n= 4 clutches analyzed per injected construct, with 40.3 embryos on average, per clutch) (NS, Not Significant).
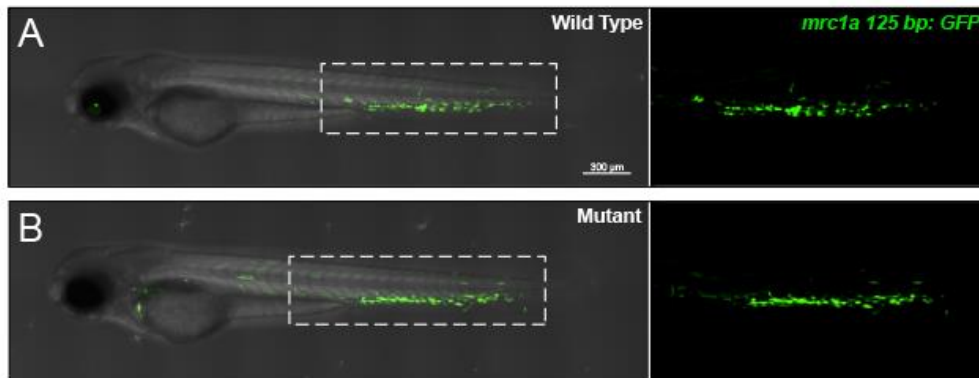
Figure 16. Expression of *125 bp mrc1a:GFP* transgenics injected with synthetic enhancer constructs. GFP expression is retained in embryos injected with the mutant enhancer constructs where mutations were targeted to intervening sequences between the Ets, Sox and NH motifs. Exemplary images of **(A)** an embryo injected with the full WT *mrc1a* enhancer construct and **(B)** its sibling injected with the mutant construct. The dashed white boxes outline the CHT region. Scale bar: 300 μm.

3.2 Transcription Factor Overexpression Induces Ectopic Niche Endothelial Gene Expression in Zebrafish Embryos

Before my arrival, the group had performed a genome-wide motif enrichment analysis of the regions of chromatin that were uniquely open in the CHT ECs. This analysis showed that the Ets, Sox and NH receptor binding motifs were most enriched in these regions. RNA-seq was then used to profile sorted CHT ECs, and it was determined that the following seven factors were the mostly highly expressed members of the Ets, Sox and NH receptor families: *fli1a*, *etv2* and *ets1* from the Ets family; *sox18* and *sox7* from the Sox family; and *nr2f2* and *rxraa* from the NH receptor family (data not shown). Given these results, we hypothesized that overexpression of a combination of these TFs in zebrafish embryos could lead to ectopic expression of niche endothelial genes outside the CHT. To this end, we injected DNA constructs in which each of the genes encoding the aforementioned TFs was under the control of a ubiquitous (*ubi*) promoter. In initial experiments, a combination of all seven TF genes (i.e., (*FLI1A*, *ETV2*, *ETS1*, *sox18*, *SOX7*, *nr2f2* and *RXRAA)* was injected into one cell-stage embryos at a total DNA concentration of 25 ng/μL plus 25 ng/μL Tol2 mRNA. Embryos were fixed at 60 hpf and analyzed by WISH for expression of *mrc1a*. Surprisingly, 21% of TF gene-injected embryos (12/57), presented what appeared to be vessels

expressing CHT endothelial genes outside the CHT (**Figure 17**), whereas control embryos, which were either injected with an empty Gateway destination vector or uninjected, did not show significant ectopic expression (23/1072) (p<.0001).
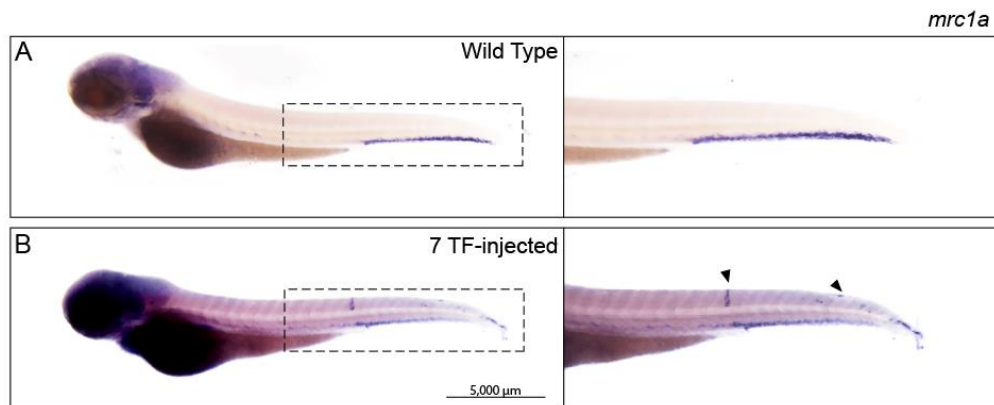
Figure 17. Overexpression of genes encoding for transcription factors from the Ets, Sox and NH receptor families results in the induction of ectopic sites of niche endothelial gene expression in zebrafish embryos. WISH for the *mrc1a* gene of **(A)** a control embryo, showing WT CHT expression, and of **(B)** an embryo injected with the seven-TF gene pool, presenting ectopic expression outside the CHT (black arrowheads). The dashed black boxes outline the region of the tail where the CHT is found. Embryos shown here were fixed at 60 hpf. Scale bar: 5,000 µm.

In order to confirm whether these ectopic regions were in fact ECs, we crossed the *mrc1a:GFP* line to the pan-endothelial marker *flk:mCherry*, and then injected the same combination of the seven TF gene constructs. Injected embryos were screened for GFP and mCherry, and subsequently analyzed at higher magnification using SDCM. Imaging at higher resolution confirmed the endothelial identity of the observed ectopic sites, as these were positive for both GFP and mCherry (**Figure 18**). Furthermore, using DIC microscopy, we determined that the ectopic vessels were connected to circulation and carried blood flow (data not shown).
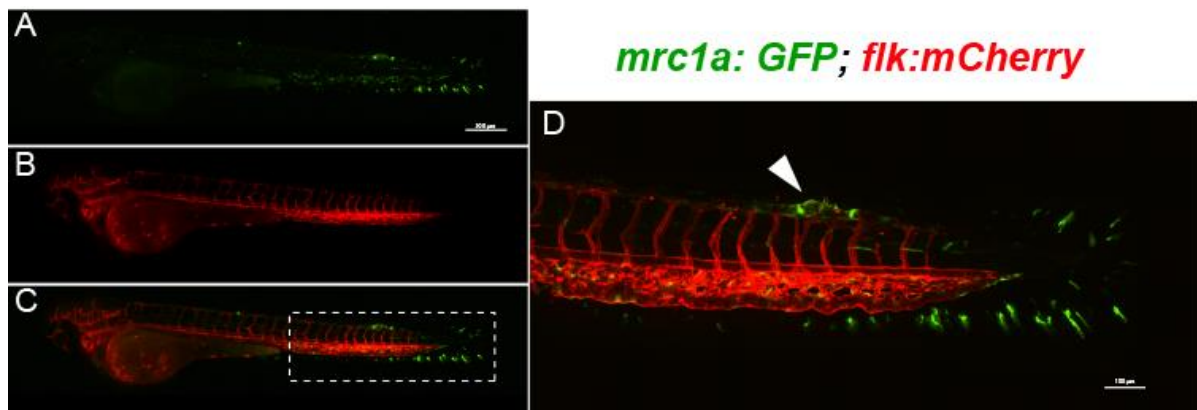
Figure 18. The regions of ectopic endothelial gene expression are composed of blood vessels. *mrc1a 125 bp:GFP; flk:mCherry* transgenic embryo photographed at 72 hpf, showing ectopic *mrc1a* expression in a dorsal region of the tail. **(A)** GFP image. **(B)** mCherry image. **(C)** GFP/mCherry overlay. Dashed white box outlines the region magnified in D. **(D)** The ectopic site, indicated by a white arrowhead, is positive for both GFP and mCherry. Scale bars: 300 μm (A-C) and 100 μm (D).

Through review of the available literature, we found that previous reports have shown that ETV2 is an ETS transcription factor that is able to convert non-endothelial cells to ECs [127], [128]. On the other hand, the Sox factors SOX7 and SOX8 play redundant roles in vascular development, where they are required for arterial specification and regulation of nr2f2 expression in venous ECs [129], [130]. Moreover, SOX7, expressed in cells from the hemogenic endothelium, has also been reported to specify the identity of such cells, thus being closely related to the emergence of HSPCs [131]. Last but not least, Nr2f2 is known to promote venous EC identity [132]. In light of these findings, we hypothesized that a combination of *ETV2*, *SOX7* and *Nr2f2*, each one representing a member from the Ets, Sox and NH receptor families, respectively, might be sufficient to induce ectopic niche endothelial gene expression. To test this hypothesis, we narrowed down the DNA construct-cocktail to the combination of these three TF genes (i.e., *ETV2*, *SOX7* and *Nr2f2*) into one cell-stage embryos. Remarkably, we observed that this combination (subsequently referred to as *ETV2* mix) resulted in significant ectopic *mrc1a* expression similar to what was observed with the seven-TF gene combination, as assessed by GFP expression in *mrc1a:GFP* transgenic embryos (**Figure 19**), or by WISH for the endogenous *mrc1a* transcript. A large number of embryos were injected and screened for ectopic *versus* normal expression of *mrc1a*. In total, 60% (384/639) of the embryos injected with the three-TF gene pool showed ectopic *mrc1a* expression (**Figure 20** and **Figure 21**), whereas control embryos did not have significant ectopic expression (25/1079) (p<.0001) (**Figure 21**).
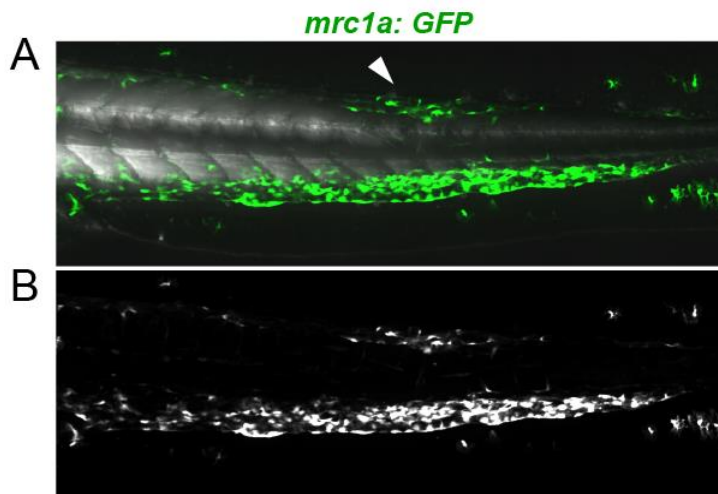
Figure 19. Injection of the *ETV2* mix into *mrc1a:GFP* transgenic embryos is sufficient to induce ectopic expression of *mrc1a* (A) GFP image. The white arrowhead indicates the ectopic *mrc1a:GFP* site. **(B)** Grayscale image of A. Embryo photographed at 72 hpf.

In order to determine the importance of the individual TFs contained in the injection mix, we injected each TF gene (i.e., *ETV2*, *SOX7* and *Nr2f2*) on its own into one cell-stage embryos. We then performed WISH for *mrc1a* and screened for ectopic expression. Embryos injected with *Nr2f2* and *SOX7* alone constructs did not show significant ectopic expression (6/214, and 9/261 respectively). Remarkably, overexpression of *ETV2* alone induced ectopic expression in 48% of the injected embryos (126/265), a significant number compared to control embryos (p<.0001) (**Figure 20** and **Figure 21**).

Next, to test whether an Ets factor other than ETV2 could similarly induce ectopic expression as a part of the three-TF gene combination, we overexpressed *SOX7*, *Nr2f2* and *ETS1* (in lieu of *ETV2*). Thereafter, we performed WISH for *mrc1a* and found that 17% of the embryos injected with this TF gene combination (subsequently referred to as *ETS1* mix) gave significant ectopic *mrc1a* expression (52/309) (p<.0001), albeit at a significantly lower frequency than the *ETV2* mix (p<.0001) (**Figure 20** and **Figure 21**). To further compare the two Ets factors, ETV2 and ETS1, we examined the individual contribution of ETS1 by injecting the DNA construct of this TF alone. Subsequent WISH for *mrc1a* revealed that only insignificant numbers of embryos presented ectopic expression (2/140) (**Figure 21**).

Collectively, these experiments suggest that the combination of three TFs, one each from the Ets, Sox and NH receptor families, can function in a synergistic fashion to induce niche endothelial gene expression, and that among these three factors, ETV2 is the most potent niche endothelial inducer.
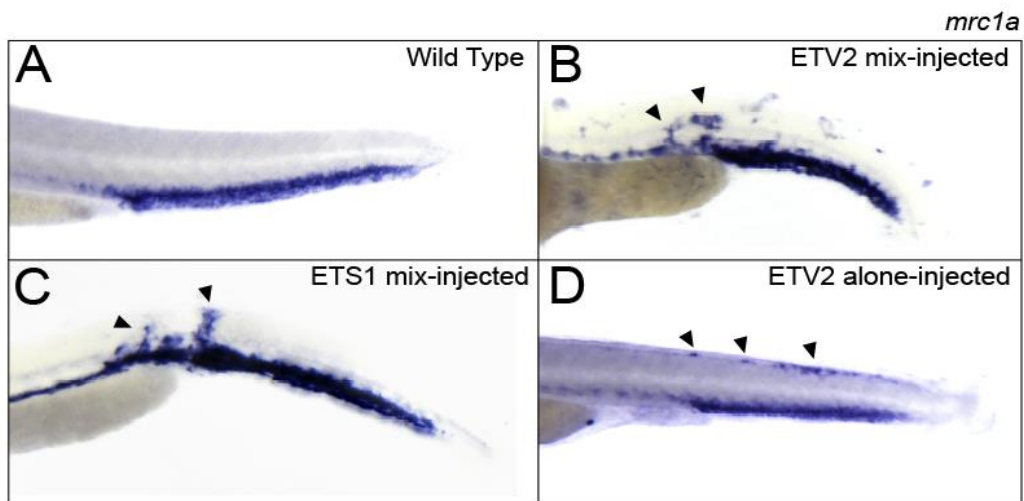
Figure 20. Injections of the three-transcription factor gene combinations and *ETV2* alone result in significant ectopic expression of *mrc1a* compared to control embryos. Close-up images of the tails of **(A)** a negative control embryo, **(B)** an *ETV2* mix-injected embryo, **(C)** an *ETS1* mix-injected embryo, and **(D)** an *ETV2* alone-injected embryo. Black arrowheads indicate ectopic *mrc1a* expression. Embryos shown here were fixed at 60 hpf.
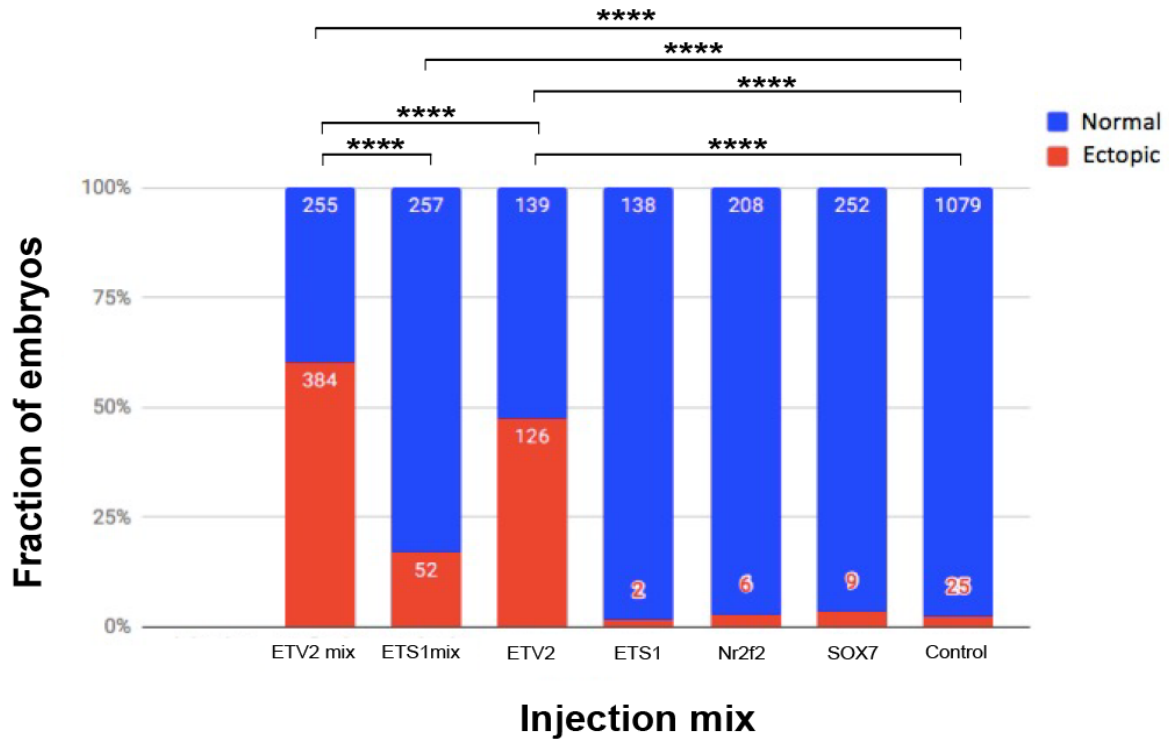
Figure 21. Injection of niche endothelial transcription factors induces ectopic expression of *mrc1a* outside the CHT. The injection of the *ETV2* mix resulted in the induction of ectopic endothelial gene expression in 384/639 injected embryos (60%). The injection of the *ETS1* mix led to formation of ectopic endothelial regions in 52/309 injected embryos (16.8%). The injection of *ETV2* alone led to ectopic endothelial gene expression in 126/265 injected embryos (48%). The uninjected or Gateway destination vector-injected counterparts served as a negative control. Only 25/1,104 (2.26%) of control embryos had expression of *mrc1a* outside the CHT. Embryos injected with both three-TF gene combinations were significantly different from control embryos (p<.0001). Overexpression of *ETV2* alone also led to significant ectopic expression (p<.0001), but significantly less than the ETV2 mix (p<.0001). In contrast, injections of *ETS1*, *Nr2f2* or *SOX7* alone did not induce significant ectopic *mrc1a* expression. A Chi-square non-parametric test was performed for pairwise comparison between two different injection mixes (e., g, *ETV2* mix *versus ETV2* alone) as well as for pairwise comparison between the TF-injected and control embryos. Not significant comparisons are not indicated in this graph.

3.3 Injection of the ETV2 Alone Construct Can Induce Ectopic Expression of other Niche Endothelial Transcription Factors

Considering that the *ETV2* alone construct also induced ectopic expression of CHT endothelial genes, we sought to find out if ETV2 on its own was capable of triggering ectopic expression of genes encoding the other TFs that we had implicated in CHT EC specification. To that end, we re-injected the *ETV2* alone construct and then performed WISH at 24 hpf for the endogenous transcripts of some zebrafish TF genes, including *sox7*, *sox18*, *fli1a*, *ets1* and *nr2f2*.

WISH for *nr2f2* showed that this gene is robustly and widely expressed outside the CHT, especially in areas associated with the notochord, the spinal cord and the head. Since it was difficult to distinguish endothelial from neural expression, this probe was not considered optimal for this experiment. WISH for *ets1* also showed that this gene is broadly expressed, particularly in dorsal areas of the tail, which made it difficult to identify whether ectopic endothelial expression of this factor was induced (**Appendix A: Supplementary Information**; **SI.4. Whole-mount in situ hybridization analysis for *ets1* and *nr2f2*)**. On the contrary, WISH analysis for *sox7*, *sox18* and *fli1a* showed that these genes are strongly expressed in the CHT and that injection of the *ETV2* alone construct is sufficient to induce their expression elsewhere (**Figure 22**). These results suggested that activation of *ETV2* alone induces aspects of the niche endothelial program due to the ability of ETV2 to transactivate other TFs involved in the transcriptional code governing the genetic identity of CHT ECs. In addition, we also performed WISH for *etv2.* Strikingly, we found that overexpression of the human TF gene results in the induction of sites of ectopic expression of the zebrafish *etv2* gene as well, suggesting that ETV2 activates its own gene expression (**Figure 22**).
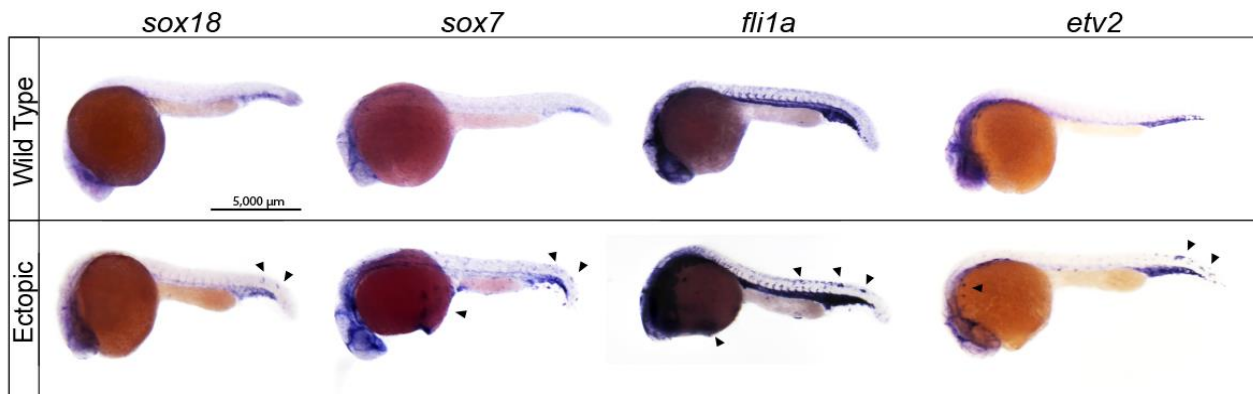
Figure 22. Injection of the *ETV2* alone construct is sufficient to induce ectopic expression of genes encoding other niche endothelial transcription factors and *etv2* itself. Upper images correspond to WT embryos, whereas lower images show embryos with ectopic expression of *sox18*, *sox7*, *fli1a* and *etv2* (from left to right). Ectopic expression is indicated by black arrowheads. Scale bars: 5,000 μm.

3.4 HSPCs Localize to Regions of Ectopic Niche Endothelial Gene Expression

To ascertain if a wider CHT endothelial genetic program was being induced within the ectopic regions of *mrc1a* expression, we performed WISH for additional CHT endothelial genes. Interestingly, ectopic expression of *sele*, *gpr182* and *legumain* (*lgmn*) was also detected in embryos injected with the *ETV2* mix, unlike control embryos where ectopic expression was insignificant (**Figure 23**). The fact that various niche endothelial genes were ectopically expressed after injection of the *ETV2* mix brought to our mind that the generated ectopic locations might be functionally similar to the endogenous CHT niche.
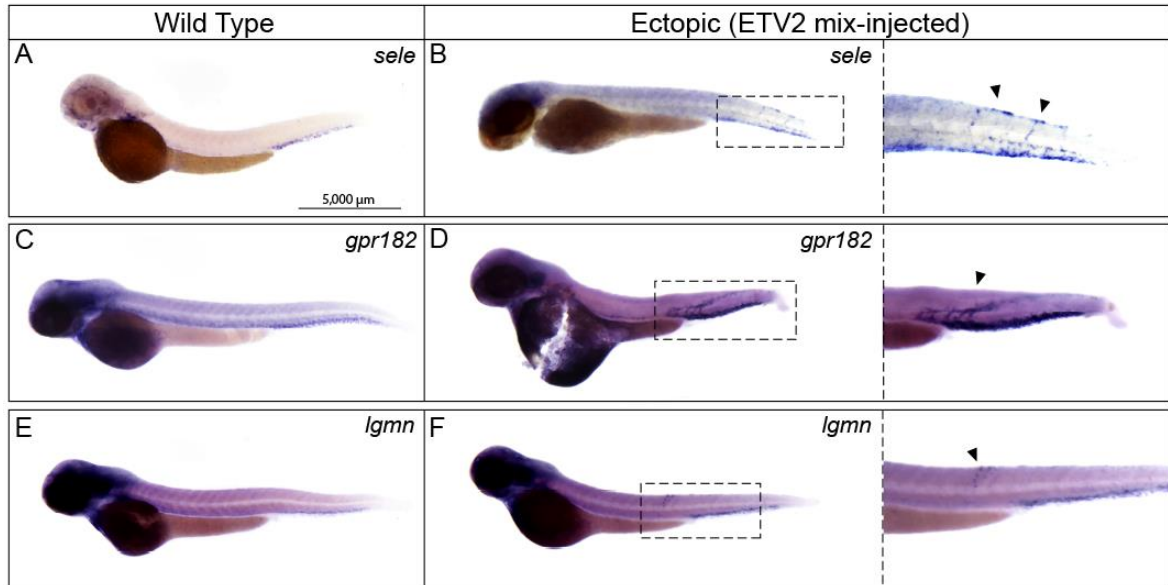
Figure 23. Transcription factor overexpression leads to ectopic expression of several niche endothelial genes other than *mrc1a*. (**A** and **B**) WISH for *sele*. (**C** and **D**) WISH for *gpr182*. (**E** and **F**) WISH for *lgmn*. A, C and E are images of WT embryos, whereas B, D and F show embryos with ectopic expression of the aforementioned genes after TF overexpression. Close-up images of B, D and F are also included. Dashed black boxes outline regions that are magnified, and black arrowheads indicate ectopic expression. Embryos shown here were fixed at 60 hpf. Scale bar: 5,000 μm.

To assess the functionality of the ectopic regions, we examined whether HSPCs were able to localize to these sites and interact therein with ectopic ECs, thereby mimicking the natural interactions occurring in the CHT niche. To that end, we injected the *ETV2* mix into *mrc1a:GFP;runx1:mCherry* transgenic embryos. Subsequently, we examined the localization of *runx1:mCherry* positive HSPCs. Strikingly, HSPCs were able to localize to regions of ectopic *mrc1a:GFP* expression. While 12/22 embryos having ectopic vascular regions of *mrc1a:GFP* presented HSPCs localizing to the ectopic regions (**Figure 24**), 27/27 control embryos did not show ectopically localized HSPCs. Furthermore, ECs were observed to behave similarly to those residing in the CHT niche, since upon arrival of HSPCs, groups of surrounding ECs were seen to remodel around single HSPCs, thus resembling the typical behaviour that ECs show when HSPCs lodge in the endogenous CHT niche (data not shown). In this way, HSPCs and ECs were found closely associated in both intraluminal and extravascular spaces within the ectopic regions (**Figure 25**). Moreover, we analyzed HSPC behavior using time-lapse microscopy to determine whether HSPCs associated with the ectopic locations were stimulated to divide. Remarkably, we could visualize dividing HSPCs

in these locations (data not shown). These findings suggested that the ectopic regions of CHT-like ECs can recruit HSPCs and sustain their division, akin to behaviors characterizing resident ECs in the CHT niche.
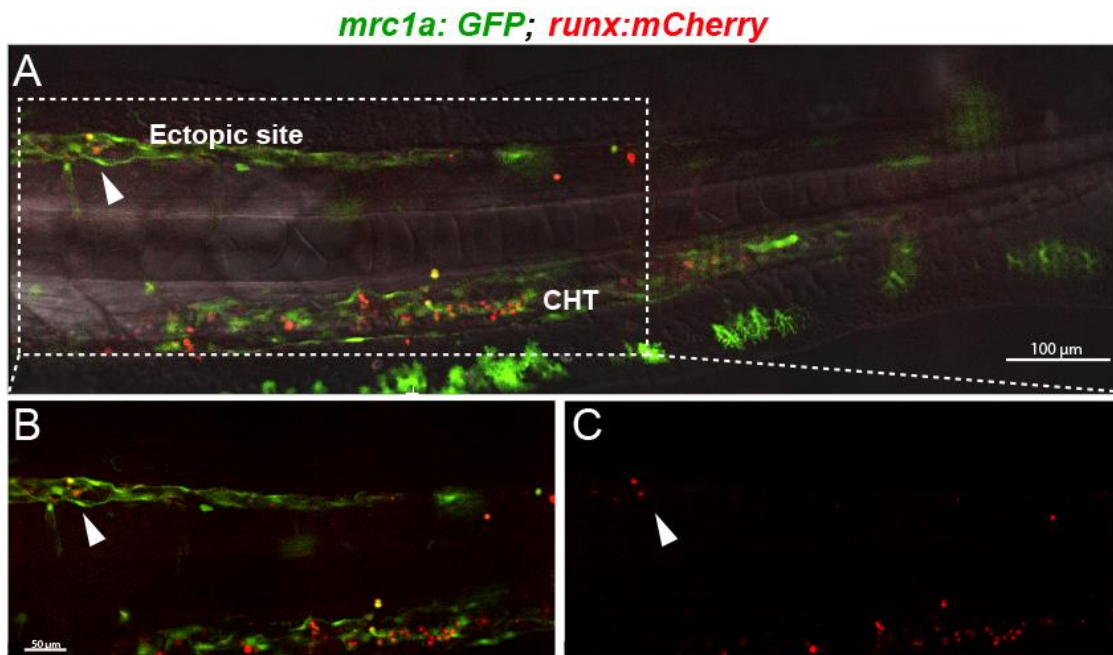
Figure 24. *runx1*:*mCherry* positive hematopoietic stem and progenitor cells are recruited to sites of ectopic *mrc1a* expression. (A) Injection of *ETV2* mix resulted in the induction of ectopic *mrc1a* expression (GFP) in a dorsal region of the tail, where HSPCs (mCherry) were observed to localize. GFP/mCherry/DIC overlay. **(B)** GFP/mCherry overlay. **(C)** mCherry image. White arrowheads indicate HSPCs. The dashed white box in A outlines the region that is magnified in B and C. Scale bars: 100 μm (A) and 50 μm (B and C).

We next examined embryos using the *runx1* probe. This confirmed our initial observations made by SDCM, since WISH for *runx1* similarly demonstrated that embryos injected with the three-factor combination had ectopic HSPC localization (**Figure 26**). Taken together, these results indicated that the observed ectopic sites function in a similar way to the endogenous CHT niche.

mrc1a: GFP; runx:mCherry
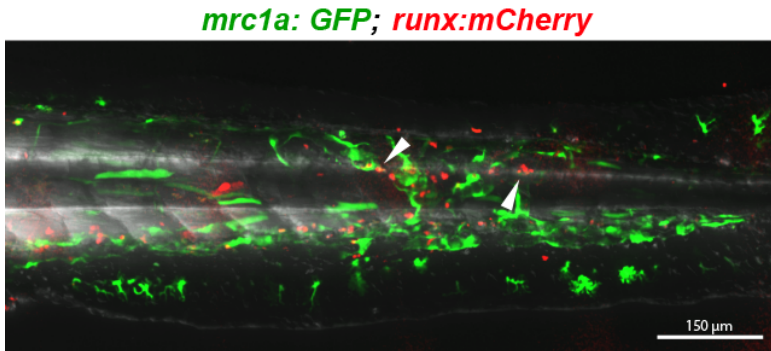
Figure 25. *Runx1* positive hematopoietic and progenitor cells are found within intraluminal and extravascular spaces in ectopic regions. HSPCs (*runx1*: mCherry) localize to ectopic regions, where they are directly associated with the ectopic *mrc1a*: GFP positive ECs. White arrowheads indicate HSPCs inside and out the blood vessels (GFP positive). Scale bar: 150 μm.
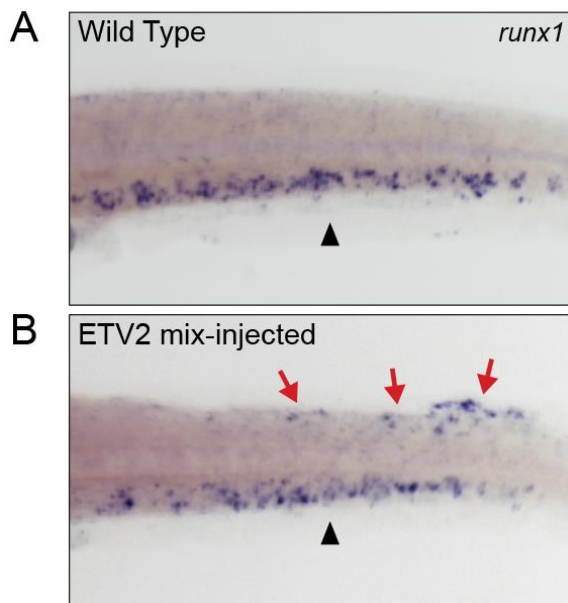
Figure 26. Whole-mount in situ hybridization for the *runx1* transcript confirms that hematopoietic and progenitor cells localize to ectopic regions outside the caudal hematopoietic tissue niche. (A) WT embryo. **(B)** Embryo injected with the *ETV2*-mix showing ectopic localization of *runx1* positive HSPCs. Black arrowheads indicate the CHT region, whereas red arrows mark ectopic *runx1* positive HSPCs.

3.5 Blood Flow is Required for Expression of Niche Endothelial Genes

After we elucidated the existence of a transcriptional code governing the genetic identity of the CHT EC population, we sought to shed light to the extrinsic cues that regulate the intrinsic gene program within these cells. Preliminary data in our laboratory showed that blockage of blood flow by injecting a morpholino designed against the cardiac troponin T (*tnnt2*; *silent heart* morpholino) transcript (3 ng) into zebrafish zygotes led to loss of expression of *gpr182*, one of the genes that is highly expressed by CHT ECs (**Figure 27**). Along with other experiments, in which it was observed that expression of other genes such as *sele* and *sox7* was also downregulated in the absence of blood flow (data not shown), this result suggested that expression of some niche-specific endothelial genes might be regulated by blood flow.
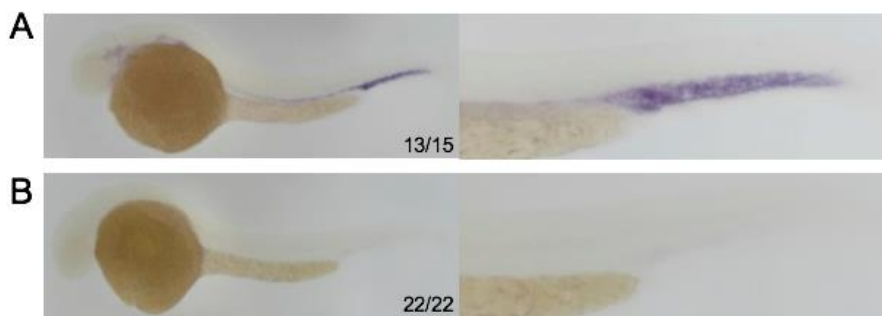
Figure 27. Blockage of blood flow causes loss of expression of *grp182*. (A) In WT embryos, *gpr182* is selectively expressed in the CHT region. **(B)** Anti-tnnt2 morpholino-injected embryos lack blood flow and do not show expression of *grp182* in the CHT. *Courtesy of Shelby Redfield.*

We next hypothesized that expression of *gpr182* could be rescued in the absence of blood flow by the overexpression of *SOX7*, one of the genes that we had implicated in the transcription factor code specifying CHT ECs and that was also downregulated in the absence of blood flow. To that end, we cloned the ORF of the *SOX7* gene under the control of the heat shock (*hsp70l*) promoter and injected such a construct into one cell-stage embryos. We then studied whether overexpression of this gene could indeed rescue the expression of *gpr182* in those embryos treated with 25 µM pimozide, concentration at which this drug is known to block blood flow in zebrafish embryos, as observed in previous experiments carried out by other colleagues in our laboratory (data not shown). *hsp70l: SOX7* transgenic embryos were heat shock-induced to express *SOX7* at two different time points: 24 hpf and 36-48 hpf. Pimozide was dissolved in DMSO to a final concentration of

25 µM in 1% (v/v) DMSO. Embryos exposed to 1% (v/v) DMSO in E3 medium or in E3 medium alone served as a negative control. Additionally, uninjected heat-shocked embryos, also exposed to 25 µM pimozide, served as the heat-shocked control to verify that the heat shock treatment itself could not rescue the expression of *gpr182*.

Treated embryos were observed by visual inspection during the treatment period (18-48 hpf). Although a minimal electrical heart activity (i.e., myocardial contractions) was detected in roughly 15% of the embryos, blood flow stopped completely in all the treated embryos compared with the control groups (i.e., 1% (v/v) DMSO and E3 medium) (data not shown). After treatment, we performed WISH for *gpr182* and examined its expression in the CHT. The intensity of *gpr182* expression in the CHT was classified as follows: no staining, low-middle staining, and strong staining (WT expression) (**Figure 28**). This study led to the confirmation that blood flow indeed plays a pivotal role in the expression of the *gpr182* gene, since the percentage of embryos showing medium-low or not staining at all was significantly higher in those embryos treated with 25 µM pimozide than in control groups (p<.0001). Unexpectedly, in the groups of pimozide-treated embryos, significantly higher numbers of embryos injected with the *hsp70l: SOX7* construct presented either medium-low expression or absence of expression of *gpr182* than those that were not heat-shocked and kept as uninjected. However, no statistically significant differences were observed between the pimozide-treated *hsp70l: SOX7* transgenics and the heat-shocked uninjected control embryos, also treated with pimozide (**Table 12**, **Table 13** and **Figure 29**). These results suggested that the combination of the pimozide exposure and the heat shock treatment severely affected the health of the embryos. This thus hindered either the outcomes of the WISH technique or the embryos' gene expression. Of note, mortality rates were between 30% and 40% in those groups that were both treated with pimozide and heat-shocked, unlike negative control groups where mortality rates were below 10%, and embryos only treated with pimozide where mortality rates were below 15%. Moreover, the surviving embryos from the group subjected to both the pimozide treatment and heat shock showed overall more severe morphological abnormalities, such as bigger heart edema, curly tail and abnormal trunk curvature, than the embryos treated with pimozide only, whereas control embryos appeared to be healthy (data not shown).

In addition, we also compared the WISH outcomes between the two negative control groups: 1% (v/v) DMSO and E3 medium. Although embryos from these groups were phenotypically similar, significantly higher numbers of embryos treated with 1% (v/v) DMSO showed medium-low or no staining in the CHT after WISH for *gpr182* than embryos incubated in E3 medium alone (p ≤ .01) (**Table 12**, **Table 13** and **Figure 29**). This suggested

that exposure to 1% (v/v) DMSO might also have an effect either on the outcomes of the WISH technique or on gene expression.
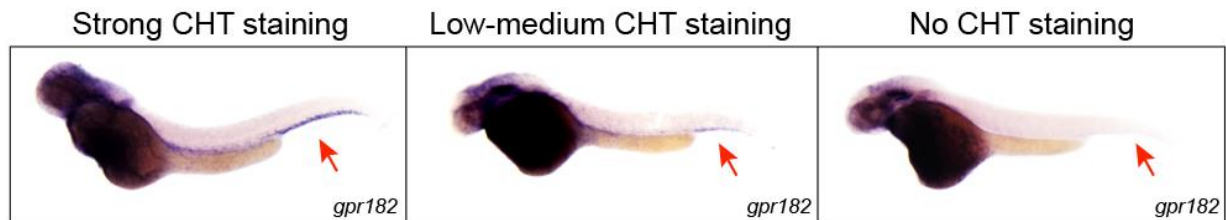
Figure 28. Classification of the whole-mount *in situ* hybridization staining for *gpr182*. The intensity of *gpr182* expression in the CHT was classified as follows: no staining, low-middle staining and strong staining (WT expression). Exemplary images of embryos treated with 25 µM pimozide are shown. Red arrows indicate the expression of *gpr182* in the CHT. Embryos presented here were fixed at 48 hpf (CHT, Caudal Hematopoietic Tissue).

Table 12. Percentages of embryos per group with different staining intensity of *gpr182* in the caudal hematopoietic tissue.

Groups — Staining in the CHT after WISH for *gpr182*	Percentages of embryos (%)		
	Strong	Middle-low	No staining
1) Uninjected in E3 medium	98,60	0,70	0,70
2) Uninjected in 1% (v/v) DMSO	91,83	8,17	0,00
3) Uninjected in 25 µM pimozide	56,37	39,71	3,92
4) Heat-shocked uninjected in 25 µM pimozide	35,87	47,83	16,30
5) Heat-shocked *hsp70l: SOX7* transgenics in 25 µM pimozide	36,96	36,96	26,09

Table 13. Total number of embryos per group with different staining intensity of *gpr182* in the caudal hematopoietic tissue.

Groups — Staining in the CHT after WISH for *gpr182*	Total # of embryos		
	Strong	Middle-low	No staining
1) Uninjected in E3 medium	141	1	1
2) Uninjected in 1% (v/v) DMSO	191	17	0
3) Uninjected in 25 µM pimozide	115	81	8
4) Heat-shocked uninjected in 25 µM pimozide	33	44	15
5) Heat-shocked *hsp70l: SOX7* transgenics in 25 µM pimozide	51	51	36
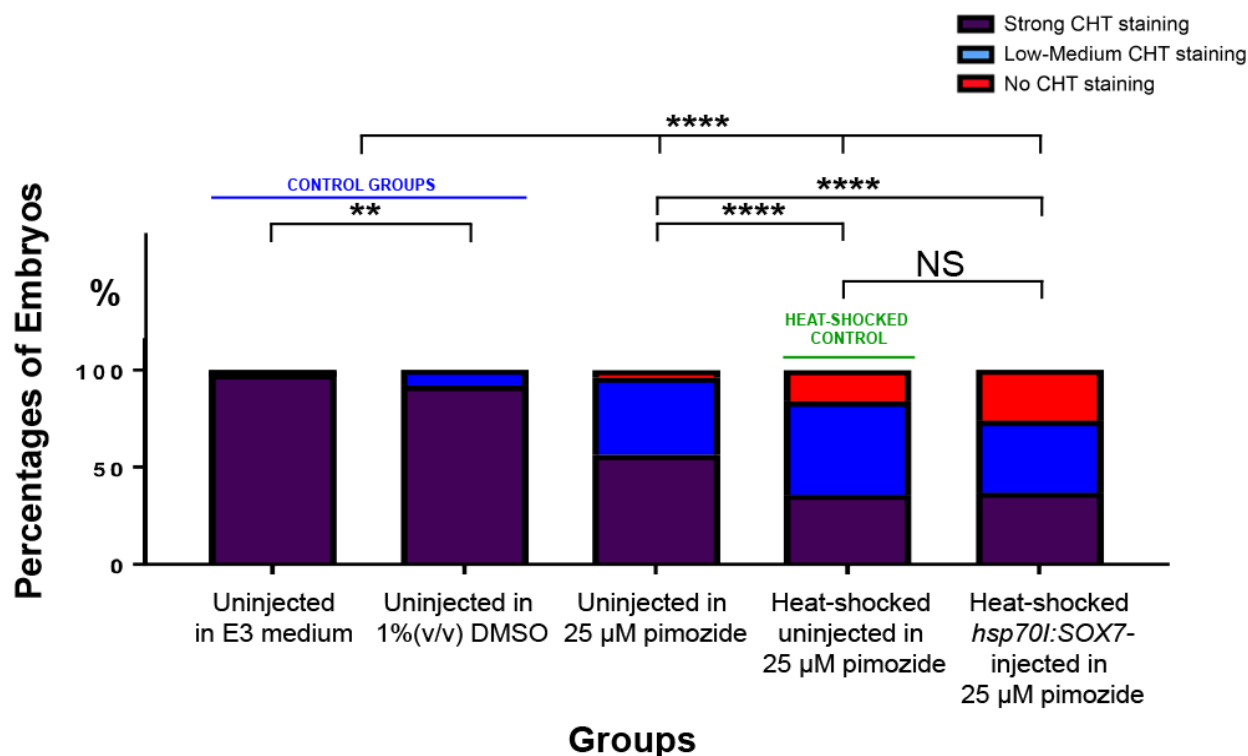
Figure 29. Outcomes of the whole-mount *in situ* hybridization analysis for *gpr182*. Exposure of zebrafish embryos to 25 µM pimozide led to significantly higher numbers of embryos with low-medium CHT staining or no staining at all than control groups (p<.0001). The injection of the *hsp70l: SOX7* led to significantly higher numbers of embryos with low-medium CHT staining or no staining at all than control groups (p<.0001), but also than uninjected embryos treated with 25 µM pimozide (p<.0001). However, no statistically significant differences were detected between the heat-shocked control and the *hsp70l: SOX7*-injected embryos. In addition, there were statistically significant differences between the two control groups (i.e., uninjected in E3 medium and uninjected in 1%(v/v) DMSO) (p<.01). A Chi-square non-parametric test was performed for comparison between the different groups (CHT, Caudal Hematopoietic Tissue; NS, Not Significant; WISH, Whole-mount In Situ Hybridization).

3.6 The Morphological Complexity of the CHT Vascular Plexus Regresses Over Time

Additionally, in this thesis work, we aimed to gain a better understanding of the CHT microenvironment as a whole, giving particular emphasis to the temporal changes of the CHT venous plexus morphology. To that end, we first in-crossed *mrc1a 125 bp*:*GFP* transgenics. GFP positive embryos were selected and raised until 14 dpf. During this period of time, embryos were analyzed using SDCM at distinct time points, starting at 3 dpf.

In our first observations, we found that a gradual decrease in the morphological complexity of the CHT vascular network occurred progressively throughout the first two weeks of development. At early stages of development (2-3 dpf), the vascular plexus, emerging from the posterior caudal vein (PCV), is characterized by a markedly complex network of sinusoidal-like venous ECs that extends towards the dorsal aorta (DA) (**Figure 30**| **A**). However, the CHT venous plexus starts regressing vertically towards the PCV at 3 dpf. In **Figure 30** the CHT vascular plexus can be compared between 3 dpf and 9 dpf. While at 3 dpf the plexus consists of a convoluted vessel network between the PCV and the DA, at 9 dpf it is largely confined to a small region above the PCV and does not extend towards the DA (**Figure 30** | **B**).
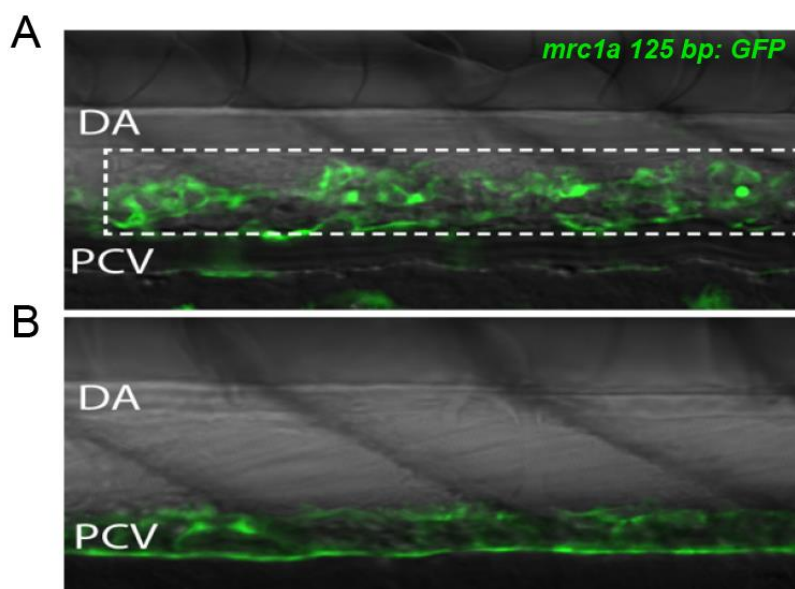
Figure 30. The morphology of the CHT vascular plexus regresses over time (A) At 3 dpf, the CHT venous plexus is a highly interconnected vascular network. The dashed white box outlines the plexus. **(B)** At 9 dpf, the CHT is mostly restricted to the PCV area, where it emerges from. (DA, Dorsal Aorta; PCV, Posterior Caudal Vein).

Given these observations, to quantitate the changes occurring in the remodelling CHT plexus, performed a quantitative analysis of the CHT plexus starting at 2 dpf until 14 dpf. For that, we out-crossed *mrc1a 125 bp*:*GFP* transgenics to *flk*:mCherry adults. Double positive embryos were selected and then analyzed by SDCM over the course of two weeks. Vessels forming the CHT plexus were both GFP and mCherry positive (**Figure 31**). This way, double transgenics allowed us to verify that the observed vessels were indeed of endothelial origin.

The CHT plexus is initially composed of an expanded plexus with a high number of interconnected vessels, among which wide, intervascular spaces are found (**Figure 32**). Between 2 dpf and 3 dpf, the plexus undergoes a remarkable dorsoventral retraction towards the PCV. The intervascular spaces significantly decrease in size, as demonstrated by comparing the mean values of the maximum height and width values (μm) of such spaces between 2 dpf and 3 dpf ($p<.001$) (**Figure 33**). Analysis of the CHT vessel network using the AngioTool software revealed that the total number of branch points, the total vessel length (μm) and the number of total endpoints decline over time, thus confirming the progressive decrease in network complexity previously observed. After 3 dpf, the morphology of the CHT continues regressing until 14 dpf, stage at which it is virtually non-existent and entirely associated with the PCV from which it originally emerged (**Figure 34** and **Figure 35**).
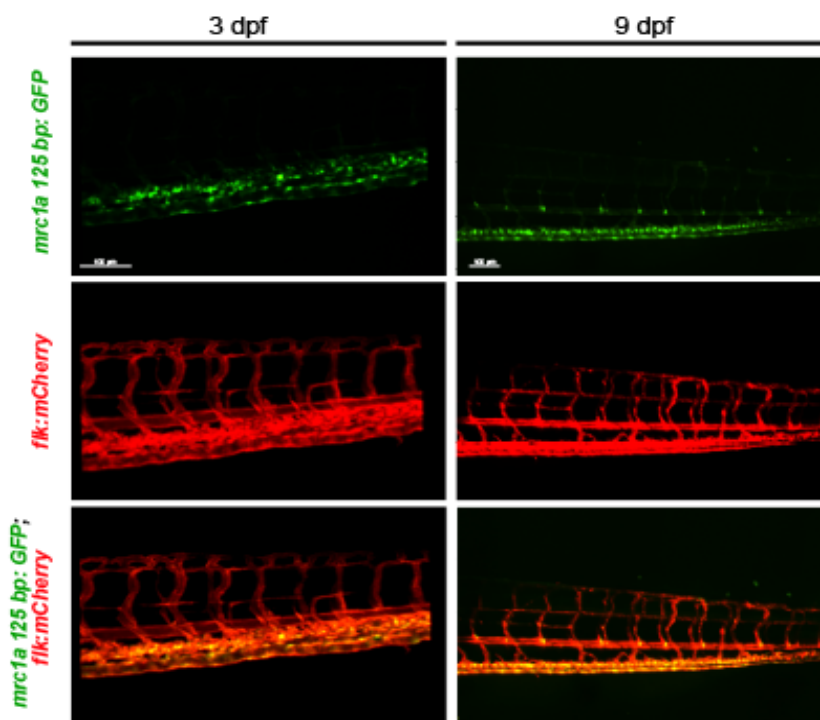
Figure 31. Double positive transgenics at 3 dpf and at 9 dpf. The CHT ECs expressed both *mrc1a:GFP* and *flk:mCherry* at the different analyzed stages – labeled in yellow as a result of the overlap between the green (*mrc1a:GFP*) and red (*flk:mCherry*) colors. Scale bar: 100 μm.
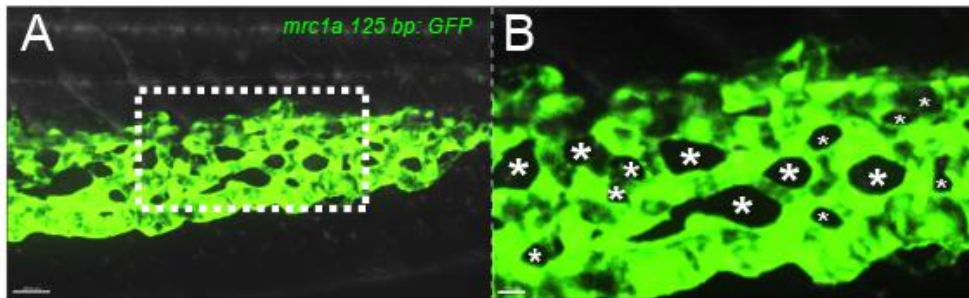
Figure 32. The caudal hematopoietic tissue at 2 dpf is comprised of a complex network of interconnected venous vessels, containing numerous intervascular spaces. **(A)** The CHT plexus at 2 dpf. The dashed white box outlines a specific region, that can be observed at a higher magnification in **(B)**. Asterisks indicate some intervascular spaces. Scale bars: 30 µm (A) and 10
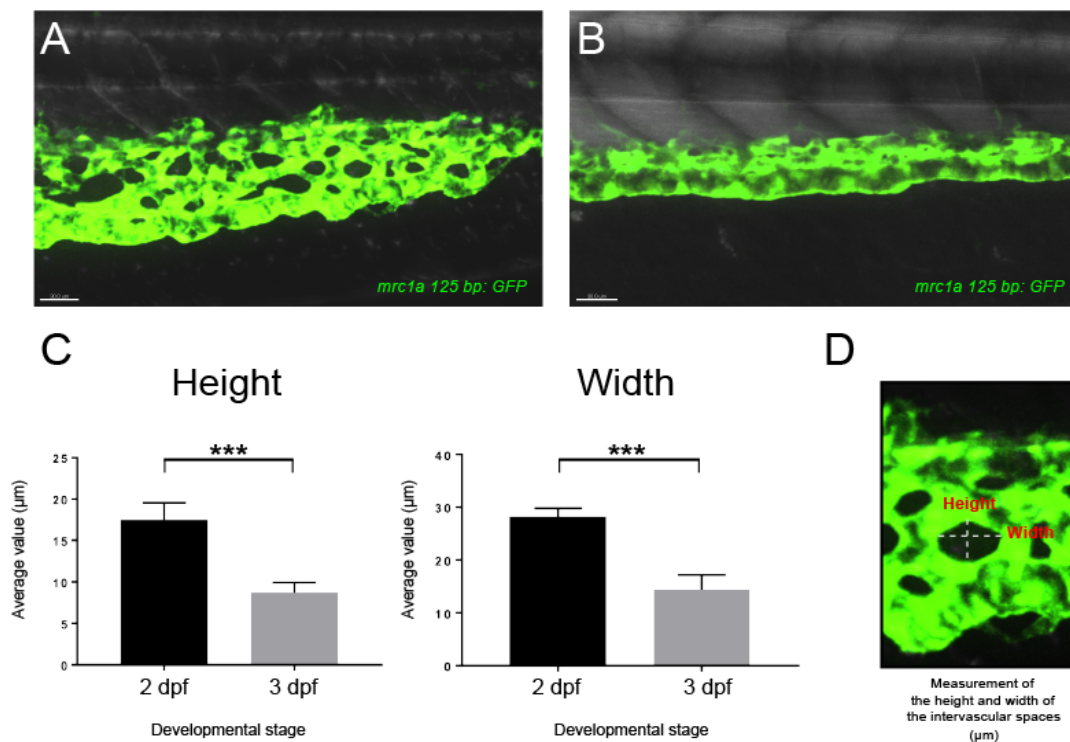
Figure 33. The dorsoventral retraction of the caudal hematopoietic tissue plexus starts after 2 dpf and is already very noticeable at 3 dpf. (A) CHT plexus at 2 dpf. **(B)** CHT plexus at 3 dpf. **(C)** The dimensions of the intervascular spaces within the plexus are significantly reduced at 3 dpf compared to 2 dpf (p<.001). Both average values of height and width notably decrease from one day to next. **(D)** Image indicating the maximum height and width of a concrete intervascular structure in the 2 dpf-CHT plexus in a 2D sagittal section. Both parameters are measured in µm. Scale bar: 30
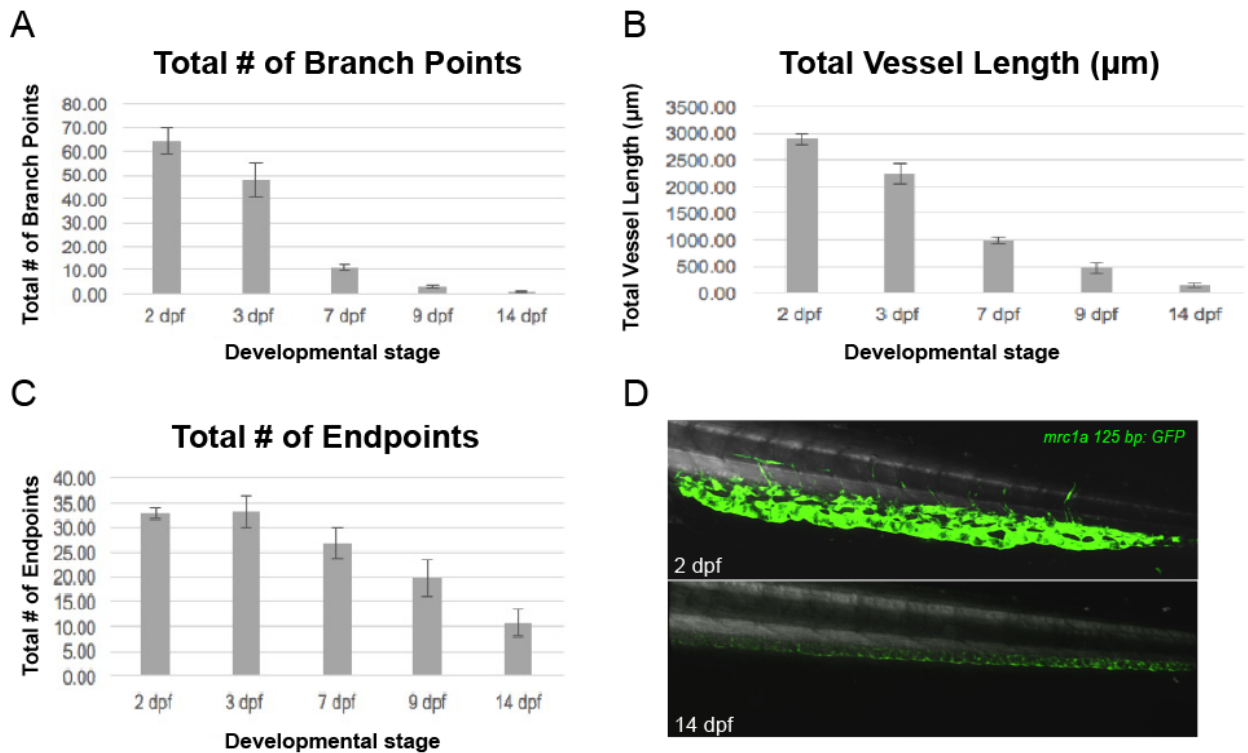
Figure 34. Graphical representation of the analysis performed on the CHT vessel network analysis of *mrc1a 125 bp*: *GFP*; *flk*: *mCherry* embryos from 2 dpf until 14 dpf. (A) Total number of branch points, **(B)** total vessel length (µm) and **(C)** total number of endpoints decline over time, thus indicating a progressive decrease in vascular network complexity throughout the first two weeks of development. **(D)** The CHT of a 2 dpf-embryo can be compared to that of a 14 dpf-embryo. While at 2 dpf the CHT is a complex network of vessels, at 14 dpf it is restricted to a single caudal vein. Data are expressed as the mean ± SEM (n = 10-15 embryos analyzed at each developmental stage).
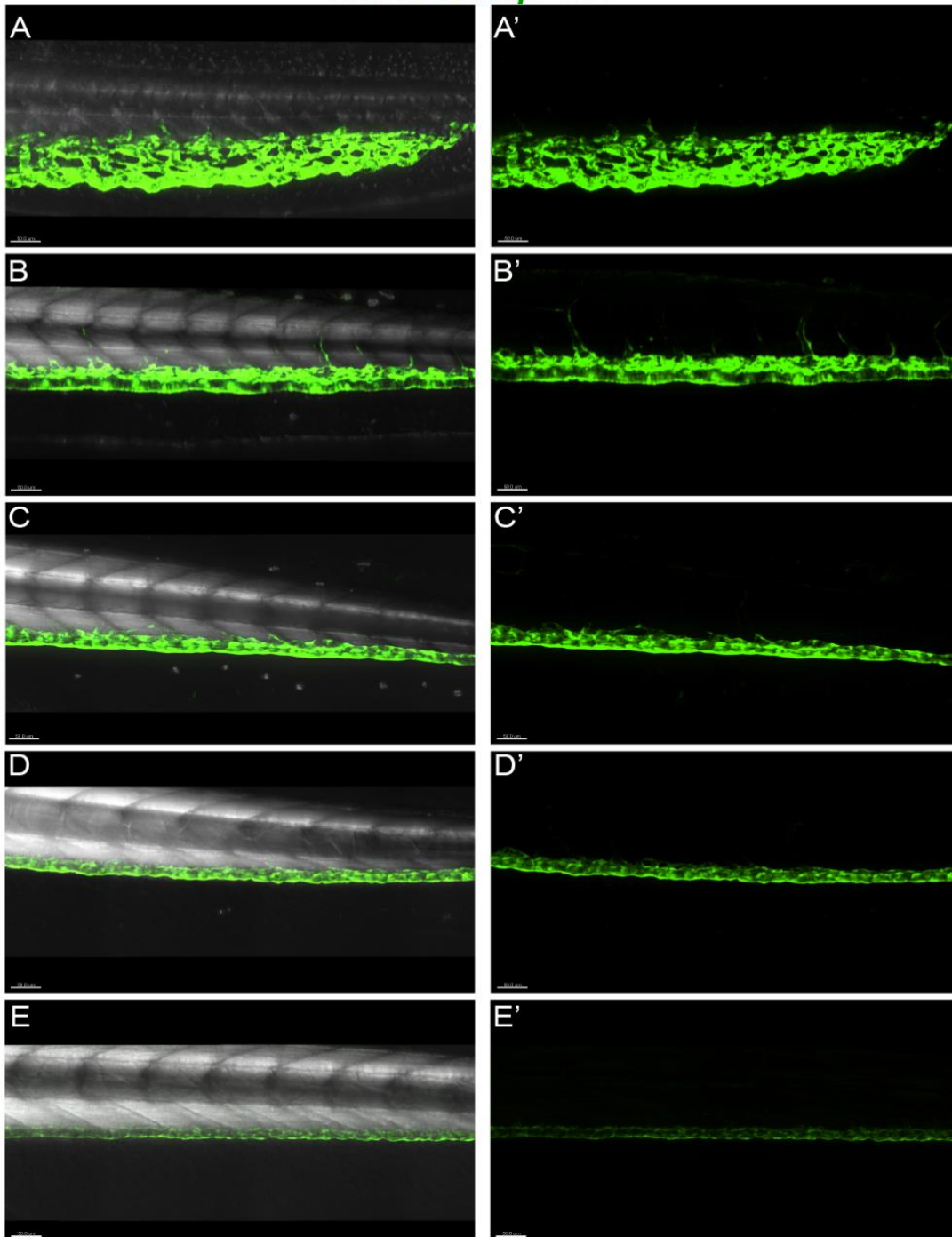
Figure 35. Progressive decrease in vascular network complexity of the CHT plexus throughout the first two weeks of development. The CHT region initially consists of a complex network of blood vessels, that regresses over time, until being finally reduced into a single caudal vein. Representative images from different developmental stages are shown**:** 2 dpf (**A** and **A'**), 3 dpf (**B** and **B')**, 7 dpf (**C** and **C'**), 9 dpf (**D** and **D'**) and 14 dpf (**E** and **E'**). Left images are GFP/DIC overlays, whereas right images are only GFP (n= 10-15 embryos per developmental stage). Scale bar: 50 μm.

3.7 HSPCs in the CHT Niche Start Decreasing in Numbers After 8 dpf, but this Region Remains Hematopoietic until 14 dpf

We next hypothesized that the CHT morphological changes are associated with the migration of HSPCs to the definitive hematopoietic niches. This led us to an important question: When do HSPCs leave the CHT niche? To address this question, we characterized precisely when that occurs. For that, we out-crossed *mrc1a 125 bp:GFP* to *runx1:mCherry* transgenics. Double positive embryos were selected, raised until 14 dpf and examined using SDCM at specific time points.

The results from the first trial indicated that some HSPCs remained in the CHT after the time the stem cell population began to migrate to the definitive sites of hematopoiesis, the kidney marrow and thymus, which takes place by 5-6 dpf, as demonstrated elsewhere [118]. However, at 14 dpf practically no *runx1* positive cells were observed in the CHT niche, suggesting that the niche had already emptied by that time (**Figure 36**).
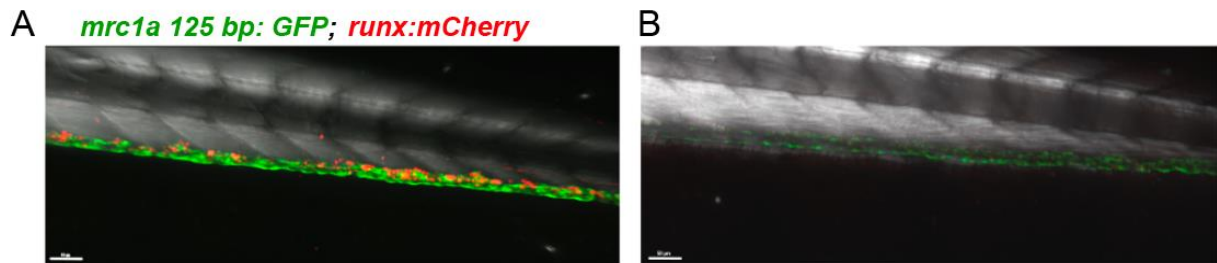
Figure 36. The CHT niche remains hematopoietic after the time HSPCs start migrating to the definitive sites of hematopoiesis (A) HSPCs (*runx1:mCherry*) were still present in the CHT vascular plexus (*mrc1a: GFP*) at 8 dfp. **(B)** Practically no HSPCs were detected in the CHT at 14 dpf. In addition, the expression of *mrc1a: GFP* is very low. Scale bar: 50 µm.

To confirm these observations, we performed a second round of imaging, in which new double *mrc1a 125 bp:GFP; runx1:mCherry* transgenics were analyzed, also using SDCM. In this round, processed images were used to count the numbers of *runx1* positive cells. Only cells present in the CHT plexus were counted, with circulating cells or cells clearly located within the lumen of the PCV being excluded from analysis. We found that the numbers of *runx1* positive cells were low at early stages but increased progressively until 8 dpf (**Figure 37**). This finding is in accordance with previous studies, in which it was demonstrated that

the CHT plexus, akin to the mammalian fetal liver, serves as an intermediate niche where arriving HSPCs expand before they seed the definitive hematopoietic organs [1],[118]. Surprisingly, the number of *runx1* positive cells happened to reach its maximum at 8 dpf, time after the HSPCs are thought to start migrating to the ultimate adult niches. This suggested that some HSPCs leave the CHT niche, while others remain in the region and keep expanding to increase the stem cell pool. After 8 dpf, the number of *runx1* positive cells notably decreased until 14 dpf, at which point essentially no HSPCs were detected in the CHT region (**Figure 37**).

The time during which HSPCs resided in the CHT niche paralleled the remodelling of the CHT plexus into the definitive PCV. At 2 dpf, when the plexus was composed of a complex network of vessels that occupied the space between the PCV and DA, circulating *runx1* positive HSPCs were observed to arrive in the CHT via the DA. At this time point, although multiple empty intervascular spaces were observed across the plexus area, most of the cells were intravascular, circulating through the dorsal-most branches of the plexus. At 3 dpf, higher numbers of *runx1* positive HSPCs were detected. Additionally, it could be observed that a noticeable remodelling of the CHT plexus had already taken place (**Figure 37** and **Figure 38**). This suggested that the plexus commenced shrinking vertically towards the PCV since the moment HSPCs were seen to lodge in the CHT. At 3 dpf, most of the HSPCs were integrated into the plexus, thus being located in middle positions of its territory (**Figure 38** I **B**). Notably, more *runx1* positive cells were visualized within the intervascular spaces than at 2 dpf (**Figure 38** I **A**), suggesting that ECs might remodel to wrap around the new coming HSPCs. This finding supports the notion that the arrival of HSPCs in the CHT region directly triggers EC remodelling, thereby changing the morphology of the CHT venous plexus.

After 3 dpf, as the plexus continued undergoing a dorsoventral retraction, more and more HSPCs were observed to circulate through the PCV, while lower numbers of cells resided in the plexus area (**Figure 37** and **Figure 39**). This fact suggested that after expansion in the CHT, HSPCs leave the CHT niche and migrate to the definitive sites of hematopoiesis via the PCV, and that these phenomena – both expansion of the hematopoietic population and migration to the definitive HSPC niches – are directly linked to CHT EC remodelling.

Total # of *runx1:mCherry* positive HSPCs in the CHT plexus
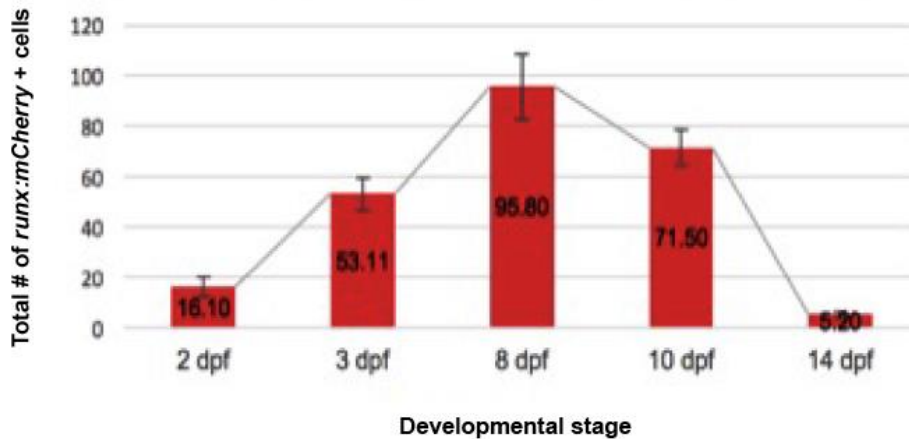
Figure 37. The numbers of *runx1:mCherry* positive HSPCs increase during the first week of development and decline through the second week. HSPCs colonize the CHT by 2 dpf. There, they expand in numbers throughout the first week of development. After 8 dpf, the numbers of HSPCs start decreasing. The CHT remains hematopoietic until 14 dpf, stage at which little-to-no numbers of HSPCs are detected. Data are expressed as the mean ± SEM (n= 8-10 embryos analyzed at each developmental stage).
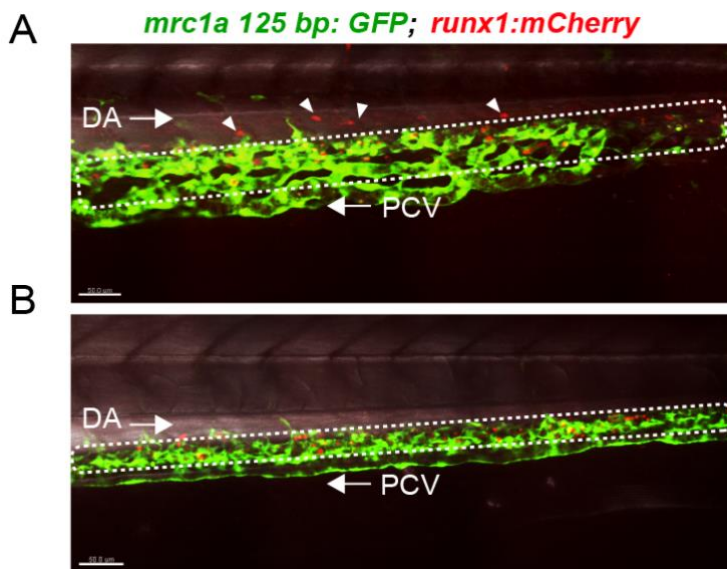
Figure 38. *Runx1* positive hematopoietic stem and progenitor cells arrive in the caudal hematopoietic tissue niche by 2 dpf and at 3 dpf they are intimately associated with niche endothelial cells. (A) Most HSPCs (*runx1:mCherry*) are found circulating through the DA and in the dorsal-most branches of the CHT plexus, as indicated by the white arrowheads. **(B)** HSPCs are in intervascular spaces surrounded by CHT ECs. The dashed white boxes outline the CHT plexus. (DA, Dorsal Aorta; PCV, Posterior Caudal Vein). Scale bar: 50 μm.
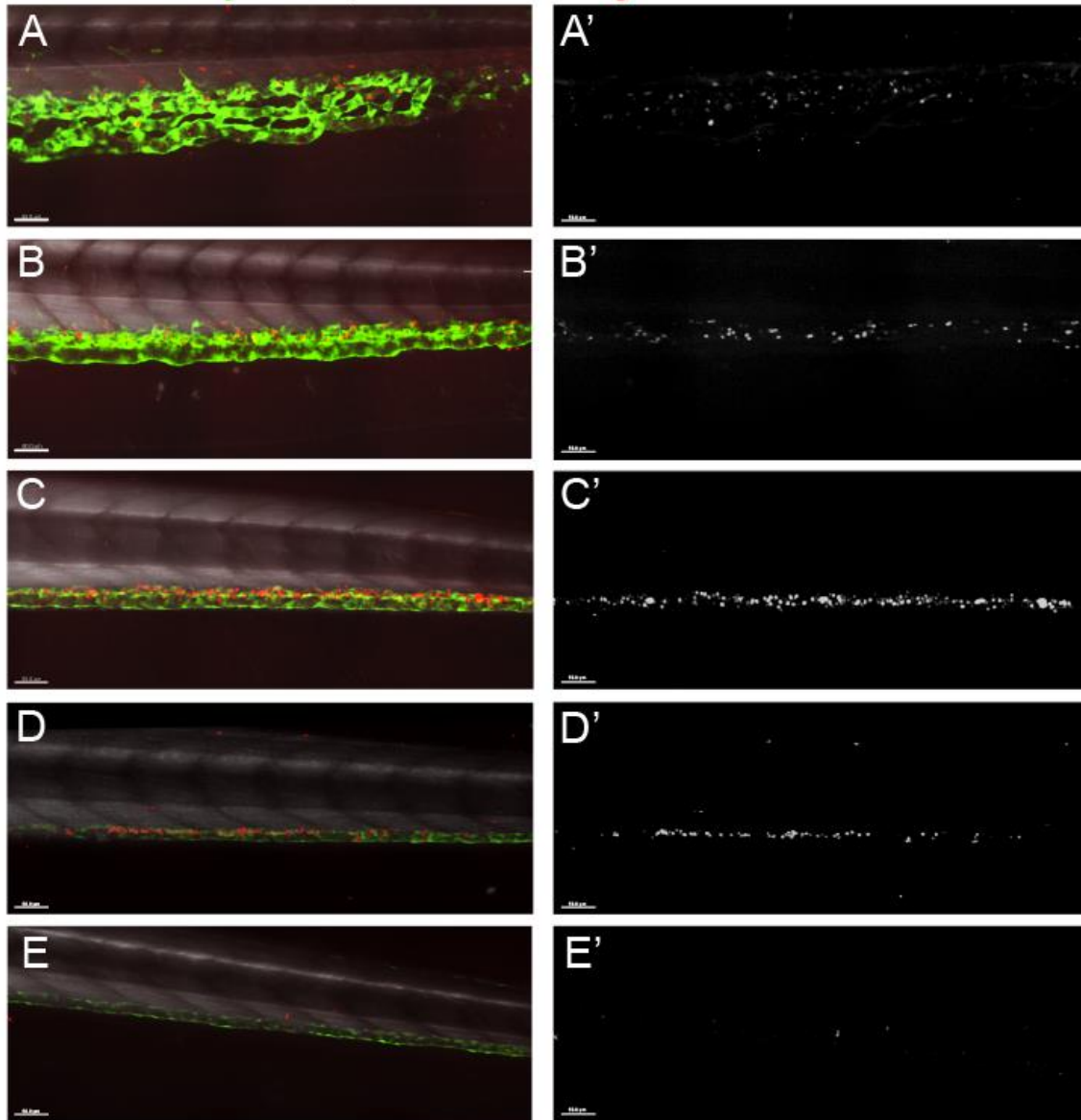
Figure 39. HSPCs arrive in the CHT region, where they increase in numbers up to 8 dpf, stage from which they start decreasing until being barely detected at 14 dpf. (A and **A')** HSPCs (*runx: mCherry*) are detected in the CHT vascular plexus (*mrc1a: GFP*) at 2 dpf. Many HSPCs, arriving in the CHT, are observed to be circulating through the DA. **(B** and **B')** At 3 dpf, HSPCs have already lodged in the CHT, where the interact with resident ECs. **(C** and **C')** At 8 dpf, the numbers of HSPCs reach the maximum. **(D** and **D')** At 10 dpf, the numbers of HSPCs have been reduced compared to 8 dpf. **(E** and **E')** At 14 dpf, HSPCs are barely detected in the CHT region. In addition, the expression of *mrc1a: GFP* is very low, and the plexus has already regressed into a single caudal vein. Left images are mCherry/GFP/DIC overlays and right images are the grayscale of the mCherry images, showing HSPCs only. Scale bar: 50 μm.

3.8 Niche Endothelial Gene Expression in the CHT Decreases After the HSPCs Migrate to the Kidney Marrow Niche

In order to better understand the spatial and temporal dynamics of CHT-specific endothelial gene expression, we performed WISH for different endothelial genes (e.g., *mrc1a*, *lgmn* and *gpr182*) on embryos fixed at specific time points – from 24 hpf until 14 dpf. For these experiments, WT Casper EKK adults were in-crossed and embryos were collected and grown until a selected time point (n=30 per clutch at each time point). The expression patterns were consistent across the different groups. as well as within the same group. Expression of CHT-specific endothelial genes could be detected up to 14 dpf, but appeared to be down-regulated over time (**Figure 40**). This suggested that the expression of such genes remains, albeit at lower levels, after the time at which HSPCs begin to migrate to the definitive hematopoietic niches, which is thought to occur around 5 - 6 dpf [1],[118].
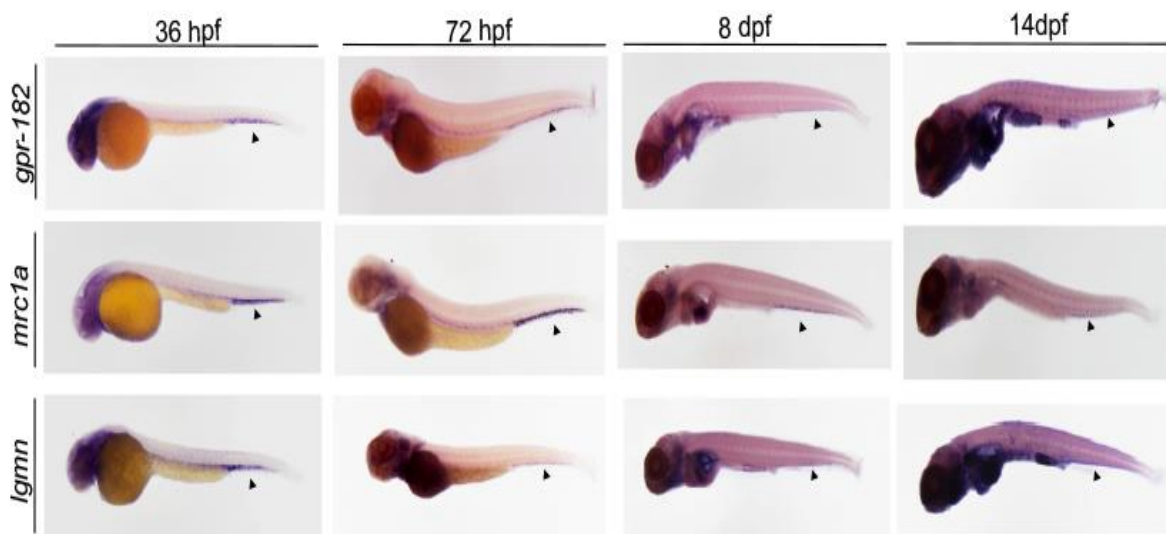
Figure 40. **Whole-mount in situ hybridization for three niche endothelial cell-enriched genes, *gpr182*, *mrc1a* and *lgmn*, on embryos fixed at four different developmental stages.** Expression of niche-specific endothelial genes remains up to 14 dpf in the CHT (black arrowheads), but appears to be downregulated over time. Expression of these genes in the CHT remains, albeit at lower levels, after the time at which HSPCs start migrating to the kidney marrow, which begins around 5-6 dpf (n=30 embryos per clutch at each time point).

Downregulation of CHT-specific endothelial genes appeared to coincide with the loss of HSPCs from the CHT niche. We thus surmised that HSPC migration from the CHT niche to the kidney marrow might correlate with the global activation status of the niche-specific EC genetic program. To that end, we isolated the CHT ECs (*mrc1a:GFP +*, *flk:mCherry +*) from whole embryos belonging to three different developmental stages (i.e., 4 dpf, 7 dpf and 14 dpf) using FACS and next performed RNA-seq on them. Unexpectedly, a subsequent genome-wide differential analysis determined that the gene expression was more similar between 4 dpf and 14 dpf, compared to the 7 dpf stage. By looking at the computed Fragments Per Kilobase of transcript per Million mapped reads (FPKM) values of different CHT-enriched endothelial genes, including *mrc1a*, *lgmn*, and *gpr182* (data not shown), we observed that whereas the values were similar between 4 dpf and 14 dpf, they were lower at 7 dpf, suggesting a gene downregulation between 4 dpf and 7 dpf, followed by an upregulation between 7 dpf and 14 dpf. These results challenged our hypothesis rooted in the idea that the CHT endothelial genes downregulate over time, as supported by our WISH analysis. They also suggest, however, that while the CHT endothelial genes downregulate during the first week of development, a similar genetic program might be turned on in the second week of development. **Figure 41** depicts a dendrogram of the three *mrc1a:GFP +*, *flk:mCherry +* EC samples that shows the similarity between samples' gene expression. To plot this dendrogram, the Jensen-Shannon (JS) distance was used as the clustering metric.
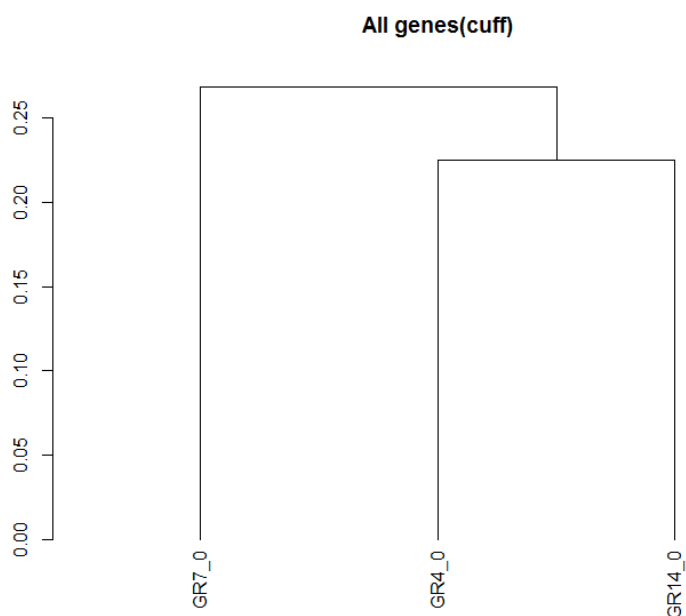
Figure 41. A dendrogram of the relationship between samples based on the expression of genes in a CuffGene set. The gene expression at 4 dpf is similar to that at 14 dpf, and more different to that at 7 dpf. The vertical axis indicates JS distances. The longer the distance, the more different the gene expression between two samples is (GR, Green (*mrc1a:GFP*) Red (*flk:mCherry*)).

4 Discussion

HSPC transplantation is often the only curative therapy available for some hematological disorders including cancer [1],[2],[133]. However, the number of cells available for transplantation is limited by the shortage of immunologically suitable donors and the small quantities of HSPCs in the body. Fueled by the ever-present demand for HSPCs in the clinic, recent research has focused on designing new methods for *in vitro* expansion of HSPCs, with a particular focus on preserving the stemness and self-renewal potential of these cells. Despite some progress, there remain significant challenges in devising more efficient and safe strategies to increase the number of HSPCs for clinical applications. Reaching the full potential of HSPC transplantation will require further investigation into the biology of HSPCs, and in particular, advanced knowledge of how the niche – the microenvironment where these cells reside and are nurtured – contributes to HSPC expansion and maintenance. A deeper understanding of the intricacy of the HSPC niche will be attained by dissecting the identity of the supporting niche cells and how they interact with stem cells [1], [2], [7], [8]. In this thesis work, we characterized the transcriptional code that defines the genetic identity of sinusoidal ECs in the CHT – the embryonic HSPC niche in zebrafish. We provide additional data on the morphological, molecular and cellular changes that occur within this niche over developmental time. Our results highlight a dynamic interplay between HSPCs and niche ECs that is likely important for proper HSPC function.

4.1 Ets, Sox and NH Receptor Binding Sites Are Specifically Required for Expression of Niche Endothelial Genes

In the present work, we define a novel transcriptional code, involving members of the Ets, Sox and NH receptor families, that specifies the genetic signature of sinusoidal ECs in the zebrafish CHT niche. In an initial phase of this project, ATAC-seq was performed on CHT ECs, and it was determined that this cell population presented 6,848 unique regions of open chromatin, that were later shown to include tissue-specific EC enhancers. Subsequent informatic analysis of these sequences identified Ets, Sox, and NH receptor sites as the most enriched TF binding motifs within these regions (data not shown). Therefore, it was hypothesized that TFs from these three families might bind the CHT EC enhancers as a part of a transcriptional network that specifies the genetic identity of these cells. The fact that TF

members from the Ets, Sox F and NH receptor families could be involved in mediating EC gene regulation was not entirely unexpected given the known roles for TFs from these families in regulating vessel development and specification [134]. However, when a similar analysis of pan-endothelial ATAC-seq regions was performed, it was found that only Ets sites, and not the Sox F and NH receptor sites, were highly enriched within these regions (data not shown). Thus, the specific enrichment of the Sox F and NH receptor motifs, in combination with Ets motifs, in niche-specific EC enhancers supported our hypothesis that members from these three families might constitute a niche-specific EC gene regulatory network.

Using mutant enhancer variants of the *mrc1a* 125 bp and *sele* 158 bp elements, we provide evidence that the Ets, Sox and NH receptor motifs are specifically required for selective expression in CHT ECs. While disruption of the specific motifs by mutation led to substantial reduction or complete loss of GFP expression (data not shown), control mutations targeting intervening sequences between the Ets, Sox and NH receptor motifs did not result in significant differences in GFP expression when compared to the full WT sequence of the enhancer (**Figure 15** and **Figure 16**). Together these results support our initial hypothesis that the Ets, Sox and NH receptor binding sites are specifically required for selective expression in niche ECs.

4.2 Induction of Ectopic Niche Endothelial Gene Expression by the Synergistic Action of Ets, Sox, and NH Receptor Factors

Before I joined the group, RNA-seq was carried out to profile the CHT EC population. Results from this analysis revealed that the following seven factors were the mostly highly expressed members of the Ets, Sox and NH receptor families: *fli1a*, *etv2* and *ets1* from the Ets family; *sox18* and *sox7* from the Sox family; and *nr2f2* and *rxraa* from the NH receptor family. In light of these results, we hypothesized that overexpression of a combination of these factors in zebrafish embryos might induce ectopic sites of niche endothelial gene expression. Therefore, we first injected the seven-factor combination and performed WISH analysis for *mrc1a*. Remarkably, we found that overexpression of these TF genes led to ectopic *mrc1a* expression in 21% of the injected embryos, whereas control embryos did not show significant ectopic expression (**Figure 17**). This finding further supported our hypothesis that TFs from the Ets, Sox and NH receptor families constitute the transcriptional network that specifies

CHT ECs.

It is well established that members of the Ets TF family are involved in EC development. Particularly, ETV2 has been reported as a potent and indispensable mediator of vessel development [94], [95], [135]. Therefore, we sought to determine whether ETV2 in concert with SOX7 and Nr2f2, each one representing a member from the Ets, Sox and NHR families, respectively, could similarly induce ectopic niche endothelial gene expression. Strikingly, we observed that 60% of embryos injected with the three-factor ETV2 mix showed ectopic *mrc1a* expression (**Figure 20** and **Figure 21**).Narrowing down the TF combination to the above-mentioned three factors made it possible to increase the injected amount of each TF gene construct, which would explain the fact that the efficiency was increased when injecting the three-factor combination compared to the initial seven-factor pool.

Next, we injected single TF gene constructs to evaluate the contribution of each TF. Whereas injection of SOX7 and Nr2f2 on their own did not lead to significant ectopic expression, 48% of the embryos injected with ETV2 alone showed significant ectopic *mrc1a* expression (**Figure 20** and **Figure 21**). This finding was consistent with recent studies, where ETV2 has been shown to activate endothelial gene expression on its own, thereby reprogramming non-endothelial cells, such as fibroblasts and skeletal muscle cells, towards an endothelial fate [96], [124], [136]. In view of our results, we wanted to test whether an alternative TF gene from the Ets family could be injected in place of ETV2 in the three-TF gene pool and similarly give rise to ectopic niche endothelial gene expression. ETS1 is an Ets factor that is known to be crucial for EC differentiation and maintenance [92] [130]. We therefore hypothesized that ETS1 might be able to function in place of ETV2 in the three-factor pool. Indeed, injection of the three-factor ETS1 mix induced *mrc1a* ectopic expression, although it was at a lower frequency compared to the three-factor ETV2 mix (**Figure 20** and **Figure 21**).

On the one hand, our results concur with the established role of ETV2 as a potent activator of the endothelial gene transcription program. On the other hand, we show that the novel combination of three TFs – either ETV2 or ETS1 with SOX7 and Nr2f2 – is sufficient to generate ectopic sites of niche endothelial gene expression. In addition, as the three-TF gene pool led to significantly higher numbers of embryos with ectopic endothelial gene expression than the single TF genes, it is likely that the combination of the three TFs, one each from the Ets, Sox and NH receptor families, function together to induce CHT endothelial gene expression (**Figure 42**). In addition, the fact that the overexpression of human TF genes led to ectopic expression of the endogenous zebrafish genes highly suggests an interspecies conservation of the niche endothelial gene program.
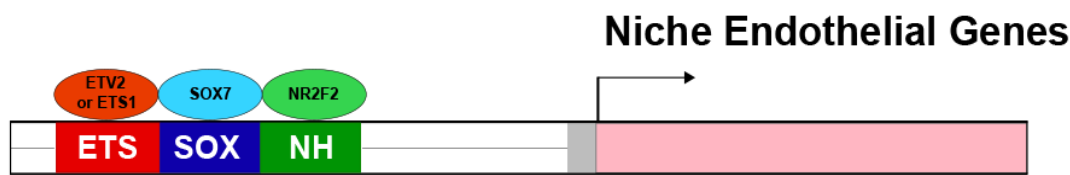
Figure 42. A model for the cooperative action of the three transcription factors, one each from the Ets, Sox and NH receptor families, in the activation of the transcription of niche endothelial genes. The combination of three TFs – either ETV2 or ETS1 with SOX7 and Nr2f2 – is sufficient to activate the niche endothelial gene program. The TFs bind the enhancer regions of the niche endothelial genes to stimulate transcriptional initiation.

4.3 ETV2 Alone Can Induce Aspects of the Niche Endothelial Gene Program

To further evaluate the role of ETV2 in the activation of the niche endothelial program, we examined embryos injected with ETV2 alone using WISH probes for the seven-factors in our initial overexpression pool, including *sox7, sox18, fli1a, ets1, etv2* and *nr2f2*. WISH for *nr2f2* resulted in a high background, particularly in the region of the spinal cord, so it was difficult to determine whether this gene was induced ectopically after injection of ETV2 alone. Consistent with this observation *nr2f2* is implicated in the development of various organs besides the vasculature, including the developing hindbrain and the mesoderm [137]. WISH for *Ets1* similarly showed that this gene is broadly expressed, particularly in dorsal areas of the tail, which made it difficult to identify whether ectopic endothelial expression of this factor was induced. WISH for *sox7*, *sox18*, *fli1a* and *etv2* (genes that are normally selectively enriched in the CHT), however, revealed that injection of ETV2 alone was sufficient to induce ectopic expression of these TFs outside the CHT (**Figure 20** and **Figure 21**).

This is in agreement with previous work, where it was established that ETV2 alone turns on key genes regulating hematopoietic and endothelial cell specification, including other TFs from the Ets family (*e.g.,* Fli1) [139].Together our data reveal that ETV2 alone is capable of triggering ectopic niche endothelial gene expression due to its ability to activate other TF genes (as well as itself) implicated in the transcriptional code governing the identity of CHT ECs.

Recent studies have proposed the role of ETV2 as a pioneer factor [143], [144]. With our results, we favor this idea in that we believe that ETV2 would be able to access closed chromatin and after stimulating the transcription of those genes encoding relevant TFs, it

would facilitate the binding of the recently transcribed non-pioneer factors to the enhancer regions of the niche endothelial genes (**Figure 43**). This could explain why ETV2 on its own has a potent effect on the induction of ectopic niche endothelial gene expression, unlike ETS1 and the other factors, whose individual overexpression did not result in significant ectopic niche endothelial gene expression (**Figure 21**). Additionally, the fact that the overexpression of ETV2 induces ectopic expression of the endogenous *etv2* gene suggests the existence of a possible auto-regulatory mechanism where ETV2 positively activates its own gene expression (**Figure 43**). This is consistent with the work of Koyano-Nagawaka *et al.* published in 2015 where it was shown that early induction of Etv2 resulted in increased endogenous Etv2 expression using an *in vitro* culture of mouse embryonic stem cells [145]. Future studies, using immunoprecipitation- and mass spectrometry-based methods, will be required to determine whether ETV2 would bind the chromatin alone or together with other TFs, as well as the precise interactions between the different TFs.
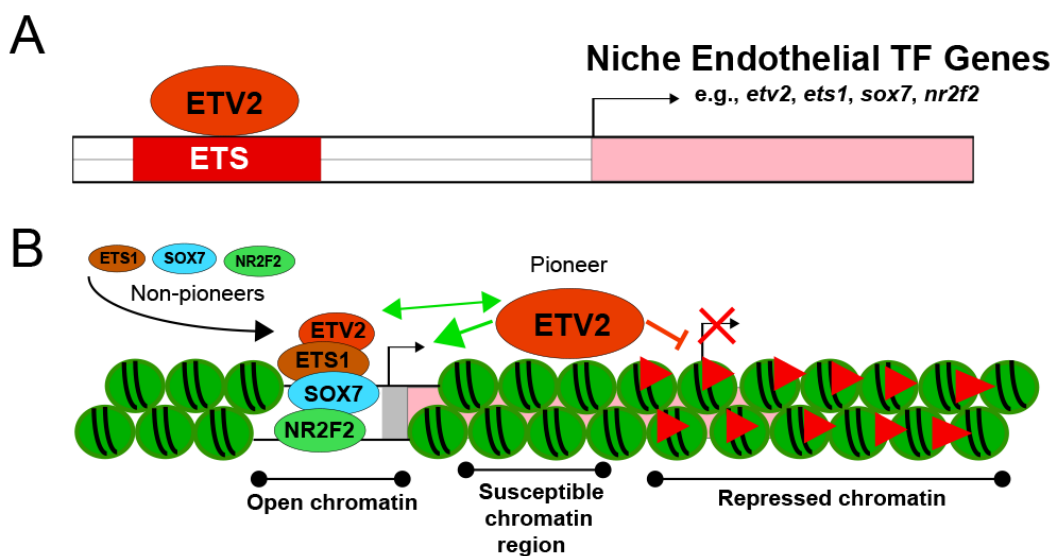
Figure 43. ETV2 transactivates other transcription factors involved in the niche endothelial transcriptional regulatory network. (A) ETV2 activates the expression of other TF genes involved in the CHT endothelial transcriptional regulatory network, as well as its own gene expression as a part of an auto-regulatory mechanism. **(B)** We believe that ETV2 is a pioneer factor capable of binding susceptible regions of chromatin and make them accessible for the other non-pioneer factors (e.g., ETS1, SOX7 and NR2F2) to bind and stimulate together the transcription of niche endothelial genes.

4.4 Blood Flow Regulates Expression of CHT Endothelial Genes

It is well established that the shear stress generated by blood flow regulates gene expression and signaling pathways in the blood vasculature [146],[147]. Additionally, previous work has demonstrated that blood flow velocities and low wall shear rates are key to HSPC homing [46], and that alterations in blood flow also lead to changes in the expression of genes involved in HSPC development and homeostasis, such as *runx1* and *c-myb* [59], [60]. Given these findings, it was logical to hypothesize that blood flow would play a critical role in the regulation of the niche EC genetic program in that lower blood flow velocities could upregulate the expression of these genes. Strikingly, according to previous experiments in our laboratory, blockage of blood flow led to the opposite effect; this is downregulation or loss of expression of some niche endothelial genes, including *sele*, *sox7* (data not shown) and *gpr182* (**Figure 27**).

By exposing zebrafish embryos to a concentration of 25 µM pimozide from 18 hpf (before the systemic blood circulation initiated [148]) to 48 hpf, we stopped blood flow. Subsequent WISH analysis for *gpr182*, a gene highly expressed by CHT ECs, revealed that a significant number of embryos treated with pimozide had substantially lower levels or complete loss of *gpr182* expression compared to sibling embryos incubated either in DMSO alone or E3 medium as a control. These results indicate that blood flow regulates the expression of *gpr182.* In an attempt to rescue the expression of this gene, we overexpressed SOX7, a TF gene whose expression was also downregulated in the absence of blood flow, as demonstrated by recent work by other colleagues in our laboratory (data not shown). To that end, we cloned the ORF of the human SOX7 gene and fused it to the *hsp70l* promoter and then injected this construct into one cell-stage embryos, that were subsequently heat-shocked at two different time points. Unexpectedly, overexpression of SOX7 led to higher number of embryos showing downregulation of *gpr182* compared to the uninjected counterparts that were exposed to 25 µM pimozide, but not heat shocked. Nevertheless, when compared with the heat-shocked control (uninjected embryos treated with pimozide that were heat shock-induced at the same time points), no statistically significant differences were observed (**Table 12**, **Table 13** and **Figure 29**). These results, along with the fact that the rates of mortality and morphological abnormality were similar in these two groups and higher than in the others, suggest that when pimozide treatment is combined with heat shock, the health of the embryos dramatically deteriorates. It is possible this hinders gene

expression or the outcomes of the WISH technique. Future experiments using untreated WT embryos would help determine whether the heat shock treatment has a negative effect on the expression of *gpr182*, as well as other niche endothelial genes. Additionally, using an alternative method to block blood flow, such as the injection of the anti-tnnt2 (*silent heart*) morpholino, could be used to test whether the results would differ from the ones obtained with the pimozide treatment.

Lastly, we made the observation that embryos treated with DMSO (1% in E3 medium), despite being morphologically normal, showed downregulation of *gpr182* compared to embryos treated with only E3 medium alone (**Table 12**, **Table 13** and **Figure 29**). This indicates that this concentration of DMSO might be sufficient to induce gene expression changes within the niche ECs. In order to investigate into the effects of DMSO on gene expression in general, WISH analysis for different genes expressed out and inside the CHT should be performed. These experiments would determine whether DMSO has a specific effect on the expression of niche endothelial genes or it generally leads to changes in gene expression, thereby affecting genes expressed elsewhere as well.

Together, our experiments demonstrate that blood flow, an extrinsic regulator of EC function, is a determinant of niche endothelial gene expression. As the expression of *gpr182* could not be rescued by heat shock-induced SOX7, however, it remains to be determined exactly how blood flow dictates the activation and maintenance of the genetic program of the niche ECs.

4.5 Dorso-ventral Regression of the CHT Plexus during the First Two Weeks of Development

In this thesis work, we have additionally characterized the temporal morphological changes of the ECs in the CHT vascular plexus. Analysis of the CHT region over the course of the first two week of development using SDCM revealed that the morphological complexity of the CHT vascular plexus progressively decreases over time and that the CHT is remodelled down until essentially only the PCV remains.

At 2 dpf, the CHT plexus consists of an interconnected network of venous sinusoids containing wide intervascular spaces (**Figure 32 I A**). At this time point, the CHT vascular region fully extends from the PCV to the DA. By contrast, just one day later, the CHT plexus is notably narrower. Within the dorsal-ventral dimension, the plexus is shorter compared to at 48 hpf (**Figure 33**). After 3 dpf, the CHT plexus continues to regress until eventually only

the PCV remains. During this morphological transformation, the number of branch points, the total vessel length and the number of endpoints steadily decrease (**Figure 34** and **Figure 35**). These results are consistent with previous work, where it was established that the CHT plexus emerges from the PCV via a process of angiogenic sprouting before 2 dpf and that later it is gradually remodelled down to the definitive PCV [118], [149], [150].

In our study we were able to carefully track the regression of the EC plexus in the CHT within the first two weeks of development. Murayama *et al.* suggested that this process of dorsal-ventral retraction was in part directed by the rostro-caudal extension of the zebrafish tail, taking place throughout the first days of development [118]. We observed that it is in fact a much longer process, however, suggesting there are likely to be other factors, such as cellular and molecular changes, contributing to this phenomenon. However, it is worth mentioning that although the PCV was excluded from our analysis, ECs from the PCV were also GFP positive. Since the CHT plexus emerges originally from the PCV, it is not surprising that the venous ECs comprising the PCV express some of the same genes as sinusoidal CHT ECs. Future studies, however, should further characterize and differentiate the different endothelial cell populations and determine whether some aspects of the niche endothelial program are shared with other endothelial subtypes.

4.6 The Dorso-ventral Retraction of the CHT Plexus Coincides with the Time During which HSPCs Reside in the CHT Niche

Recent work, demonstrating that HSPCs are able to induce active remodelling of the zebrafish perivascular niche upon their arrival [22], prompted us to investigate whether the observed regression of the CHT plexus coincided with the period of time during which HSPCs are found in this region. In this scenario, the arrival and maintenance of HSPCs in the CHT and the remodelling of CHT ECs would be closely related processes.

HSPCs migrate to the CHT for amplification and differentiation, before homing to the kidney marrow and thymus – the adult HSPC niches [118], [147]. At 2 dpf, HSPCs are already detected in the CHT, albeit at low numbers. At this stage, most of the *runx1* positive HSPCs are found within the lumen of the dorsal-most branches, but also many of them are observed to circulate through the DA and enter the CHT plexus (**Figure 38** I **A**). This fact points out that the HSPCs arriving in the CHT derive from the AGM region and colonize the CHT by 2 dpf, as already demonstrated by previous studies [22], [118], [149], [151], [152].

By 3 dpf, HSPCs are mostly located within the intervascular spaces across the plexus (**Figure 38** I **B**). The size of such spaces has significantly decreased compared to what is observed a day earlier (**Figure 33** and **Figure 38**). This might be associated with the fact that HSPCs become tightly wrapped by surrounding CHT ECs once they arrive in the niche, a phenomenon described in the study of Tamplin *et al.*, where ECs were shown to form pockets around HSPCs after their lodgement in the CHT [22]. Also importantly, we hypothesize that the striking regression of the CHT plexus occurring between 2 dpf and 3 dpf might be triggered during or after the colonization of the niche by HSPCs.

Murayama *et al.* observed that the CHT plexus reaches its peak activity by 5-6 dpf [118]. We detected, however, the maximum numbers of HSPCs at 8 dpf. After that, the numbers of HSPCs start decreasing (**Figure 37** and **Figure 39**). Our results suggest that after HSPC lodgement in the CHT, the hematopoietic cell population begins to expand. Throughout the first week of development, HSPCs continue to expand until 8 dpf. Presumably, HSPCs begin to migrate to the definitive niches while they are still expanding in the CHT. HSPC expansion then slows down at or after 8 dpf, and the cell numbers start decreasing progressively until 14 dpf. At this latter stage, little-to-no numbers of HSPCs are detected in the CHT (**Figure 37** and **Figure 39**). We thus think that it can be considered that the CHT niche empties by that time. At the later stages of development, it is possible that the regression of the plexus somehow facilitates the release of HSPCs into the lumen of the PCV. Then, HSPCs will subsequently migrate to the kidney marrow and thymus. This is also consistent with the data obtained from the *in vivo* cell tracing experiments performed by Murayama *et al,* in which they used *gata1:red fluorescent protein (dsred)* (a marker of erythroid cells); *CD41:GFP* (a marker of HSPCs) double transgenics [118]. It is worth stressing, however, that in our experiments we used the *runx1:mCherry* transgenic line. According to recent observations in our laboratory, this line marks more myeloid progenitors than stem cells when compared to the *runx1:GFP* line [22]. Therefore, these experiments could be repeated using the *runx1:GFP* line to more definitively assess whether the *runx1:mCherry* positive cells that remain in the CHT niche during the second week of development are mainly stem cells or are rather lineage-restricted progenitor cells. Additionally, in a future study, a time point between 3 dpf and 8 dpf (e.g., 5 dpf) should be analyzed in order to determine whether the CHT expansion of the hematopoietic cell population occurs either continuously or in different successive waves. Taken together, these experiments demonstrate that the *mrc1a 125 bp:GFP; runx1: mCherry* double transgenics, that have been generated for the first time in our laboratory, are optimal for specifically studying the morphological and cellular dynamics of ECs and HSPCs in the CHT niche.

Lastly, we sought to establish a correlation between the morphological and cellular dynamics observed in the CHT and the CHT endothelial gene expression program. Performing WISH analysis, we observed that the expression of CHT-specific endothelial genes, including *mrc1a*, *gpr182* and *lgmn*, appeared to be down-regulated over time, although it could be detected up to 14 dpf (**Figure 40**). Based on these results, we hypothesized that the downregulation of the CHT endothelial genes might direct in a way the morphological transformation of the CHT plexus, as well as the cellular dynamics in the niche. Our hypothesis was then rooted in the following idea: as long as the niche-specific EC genetic program remains activated in the CHT, this niche will be still optimal for HSPCs. In order to test this hypothesis, we isolated double positive *mrc1a:GFP*; *flk:mCherry* ECs from whole embryos from three different developmental stages (4 dpf, 7 dpf and 14 dpf) and performed RNA-seq on them. After a differential gene analysis between the different stages, we observed that indeed the expression of CHT-enriched genes was downregulated at 7 dpf in comparison with 4 dpf. However, we detected an unexpected upregulation of this set of genes at 14 dpf when compared to 7 dpf, and that the gene expression was thus more similar between 4 dpf and 14 dpf than between 4 dpf and 7 dpf (**Figure 41**). Due to the low number of samples, as well as the lack of biological replicates, it is difficult to draw a clear conclusion from these results, and therefore a repetition of this experiment should be carried out in the future, since the obtained data might be either the result of stochasticity or a consequence of a human error while equalizing index concentration, which might have led to a higher concentration of the 14 dpf-sample and therefore false over-expression of the genes at 14 dpf. In case future experiments showed, however, the same gene expression pattern, that could indicate that a similar niche endothelial genetic program is turned on in the second week of development, presumably in the kidney marrow where we believe a similar gene program might be upregulated. In this scenario, we could surmise that the lower CHT endothelial gene expression, the greater the number of stem cells that will leave the CHT niche to lodge in the kidney marrow. However, this would also challenge our *runx1* positive HSPC cell tracing experiments, in which we determined that the number of HSPCs reach its maximum at 8 dpf. From that, we could also hypothesize that the *runx1* positive HSPCs that we observed might be myeloid progenitors that remain in the CHT rather than stem cells. This will also push the repetition of the HSPC tracing experiments using the *runx1:GFP* line instead, that as previously outlined, has been recently shown to mark more stem cells than progenitor cells.

Bibliography

[1]   J. R. Perlin, A. L. Robertson, and L. I. Zon, "Efforts to enhance blood stem cell engraftment: Recent insights from zebrafish hematopoiesis," *J. Exp. Med.*, Aug. 2017.

[2]   R. Aggarwal, J. Lu, V. J. Pompili, and H. Das, "Hematopoietic Stem Cells: Transcriptional Regulation, Ex Vivo Expansion and Clinical Application," *Curr. Mol. Med.*, vol. 12, no. 1, pp. 34–49, Jan. 2012.

[3]   O. Hequet, "Hematopoietic stem and progenitor cell harvesting: technical advances and clinical utility," *J. Blood Med.*, vol. 6, pp. 55–67, Feb. 2015.

[4]   G. Q. Daley, "The Promise and Perils of Stem Cell Therapeutics," *Cell Stem Cell*, vol. 10, no. 6, pp. 740–749, Jun. 2012.

[5]   C. B. Mahony, R. J. Fish, C. Pasche, and J. Y. Bertrand, "tfec controls the hematopoietic stem cell vascular niche during zebrafish embryogenesis.," *Blood*, vol. 128, no. 10, pp. 1336–1345, Sep. 2016.

[6]   J. Boisset and C. Robin, "On the origin of hematopoietic stem cells : Progress and controversy," *Stem Cell Res.*, pp. 1–13, Jan. 2012.

[7]   N. Pineault and A. Abu-Khader, "Advances in umbilical cord blood stem cell expansion and clinical translation," *Exp. Hematol.*, vol. 43, no. 7, pp. 498–513, Jul. 2015.

[8]   L. Gragert, M. Eapen, E. Williams, J. Freeman, S. Spellman, R. Baitty, R. Hartzman, J. D. Rizzo, M. Horowitz, D. Confer, and M. Maiers, "HLA match likelihoods for hematopoietic stem-cell grafts in the U.S. registry.," *N. Engl. J. Med.*, vol. 371, no. 4, pp. 339–348, Jul. 2014.

[9]   J. R. Perlin, A. Sporrij, and L. I. Zon, "Blood on the tracks : hematopoietic stem cell-endothelial cell interactions in homing and engraftment," *J. Mol. Med.*, vol. 95, no. 8, pp. 809–819, Aug. 2017.

[10]   E. J. Hagedorn, J. R. Perlin, C. Mao, S. E. Redfield, M. L. Daily, S. H. Collins, C. R. D'Amato, R. Riquelme, B. Li, S. J. Wattrus, K. Holler, A. van Oudenaarden, J. P. Junker, and L. I. Zon, "Defining the Transcriptional Code That Specifies Sinusoidal Endothelial Cells in the HSPC Niche," *Blood*, vol. 130, no. Suppl 1, p. 136 LP-136, Dec. 2017.

[11]   J. P. Sasine, K. T. Yeo, and J. P. Chute, "Concise Review: Paracrine Functions of Vascular Niche Cells in Regulating Hematopoietic Stem Cell Fate," *Stem Cells Transl. Med.*, vol. 6, no. 2, pp. 482–489, Feb. 2017.

[12]   B. Waas and I. Maillard, "Fetal hematopoietic stem cells are making waves," *Stem Cell Investig.*, vol. 4, p. 25, Apr. 2017.

[13]   J. L. Galloway and L. I. Zon, "Ontogeny of hematopoiesis: Examining the emergence of hematopoietic cells in the vertebrate embryo," *Curr. Top. Dep. Bio.*, vol. 53, Academic Press, 2003, pp. 139–158.

[14]   E. J. Paik and L. I. Zon, "Hematopoietic development in the zebrafish," *Int. J. Dep. Biol.,* vol. 54, no 6-7. July, pp. 1127–1137, 2010.

[15]   S. H. Orkin and L. I. Zon, "Hematopoiesis: an evolving paradigm for stem cell biology.,"

Cell, vol. 132, no. 4, pp. 631–644, Feb. 2008.

[16] E. Dejana, K. K. Hirschi, and M. Simons, "The molecular basis of endothelial cell plasticity," *Nat. Commun.*, vol. 8, p. 14361, Feb. 2017.

[17] A. Ciau-Uitz, R. Monteiro, A. Kirmizitas, and R. Patient, "Developmental hematopoiesis: Ontogeny, genetic programming and conservation," *Exp. Hematol.*, vol. 42, no. 8, pp. 669–683, Aug. 2014.

[18] P. E. Boulais and P. S. Frenette, "Making sense of hematopoietic stem cell niches," *Blood*, vol. 125, no. 17, pp. 2621–2629, Apr. 2015.

[19] T. V Bowman and L. I. Zon, "Lessons from the Niche for Generation and Expansion of Hematopoietic Stem Cells," *Drug Discov. Today. Ther. Strateg.*, vol. 6, no. 4, pp. 135–140, 2009.

[20] H. K. A. Mikkola and S. H. Orkin, "The journey of developing hematopoietic stem cells," *Development*, vol. 133, no. 19, p. 3733 LP-3744, Oct. 2006.

[21] M. O. Muench and A. Barcena, "Stem cell transplantation in the fetus.," *Cancer Control*, vol. 11, no. 2, pp. 105–118, 2004.

[22] O. J. Tamplin, E. M. Durand, L. A. Carr, S. J. Childs, E. J. Hagedorn, P. Li, A. D. Yzaguirre, N. A. Speck, and L. I. Zon, "Hematopoietic stem cell arrival triggers dynamic remodeling of the perivascular niche," *Cell*, vol. 160, no. 0, pp. 241–252, Jan. 2015.

[23] R. Schofield, "The relationship between the spleen colony-forming cell and the haemopoietic stem cell.," *Blood Cells*, vol. 4, no. 1–2, pp. 7–25, 1978.

[24] S. J. Morrison and D. T. Scadden, "The bone marrow niche for haematopoietic stem cells," *Nature*, vol. 505, no. 7483, pp. 327–334, Jan. 2014.

[25] C. Mazzon, A. Anselmo, J. Cibella, C. Soldani, A. Destro, N. Kim, M. Roncalli, S. J. Burden, M. L. Dustin, A. Sarukhan, and A. Viola, "The critical role of agrin in the hematopoietic stem cell niche," *Blood*, vol. 118, no. 10, pp. 2733–2742, Sep. 2011.

[26] J. Lessard, A. Faubert, and G. Sauvageau, "Genetic programs regulating HSC specification, maintenance and expansion," *Oncogene*, vol. 23, p. 7199, Sep. 2004.

[27] G. S. Travlos, "Normal structure, function, and histology of the bone marrow.," *Toxicol. Pathol.*, vol. 34, no. 5, pp. 548–565, 2006.

[28] I. Beerman, T. C. Luis, S. Singbrant, C. Lo Celso, and S. Mendez-Ferrer, "The evolving view of the hematopoietic stem cell niche.," *Exp. Hematol.*, vol. 50, pp. 22–26, Jun. 2017.

[29] K. Schepers, T. B. Campbell, and E. Passegué, "Normal and Leukemic Stem Cell Niches: Insights and Therapeutic Opportunities," *Cell Stem Cell*, vol. 16, no. 3, pp. 254–267, Mar. 2015.

[30] A. Abarrategi, S. A. Mian, D. Passaro, K. Rouault-Pierre, W. Grey, and D. Bonnet, "Modeling the human bone marrow niche in mice: From host bone marrow engraftment to bioengineering approaches," *J. Exp. Med.*, Feb. 2018.

[31] B. S. Guerrouahen, I. Al-Hijji, and A. R. Tabrizi, "Osteoblastic and vascular endothelial

niches, their control on normal hematopoietic stem cells, and their consequences on the development of leukemia.," *Stem Cells Int.*, vol. 2011, p. 375857, 2011.

[32] J.-P. Lévesque, F. M. Helwani, and I. G. Winkler, "The endosteal 'osteoblastic' niche and its role in hematopoietic stem cell homing and mobilization," *Leukemia*, vol. 24, p. 1979, Sep. 2010.

[33] J. Zhang, C. Niu, L. Ye, H. Huang, X. He, W.-G. Tong, J. Ross, J. Haug, T. Johnson, J. Q. Feng, S. Harris, L. M. Wiedemann, Y. Mishina, and L. Li, "Identification of the haematopoietic stem cell niche and control of the niche size," *Nature*, vol. 425, p. 836, Oct. 2003.

[34] L. M. Calvi, G. B. Adams, K. W. Weibrecht, J. M. Weber, D. P. Olson, M. C. Knight, R. P. Martin, E. Schipani, P. Divieti, F. R. Bringhurst, L. A. Milner, H. M. Kronenberg, and D. T. Scadden, "Osteoblastic cells regulate the haematopoietic stem cell niche," *Nature*, vol. 425, p. 841, Oct. 2003.

[35] Y. D. Ma, C. Park, H. Zhao, K. A. Oduro, X. Tu, F. Long, P. M. Allen, S. L. Teitelbaum, and K. Choi, "Defects in osteoblast function but no changes in long-term repopulating potential of hematopoietic stem cells in a mouse chronic inflammatory arthritis model," *Blood*, vol. 114, no. 20, pp. 4402–4410, Nov. 2009.

[36] C. K. F. Chan, C.-C. Chen, C. A. Luppen, D. L. Kraft, J.-B. Kim, A. DeBoer, K. Wei, and I. L. Weissman, "Endochondral ossification is required for hematopoietic stem cell niche formation," *Nature*, vol. 457, no. 7228, pp. 490–494, Jan. 2009.

[37] Y. Xie, T. Yin, W. Wiegraebe, X. C. He, D. Miller, D. Stark, K. Perko, R. Alexander, J. Schwartz, J. C. Grindley, J. Park, J. S. Haug, J. P. Wunderlich, H. Li, S. Zhang, T. Johnson, R. A. Feldman, and L. Li, "Detection of functional haematopoietic stem cell niche using real-time imaging.," *Nature*, vol. 457, no. 7225, pp. 97–101, Jan. 2009.

[38] N. He, L. Zhang, J. Cui, and Z. Li, "Bone Marrow Vascular Niche: Home for Hematopoietic Stem Cells," *Bone Marrow Res.*, vol. 2014, p. 128436, Apr. 2014.

[39] I.-H. Oh and K.-R. Kwon, "Concise review: multiple niches for hematopoietic stem cell regulations.," *Stem Cells*, vol. 28, no. 7, pp. 1243–1249, Jul. 2010.

[40] M. J. Kiel and S. J. Morrison, "Uncertainty in the niches that maintain haematopoietic stem cells.," *Nat. Rev. Immunol.*, vol. 8, no. 4, pp. 290–301, Apr. 2008.

[41] T. Sugiyama, H. Kohara, M. Noda, and T. Nagasawa, "Maintenance of the hematopoietic stem cell pool by CXCL12-CXCR4 chemokine signaling in bone marrow stromal cell niches.," *Immunity*, vol. 25, no. 6, pp. 977–988, Dec. 2006.

[42] S. Pinho, T. Marchand, E. Yang, Q. Wei, C. Nerlov, and P. S. Frenette, "Lineage-Biased Hematopoietic Stem Cells Are Regulated by Distinct Niches," *Dev. Cell*, vol. 44, no. 5, p. 634–641.e4, Mar. 2018.

[43] H. Mayani, "The regulation of hematopoietic stem cell populations," *F1000Research*, vol. 5, p. F1000 Faculty Rev-1524, Jun. 2016.

[44] H. Mayani, "A Glance into Somatic Stem Cell Biology: Basic Principles, New Concepts, and Clinical Relevance," *Arch. Med. Res.*, vol. 34, no. 1, pp. 3–15, 2003.

[45] T. Morikawa and K. Takubo, "Hypoxia regulates the hematopoietic stem cell niche.," *Pflugers Arch.*, Oct. 2015.

[46] M. G. Bixel, A. P. Kusumbe, S. K. Ramasamy, K. K. Sivaraj, S. Butz, D. Vestweber, and R. H. Adams, "Flow Dynamics and HSPC Homing in Bone Marrow Microvessels," *Cell Rep.*, vol. 18, no. 7, pp. 1804–1816, Feb. 2017.

[47] K. Lam and D.-E. Zhang, "RUNX1 and RUNX1-ETO: roles in hematopoiesis and leukemogenesis," *Front. Biosci.*, vol. 17, pp. 1120–1139, Jan. 2012.

[48] T.-G. Kim, S. Kim, S. Jung, M. Kim, B. Yang, M.-G. Lee, and H.-P. Kim, "CCCTC-binding factor is essential to the maintenance and quiescence of hematopoietic stem cells in mice," *Exp. & Amp; Mol. Med.*, vol. 49, p. e371, Aug. 2017.

[49] C. Lo Celso and D. T. Scadden, "The haematopoietic stem cell niche at a glance," *J. Cell Sci.*, vol. 124, no. 21, p. 3529 LP-3535, Nov. 2011.

[50] I. Park, D. Qian, M. Kiel, M. W. Becker, M. Pihalja, I. L. Weissman, S. J. Morrison, and M. F. Clarke, "Bmi-1 is required for maintenance of adult self-renewing haematopoietic stem cells," *Nature*, vol. 423, p. 302, Apr. 2003.

[51] R. Ferreira, K. Ohneda, M. Yamamoto, and S. Philipsen, "GATA1 Function, a Paradigm for Transcription Factors in Hematopoiesis," *Mol. Cell. Biol.*, vol. 25, no. 4, p. 1215 LP-1227, Feb. 2005.

[52] N. K. Wilson, F. J. Calero-Nieto, R. Ferreira, and B. Göttgens, "Transcriptional regulation of haematopoietic transcription factors," *Stem Cell Res. Ther.*, vol. 2, no. 1, p. 6, Feb. 2011.

[53] Y. Lee, M. Decker, H. Lee, and L. Ding, "Extrinsic regulation of hematopoietic stem cells in development, homeostasis and diseases.," *Wiley Interdiscip. Rev. Dev. Biol.*, vol. 6, no. 5, Sep. 2017.

[54] M. Rehn, A. Olsson, K. Reckzeh, E. Diffner, P. Carmeliet, G. Landberg, and J. Cammenga, "Hypoxic induction of vascular endothelial growth factor regulates murine hematopoietic stem cell function in the low-oxygenic niche.," *Blood*, vol. 118, no. 6, pp. 1534–1543, Aug. 2011.

[55] H.-J. Kwak, P. Liu, B. Bajrami, Y. Xu, S.-Y. Park, C. Nombela-Arrieta, S. Mondal, Y. Sun, H. Zhu, L. Chai, L. E. Silberstein, T. Cheng, and H. R. Luo, "Myeloid cell-derived reactive oxygen species externally regulate the proliferation of myeloid progenitors in emergency granulopoiesis.," *Immunity*, vol. 42, no. 1, pp. 159–171, Jan. 2015.

[56] K. Parmar, P. Mauch, J.-A. Vergilio, R. Sackstein, and J. D. Down, "Distribution of hematopoietic stem cells in the bone marrow according to regional hypoxia.," *Proc. Natl. Acad. Sci. U. S. A.*, vol. 104, no. 13, pp. 5431–5436, Mar. 2007.

[57] Y. Kunisaki, I. Bruns, C. Scheiermann, J. Ahmed, S. Pinho, D. Zhang, T. Mizoguchi, Q. Wei, D. Lucas, K. Ito, J. C. Mar, A. Bergman, and P. S. Frenette, "Arteriolar niches maintain haematopoietic stem cell quiescence," *Nature*, vol. 502, no. 7473, pp. 637–643, Oct. 2013.

[58] N. Urao and M. Ushio-Fukai, "Redox Regulation of Stem/Progenitor Cells and Bone Marrow Niche," *Free Radic. Biol. Med.*, vol. 54, pp. 26–39, Jan. 2013.

[59] L. Adamo, O. Naveiras, P. L. Wenzel, S. McKinney-Freeman, P. J. Mack, J. Gracia-Sancho, A. Suchy-Dicey, M. Yoshimoto, M. W. Lensch, M. C. Yoder, G. García-Cardeña, and G. Q. Daley, "Biomechanical forces promote embryonic

haematopoiesis," *Nature*, vol. 459, no. 7250, pp. 1131–1135, Jun. 2009.

[60]   L. Wang, P. Zhang, Y. Wei, Y. Gao, R. Patient, and F. Liu, "A blood flow-dependent klf2a-NO signaling cascade is required for stabilization of hematopoietic stem cell programming in zebrafish embryos.," *Blood*, vol. 118, no. 15, pp. 4102–4110, Oct. 2011.

[61]   C. Lee-Thedieck and J. P. Spatz, "Biophysical regulation of hematopoietic stem cells," *Biomater. Sci.*, vol. 2, no. 11, pp. 1548–1561, 2014.

[62]   J. Seita, H. Ema, J. Ooehara, S. Yamazaki, Y. Tadokoro, A. Yamasaki, K. Eto, S. Takaki, K. Takatsu, and H. Nakauchi, "Lnk negatively regulates self-renewal of hematopoietic stem cells by modifying thrombopoietin-mediated signal transduction.," *Proc. Natl. Acad. Sci. U. S. A.*, vol. 104, no. 7, pp. 2349–2354, Feb. 2007.

[63]   S. Coskun and K. K. Hirschi, "Establishment and Regulation of the HSC Niche: Roles of Osteoblastic and Vascular Compartments," *Birth Defects Res. C. Embryo Today*, vol. 90, no. 4, pp. 229–242, Dec. 2010.

[64]   M. J. Kiel, G. L. Radice, and S. J. Morrison, "Lack of evidence that hematopoietic stem cells depend on N-cadherin-mediated adhesion to osteoblasts for their maintenance.," *Cell Stem Cell*, vol. 1, no. 2, pp. 204–217, Aug. 2007.

[65]   S. Lymperi, N. Horwood, S. Marley, M. Y. Gordon, A. P. Cope, and F. Dazzi, "Strontium can increase some osteoblasts without increasing hematopoietic stem cells.," *Blood*, vol. 111, no. 3, pp. 1173–1181, Feb. 2008.

[66]   L. M. Calvi, O. Bromberg, Y. Rhee, J. M. Weber, J. N. P. Smith, M. J. Basil, B. J. Frisch, and T. Bellido, "Osteoblastic expansion induced by parathyroid hormone receptor signaling in murine osteocytes is not sufficient to increase hematopoietic stem cells.," *Blood*, vol. 119, no. 11, pp. 2489–2499, Mar. 2012.

[67]   C. Nombela-Arrieta, G. Pivarnik, B. Winkel, K. J. Canty, B. Harley, J. E. Mahoney, S.-Y. Park, J. Lu, A. Protopopov, and L. E. Silberstein, "Quantitative imaging of haematopoietic stem and progenitor cell localization and hypoxic status in the bone marrow microenvironment.," *Nat. Cell Biol.*, vol. 15, no. 5, pp. 533–543, May 2013.

[68]   M. J. Kiel, O. H. Yilmaz, T. Iwashita, O. H. Yilmaz, C. Terhorst, and S. J. Morrison, "SLAM family receptors distinguish hematopoietic stem and progenitor cells and reveal endothelial niches for stem cells.," *Cell*, vol. 121, no. 7, pp. 1109–1121, Jul. 2005.

[69]   S. Mendez-Ferrer, T. V Michurina, F. Ferraro, A. R. Mazloom, B. D. Macarthur, S. A. Lira, D. T. Scadden, A. Ma'ayan, G. N. Enikolopov, and P. S. Frenette, "Mesenchymal and haematopoietic stem cells form a unique bone marrow niche.," *Nature*, vol. 466, no. 7308, pp. 829–834, Aug. 2010.

[70]   N. Mukaida, Y. Tanabe, and T. Baba, "Chemokines as a Conductor of Bone Marrow Microenvironment in Chronic Myeloid Leukemia.," *Int. J. Mol. Sci.*, vol. 18, no. 8, Aug. 2017.

[71]   C. Michiels, "Endothelial cell functions.," *J. Cell. Physiol.*, vol. 196, no. 3, pp. 430–443, Sep. 2003.

[72]   M. K. Pugsley and R. Tabrizchi, "The vascular system. An overview of structure and

function.," *J. Pharmacol. Toxicol. Methods*, vol. 44, no. 2, pp. 333–340, 2000.

[73] D. J. Nolan, M. Ginsberg, E. Israely, B. Palikuqi, M. G. Poulos, D. James, B.-S. Ding, W. Schachterle, Y. Liu, Z. Rosenwaks, J. M. Butler, J. Xiang, A. Rafii, K. Shido, S. Y. Rabbany, O. Elemento, and S. Rafii, "Molecular signatures of tissue-specific microvascular endothelial cell heterogeneity in organ maintenance and regeneration.," *Dev. Cell*, vol. 26, no. 2, pp. 204–219, Jul. 2013.

[74] N. G. dela Paz and P. A. D'Amore, "Arterial versus venous endothelial cells," *Cell Tissue Res.*, vol. 335, no. 1, pp. 5–16, Jan. 2009.

[75] B. Li, A. S. Bailey, S. Jiang, B. Liu, D. C. Goldman, and W. H. Fleming, "Endothelial cells mediate the regeneration of hematopoietic stem cells," *Stem Cell Res.*, vol. 4, no. 1, pp. 17–24, Jan. 2010.

[76] S. Shahrabi, H. Rezaeeyan, A. Ahmadzadeh, M. Shahjahani, and N. Saki, "Bone Marrow Blood Vessels: Normal and Neoplastic Niche," *Oncol. Rev.*, vol. 10, no. 2, p. 306, Oct. 2016.

[77] S. K. Ramasamy, "Structure and Functions of Blood Vessels and Vascular Niches in Bone," *Stem Cells Int.*, vol. 2017, p. 5046953, Sep. 2017.

[78] S. Inoue and D. G. Osmond, "Basement membrane of mouse bone marrow sinusoids shows distinctive structure and proteoglycan composition: a high resolution ultrastructural study.," *Anat. Rec.*, vol. 264, no. 3, pp. 294–304, Nov. 2001.

[79] K. B. Schoedel, M. N. F. Morcos, T. Zerjatke, I. Roeder, T. Grinenko, D. Voehringer, J. R. Gothert, C. Waskow, A. Roers, and A. Gerbaulet, "The bulk of the hematopoietic stem cell population is dispensable for murine steady-state and stress hematopoiesis.," *Blood*, vol. 128, no. 19, pp. 2285–2296, Nov. 2016.

[80] M. Zhao and L. Li, "Dissecting the bone marrow HSC niches," *Cell Res.*, vol. 26, p. 975, Jun. 2016.

[81] T. Itkin, S. Gur-Cohen, J. A. Spencer, A. Schajnovitz, S. K. Ramasamy, A. P. Kusumbe, G. Ledergor, Y. Jung, I. Milo, M. G. Poulos, A. Kalinkovich, A. Ludin, K. Golan, E. Khatib, A. Kumari, O. Kollet, G. Shakhar, J. M. Butler, S. Rafii, R. H. Adams, D. T. Scadden, C. P. Lin, and T. Lapidot, "Distinct bone marrow blood vessels differentially regulate haematopoiesis," *Nature*, vol. 532, p. 323, Apr. 2016.

[82] A. O. Sahin and M. Buitenhuis, "Molecular mechanisms underlying adhesion and migration of hematopoietic stem cells," *Cell Adh. Migr.*, vol. 6, no. 1, pp. 39–48, Jan. 2012.

[83] R. Tamma and D. Ribatti, "Bone Niches, Hematopoietic Stem Cells, and Vessel Formation," *Int. J. Mol. Sci.*, vol. 18, no. 1, p. 151, Jan. 2017.

[84] I. G. Winkler, V. Barbier, B. Nowlan, R. N. Jacobsen, C. E. Forristal, J. T. Patton, J. L. Magnani, and J.-P. Levesque, "Vascular niche E-selectin regulates hematopoietic stem cell dormancy, self renewal and chemoresistance.," *Nat. Med.*, vol. 18, no. 11, pp. 1651–1657, Nov. 2012.

[85] Y.-S. Tzeng, H. Li, Y.-L. Kang, W.-C. Chen, W.-C. Cheng, and D.-M. Lai, "Loss of Cxcl12/Sdf-1 in adult mice decreases the quiescent state of hematopoietic stem/progenitor cells and alters the pattern of hematopoietic regeneration after

myelosuppression.," *Blood*, vol. 117, no. 2, pp. 429–439, Jan. 2011.

[86] L. Yao, T. Yokota, L. Xia, P. W. Kincade, and R. P. McEver, "Bone marrow dysfunction in mice lacking the cytokine receptor gp130 in endothelial cells.," *Blood*, vol. 106, no. 13, pp. 4093–4101, Dec. 2005.

[87] L. Ding, T. L. Saunders, G. Enikolopov, and S. J. Morrison, "Endothelial and perivascular cells maintain haematopoietic stem cells.," *Nature*, vol. 481, no. 7382, pp. 457–462, Jan. 2012.

[88] L. Lamalice, F. Le Boeuf, and J. Huot, "Endothelial cell migration during angiogenesis.," *Circ. Res.*, vol. 100, no. 6, pp. 782–794, Mar. 2007.

[89] D. Kanz, M. Konantz, E. Alghisi, T. E. North, and C. Lengerke, "Endothelial-to-hematopoietic transition: Notch-ing vessels into blood.," *Ann. N. Y. Acad. Sci.*, vol. 1370, no. 1, pp. 97–108, Apr. 2016.

[90] J. M. Vieira, C. Ruhrberg, and Q. Schwarz, "VEGF receptor signaling in vertebrate development," *Organogenesis*, vol. 6, no. 2, pp. 97–106, Apr. 2010.

[91] H. Ishitobi, A. Wakamatsu, F. Liu, T. Azami, M. Hamada, K. Matsumoto, H. Kataoka, M. Kobayashi, K. Choi, S. Nishikawa, S. Takahashi, and M. Ema, "Molecular basis for Flk1 expression in hemato-cardiovascular progenitors in the mouse," *Development*, vol. 138, no. 24, pp. 5357–5368, Dec. 2011.

[92] J. E. Fish and J. D. Wythe, "The molecular regulation of arteriovenous specification and maintenance.," *Dev. Dyn.*, vol. 244, no. 3, pp. 391–409, Mar. 2015.

[93] G. Wei, R. Srinivasan, C. Z. Cantemir-Stone, S. M. Sharma, R. Santhanam, M. Weinstein, N. Muthusamy, A. K. Man, R. G. Oshima, G. Leone, and M. C. Ostrowski, "Ets1 and Ets2 are required for endothelial cell survival during embryonic angiogenesis," *Blood*, vol. 114, no. 5, pp. 1123–1130, Jul. 2009.

[94] C.-X. Xu, T.-J. Lee, N. Sakurai, K. Krchma, F. Liu, D. Li, T. Wang, and K. Choi, "ETV2/ER71 regulates hematopoietic regeneration by promoting hematopoietic stem cell proliferation," *J. Exp. Med.*, Apr. 2017.

[95] S. Sumanas and S. Lin, "Ets1-related protein is a key regulator of vasculogenesis in zebrafish.," *PLoS Biol.*, vol. 4, no. 1, p. e10, Jan. 2006.

[96] M. C. Salanga, S. M. Meadows, C. T. Myers, and P. A. Krieg, "The ETS family protein, ETV2, is required for initiation of the endothelial lineage but not the hematopoietic lineage in the Xenopus embryo," *Dev. Dyn.*, vol. 239, no. 4, pp. 1178–1187, Apr. 2010.

[97] S. De Val, N. C. Chi, S. M. Meadows, S. Minovitsky, J. P. Anderson, I. S. Harris, M. L. Ehlers, P. Agarwal, A. Visel, S.-M. Xu, L. A. Pennacchio, I. Dubchak, P. A. Krieg, D. Y. R. Stainier, and B. L. Black, "Combinatorial regulation of endothelial gene expression by ets and forkhead transcription factors.," *Cell*, vol. 135, no. 6, pp. 1053–1064, Dec. 2008.

[98] S. De Val and B. L. Black, "Transcriptional Control of Endothelial Cell Development," *Dev. Cell*, vol. 16, no. 2, pp. 180–195, Feb. 2009.

[99] H. Kang, W.-T. Mesquitta, H. S. Jung, O. V Moskvin, J. A. Thomson, and I. I. Slukvin, "GATA2 Is Dispensable for Specification of Hemogenic Endothelium but Promotes Endothelial-to-Hematopoietic Transition," *Stem Cell Reports*, vol. 11, no. 1, pp. 197–

211, 2018.

[100] B. Park, K. H. Yoo, and C. Kim, "Hematopoietic stem cell expansion and generation : the ways to make a breakthrough," vol. 50, no. 4, 2015.

[101] S. Kumar and H. Geiger, "HSC Niche Biology and HSC Expansion Ex Vivo," *Trends Mol. Med.*, vol. 23, no. 9, pp. 799–819, Sep. 2017.

[102] N. Li, A. Eljaafari, D. Bensoussan, Y. Wang, V. Latger-Cannard, B. Serrurier, C. Boura, A. Kennel, J. Stoltz, and P. Feugier, "Human umbilical vein endothelial cells increase ex vivo expansion of human CD34(+) PBPC through IL-6 secretion.," *Cytotherapy*, vol. 8, no. 4, pp. 335–342, 2006.

[103] S. T. Avecilla, K. Hattori, B. Heissig, R. Tejada, F. Liao, K. Shido, D. K. Jin, S. Dias, F. Zhang, T. E. Hartman, N. R. Hackett, R. G. Crystal, L. Witte, D. J. Hicklin, P. Bohlen, D. Eaton, D. Lyden, F. de Sauvage, and S. Rafii, "Chemokine-mediated interaction of hematopoietic progenitors with the bone marrow vascular niche is required for thrombopoiesis.," *Nat. Med.*, vol. 10, no. 1, pp. 64–71, Jan. 2004.

[104] C. C. Zhang and H. F. Lodish, "Cytokines regulating hematopoietic stem cell function," *Curr. Opin. Hematol.*, vol. 15, no. 4, pp. 307–311, Jul. 2008.

[105] A. T. Hooper, J. M. Butler, D. J. Nolan, A. Kranz, K. Iida, M. Kobayashi, H.-G. Kopp, K. Shido, I. Petit, K. Yanger, D. James, L. Witte, Z. Zhu, Y. Wu, B. Pytowski, Z. Rosenwaks, V. Mittal, T. N. Sato, and S. Rafii, "Engraftment and reconstitution of hematopoiesis is dependent on VEGFR2-mediated regeneration of sinusoidal endothelial cells.," *Cell Stem Cell*, vol. 4, no. 3, pp. 263–274, Mar. 2009.

[106] A. Mendelson and P. S. Frenette, "Hematopoietic stem cell niche maintenance during homeostasis and regeneration," *Nat. Med.*, vol. 20, no. 8, pp. 833–846, Aug. 2014.

[107] H. J. Lee, N. Li, S. M. Evans, M. F. Diaz, and P. L. Wenzel, "Biomechanical force in blood development: extrinsic physical cues drive pro-hematopoietic signaling," *Differentiation.*, vol. 86, no. 3, pp. 92–103, Oct. 2013.

[108] H. Kobayashi, J. M. Butler, R. O'Donnell, M. Kobayashi, B.-S. Ding, B. Bonner, V. K. Chiu, D. J. Nolan, K. Shido, L. Benjamin, and S. Rafii, "Angiocrine factors from Akt-activated endothelial cells balance self-renewal and differentiation of haematopoietic stem cells," *Nat. Cell Biol.*, vol. 12, no. 11, pp. 1046–1056, Nov. 2010.

[109] M. Simons, E. Gordon, and L. Claesson-Welsh, "Mechanisms and regulation of endothelial VEGF receptor signalling.," *Nat. Rev. Mol. Cell Biol.*, vol. 17, no. 10, pp. 611–625, Oct. 2016.

[110] T. Kai and A. Spradling, "An empty Drosophila stem cell niche reactivates the proliferation of ectopic cells," *Proc. Natl. Acad. Sci. U. S. A.*, vol. 100, no. 8, pp. 4633–4638, Apr. 2003.

[111] A. A. Kiger, D. L. Jones, C. Schulz, M. B. Rogers, and M. T. Fuller, "Stem Cell Self-Renewal Specified by JAK-STAT Activation in Response to a Support Cell Cue," *Science (80-.).*, vol. 294, no. 5551, p. 2542 LP-2545, Dec. 2001.

[112] V. Silva-Vargas, C. Lo Celso, A. Giangreco, T. Ofstad, D. M. Prowse, K. M. Braun, and F. M. Watt, "β-Catenin and Hedgehog Signal Strength Can Specify Number and Location of Hair Follicles in Adult Epidermis without Recruitment of Bulge Stem Cells,"

Dev. Cell, vol. 9, no. 1, pp. 121–131, 2005.

[113] S. Coşkun, H. Chao, H. Vasavada, K. Heydari, N. Gonzales, X. Zhou, B. de Crombrugghe, and K. K. Hirschi, "Development of the fetal bone marrow niche and regulation of HSC quiescence and homing ability by emerging osteolineage cells," *Cell Rep.*, vol. 9, no. 2, pp. 581–590, Oct. 2014.

[114] A. Oda, T. Tezuka, Y. Ueno, S. Hosoda, Y. Amemiya, C. Notsu, T. Kasahara, C. Nishiyama, and R. Goitsuka, "Niche-induced extramedullary hematopoiesis in the spleen is regulated by the transcription factor Tlx1," *Sci. Rep.*, vol. 8, no. 1, p. 8308, 2018.

[115] E. E. Patton and L. I. Zon, "The art and design of genetic screens: zebrafish.," *Nat. Rev. Genet.*, vol. 2, no. 12, pp. 956–966, Dec. 2001.

[116] C. B. Kimmel, W. W. Ballard, S. R. Kimmel, B. Ullmann, and T. F. Schilling, "Stages of embryonic development of the zebrafish.," *Dev. Dyn.*, vol. 203, no. 3, pp. 253–310, Jul. 1995.

[117] A. T. Chen and L. I. Zon, "Zebrafish blood stem cells.," *J. Cell. Biochem.*, vol. 108, no. 1, pp. 35–42, Sep. 2009.

[118] E. Murayama, K. Kissa, A. Zapata, E. Mordelet, V. Briolat, H.-F. Lin, R. I. Handin, and P. Herbomel, "Tracing Hematopoietic Precursor Migration to Successive Hematopoietic Organs during Zebrafish Development," *Immunity*, vol. 25, no. 6, pp. 963–975, 2006.

[119] S. Higashijima, "Transgenic zebrafish expressing fluorescent proteins in central nervous system neurons.," *Dev. Growth Differ.*, vol. 50, no. 6, pp. 407–413, Aug. 2008.

[120] J. P. Junker, E. S. Noël, V. Guryev, K. A. Peterson, G. Shah, J. Huisken, A. P. McMahon, E. Berezikov, J. Bakkers, and A. van Oudenaarden, "Genome-wide RNA Tomography in the Zebrafish Embryo," *Cell*, vol. 159, no. 3, pp. 662–675, 2014.

[121] J. Buenrostro, B. Wu, H. Chang, and W. Greenleaf, "ATAC-seq: A Method for Assaying Chromatin Accessibility Genome-Wide," *Curr. Protoc. Mol. Biol.*, vol. 109, p. 21.29.1-21.29.9, Jan. 2015.

[122] W. Krebs, S. V Schmidt, A. Goren, D. De Nardo, L. Labzin, A. Bovier, T. Ulas, H. Theis, M. Kraut, E. Latz, M. Beyer, and J. L. Schultze, "Optimization of transcription factor binding map accuracy utilizing knockout-mouse models," *Nucleic Acids Res.*, vol. 42, no. 21, pp. 13051–13060, Dec. 2014.

[123] J. N. Rosen, M. F. Sweeney, and J. D. Mably, "Microinjection of Zebrafish Embryos to Analyze Gene Function," *J. Vis. Exp.*, no. 25, p. 1115, Mar. 2009.

[124] V. N. Pham, N. D. Lawson, J. W. Mugford, L. Dye, D. Castranova, B. Lo, and B. M. Weinstein, "Combinatorial function of ETS transcription factors in the developing vasculature," *Dev. Biol.*, vol. 303, no. 2, pp. 772–783, Mar. 2007.

[125] C. T. Nguyen, Q. Lu, Y. Wang, and J.-N. Chen, "Zebrafish as a model for cardiovascular development and disease," *Drug Discov. Today. Dis. Models*, vol. 5, no. 3, pp. 135–140, 2008.

[126] C. Thisse and B. Thisse, "High-resolution in situ hybridization to whole-mount

zebrafish embryos," *Nat. Protoc.*, vol. 3, p. 59, Dec. 2007.

[127] S. Lee, C. Park, J. W. Han, J. Y. Kim, K. Cho, E. J. Kim, S. Kim, S.-J. Lee, S. Y. Oh, Y. Tanaka, I.-H. Park, H. J. An, C. M. Shin, S. Sharma, and Y.-S. Yoon, "Direct Reprogramming of Human Dermal Fibroblasts Into Endothelial Cells Using ER71/ETV2.," *Circ. Res.*, vol. 120, no. 5, pp. 848–861, Mar. 2017.

[128] R. Morita, M. Suzuki, H. Kasahara, N. Shimizu, T. Shichita, T. Sekiya, A. Kimura, K. Sasaki, H. Yasukawa, and A. Yoshimura, "ETS transcription factor ETV2 directly converts human fibroblasts into functional endothelial cells.," *Proc. Natl. Acad. Sci. U. S. A.*, vol. 112, no. 1, pp. 160–165, Jan. 2015.

[129] S. Cermenati, S. Moleri, S. Cimbro, P. Corti, L. Del Giacco, R. Amodeo, E. Dejana, P. Koopman, F. Cotelli, and M. Beltrame, "Sox18 and Sox7 play redundant roles in vascular development.," *Blood*, vol. 111, no. 5, pp. 2657–2666, Mar. 2008.

[130] M. R. Swift, V. N. Pham, D. Castranova, K. Bell, R. J. Poole, and B. M. Weinstein, "SoxF factors and Notch regulate nr2f2 gene expression during venous differentiation in zebrafish.," *Dev. Biol.*, vol. 390, no. 2, pp. 116–125, Jun. 2014.

[131] G. Costa, A. Mazan, A. Gandillet, S. Pearson, G. Lacaud, and V. Kouskoff, "SOX7 regulates the expression of VE-cadherin in the haemogenic endothelium at the onset of haematopoietic development," *Development*, vol. 139, no. 9, p. 1587 LP-1598, May 2012.

[132] X. Cui, Y. W. Lu, V. Lee, D. Kim, T. Dorsey, Q. Wang, Y. Lee, P. Vincent, J. Schwarz, and G. Dai, "Venous Endothelial Marker COUP-TFII Regulates the Distinct Pathologic Potentials of Adult Arteries and Veins," *Sci. Rep.*, vol. 5, p. 16193, Nov. 2015.

[133] S. D. Tran and B. H. Nguyen, "Human umbilical cord blood hematopoietic stem cell expansion by the RNA-binding protein Musashi-2.," *Oral Dis.*, vol. 23, no. 5, pp. 548–550, Jul. 2017.

[134] C. Park, T. M. Kim, and A. B. Malik, "Transcriptional Regulation oa Endothelial Cell And Vascular Development," *Circ. Res.*, vol. 112, no. 10, pp. 1380–1400, May 2013.

[135] K. S. Wong, K. Proulx, M. S. Rost, and S. Sumanas, "Identification of vasculature-specific genes by microarray analysis of Etsrp/Etv2 overexpressing zebrafish embryos.," *Dev. Dyn.*, vol. 238, no. 7, pp. 1836–1850, Jul. 2009.

[136] M. B. Veldman, C. Zhao, G. A. Gomez, A. G. Lindgren, H. Huang, H. Yang, S. Yao, B. L. Martin, D. Kimelman, and S. Lin, "Transdifferentiation of fast skeletal muscle into functional endothelium in vivo by transcription factor Etv2.," *PLoS Biol.*, vol. 11, no. 6, p. e1001590, 2013.

[137] C. E. Love and V. E. Prince, "Expression and retinoic acid regulation of the zebrafish nr2f orphan nuclear receptor genes," *Dev. Dyn.*, vol. 241, no. 10, pp. 1603–1615, Oct. 2012.

[138] A. Rada-Iglesias, R. Bajpai, S. Prescott, S. Brugmann, T. Swigut, and J. Wysocka, "Epigenomic annotation of enhancers predicts transcriptional regulators of human neural crest," *Cell Stem Cell*, vol. 11, no. 5, pp. 633–648, Nov. 2012.

[139] F. Liu, D. Li, Y. Y. L. Yu, I. Kang, M.-J. Cha, J. Y. Kim, C. Park, D. K. Watson, T. Wang, and K. Choi, "Induction of hematopoietic and endothelial cell program

orchestrated by ETS transcription factor ER71/ETV2.," *EMBO Rep.*, vol. 16, no. 5, pp. 654–669, May 2015.

[140] T. L. Rasmussen, J. Kweon, M. A. Diekmann, F. Belema-Bedada, Q. Song, K. Bowlin, X. Shi, A. Ferdous, T. Li, M. Kyba, J. M. Metzger, N. Koyano-Nakagawa, and D. J. Garry, "ER71 directs mesodermal fate decisions during embryogenesis," *Development*, vol. 138, no. 21, pp. 4801–4812, Nov. 2011.

[141] X. Shi, K. M. Zirbes, T. L. Rasmussen, A. Ferdous, M. G. Garry, N. Koyano-Nakagawa, and D. J. Garry, "The transcription factor Mesp1 interacts with cAMP-responsive element binding protein 1 (Creb1) and coactivates Ets variant 2 (Etv2) gene expression.," *J. Biol. Chem.*, vol. 290, no. 15, pp. 9614–9625, Apr. 2015.

[142] S. J. Tapscott, "The circuitry of a master switch: Myod and the regulation of skeletal muscle gene transcription.," *Development*, vol. 132, no. 12, pp. 2685–2695, Jun. 2005.

[143] Y. Kanki, R. Nakaki, T. Shimamura, T. Matsunaga, K. Yamamizu, S. Katayama, J. Suehiro, T. Osawa, H. Aburatani, T. Kodama, Y. Wada, J. K. Yamashita, and T. Minami, "Dynamically and epigenetically coordinated GATA/ETS/SOX transcription factor expression is indispensable for endothelial cell differentiation," *Nucleic Acids Res.*, vol. 45, no. 8, pp. 4344–4358, May 2017.

[144] A. Mayran and J. Drouin, "Pioneer transcription factors shape the epigenetic landscape.," *J. Biol. Chem.*, vol. 293, no. 36, pp. 13795–13804, Sep. 2018.

[145] N. Koyano-Nakagawa, X. Shi, T. L. Rasmussen, S. Das, C. A. Walter, and D. J. Garry, "Feedback Mechanisms Regulate Ets Variant 2 (Etv2) Gene Expression and Hematoendothelial Lineages.," *J. Biol. Chem.*, vol. 290, no. 47, pp. 28107–28119, Nov. 2015.

[146] S. Chien, S. Li, and Y. J. Shyy, "Effects of mechanical forces on signal transduction and gene expression in endothelial cells.," *Hypertens. (Dallas, Tex. 1979)*, vol. 31, no. 1 Pt 2, pp. 162–169, Jan. 1998.

[147] J. N. Topper and M. A. J. Gimbrone, "Blood flow and vascular gene expression: fluid shear stress as a modulator of endothelial phenotype.," *Mol. Med. Today*, vol. 5, no. 1, pp. 40–46, Jan. 1999.

[148] C. L. Winata, S. Korzh, I. Kondrychyn, V. Korzh, and Z. Gong, "The role of vasculature and blood circulation in zebrafish swimbladder development," *BMC Dev. Biol.*, vol. 10, p. 3, Jan. 2010.

[149] S. Isogai, M. Horiguchi, and B. M. Weinstein, "The Vascular Anatomy of the Developing Zebrafish: An Atlas of Embryonic and Early Larval Development," *Dev. Biol.*, vol. 230, no. 2, pp. 278–301, 2001.

[150] K. Mouillesseaux and J.-N. Chen, "Mutation in utp15 disrupts vascular patterning in a p53-dependent manner in zebrafish embryos.," *PLoS One*, vol. 6, no. 9, p. e25013, 2011.

[151] J. Y. Bertrand, A. D. Kim, S. Teng, and D. Traver, "CD41(+) c-myb(+) precursors colonize the zebrafish pronephros by a novel migration route to initiate adult hematopoiesis," *Development*, vol. 135, no. 10, pp. 1853–1862, May 2008.

[152] J.-C. Boisset, W. van Cappellen, C. Andrieu-Soler, N. Galjart, E. Dzierzak, and C. Robin, "In vivo imaging of haematopoietic cells emerging from the mouse aortic endothelium.," *Nature*, vol. 464, no. 7285, pp. 116–120, Mar. 2010.

List of Figures

List of Tables

List of Abbreviations

AGM	Aorta-Gonad Mesonephros
Akt1	AKT Serine/Threonine Kinase 1
ANGPT1	Angiopoietin 1
AP	Alkaline Phosphatase
AV	ArterioVenous
ATAC-seq	Assay for Transposase-Accessible Chromatin with Sequencing
Bcl-xL	B-Cell Lymphoma-eXtra Large
BCIP	5-Bromo-4-Chloro-3-Indolyl-Phosphate
BM	Bone Marrow
BMI-1	B lymphoma Mo-MLV Insertion region 1 homolog
BMP	Bone Morphogenetic Protein
BSA	Bovine Serum Albumin
CAR	CXCL12-Abundant Reticular
CFU-S	Spleen Colony-Forming Cells
CD34	Cluster of Differentiation 34 antigen
CHT	Caudal Hematopoietic Tissue
DA	Dorsal Aorta
ddH$_2$O	Distilled Water
DEPC	DiEthylPyroCarbonate
DIC	Differential Interference Contrast
DMSO	DiMethyl SulfOxide
dNTPs	DeoxyNucleotide TriPhosphates
DPP	DecaPentaPlegic
dpf	Days Post Fertilization
dsred	Red Fluorescent Protein
EC(s)	Endothelial Cell(s)
ECM	ExtraCellular Matrix
EHT	Endothelial-to-Hemtopoietic cell transition
EPO	ErytroPOietin
ETV2	Ets Translocation Variant 2
ETS	E26 Transformation-Specific
FACS	Fluorescent-Activated Cell Sorting
FBS	Fetal Bovine Serum
FPKM	Fragments Per Kilobase of transcript per Million mapped reads
Flk-1	Fetal Liver Kinase-1
Fli-1	Friend Leukemia Virus Integration-1
FOX	Forkhead Box
GATA-2	GATA binding factor-2
gDNA	Genomic DNA
G-CSF	Granulocyte-Colony Stimulating Factor
GFP	Green Fluorescent Protein
Gp130	GlycoProtein 130
Gpr182	G Protein-coupled Receptor 182
GR	Green Red
hpf	Hours Post Fertilization
HSC(s)	Hematopoietic Stem Cell(s)
HSPC(s)	Hematopoietic Stem and Progenitor Cell(s)
hsp70l	Heat Shock cognate 70-kd Protein, Like
HUVEC(s)	Human Umbilical Vein Endothelial Cell(s)
Hyb+/Hyb-	Hybridization solution/ Hybridization Negative solution
HOMER	Hypergeometric Optimization of Motif EnRichment
IL	Interleukin
JS	Jensen-Shannon
KDR	Kinase insert Domain Receptor

KITL	Kit Ligand
LB	Luria Bertani
LepR	Leptin Receptor
lgmn	Legumain
LMO2	LiM domain Only 2
LPA	Linear PolyAcrylamide
LT	Long-Term
mrc1a	Mannose Receptor C type 1a
mTOR	Mammalian Target of Rapamycin
MPPs	Multipotent Progenitors
NBT	NitroBlue Tetrazolium chloride
NCC	Neural Crest Cells
NEB	T4 DNA ligase
NH	Nuclear Hormone
NO	Nitric Oxid
NR2F2	Nuclear Receptor subfamily 2, group F, member 2
NRT	No Reverse Transcriptase
n/a	Not Applicable
OPN	Osteopontin
ORF	Open Reading Frame
OSX	Osterix
PAS	Para-Aortic Splanchnopleura
PBS	Phosphate Buffered Saline
PBTw	PBS-Tween20
PcG	PolyComb Group
PDGFRα	Platelet-Derived Growth Factor Receptor α
PCR	Polymerase Chain Reaction
PCV	Posterior Caudal Vein
PFA	Paraformaldehyde
PI3K	PhosphoInositide 3-kinase
PSGL-1	P-Selectin Glycoprotein Ligand-1
PTH	ParaThyroid Hormone
PTHrP	PTH-Related Peptide
RIN	RNA Integrity Number
RNA-seq	RNA sequencing
ROS	Reactive Oxygen Species
Runx1	Runt Related Transcription Factor
Sca-1	Stem Cell Antigen-1
SCF	Stem Cell Factor
Scl	Stem Cell Leukemia
SDCM	Spinning Disk Confocal Microscopy
SDF-1	Stromal-Derived Factor-1
sele	selectin-e
SHH	Sonic HedgeHog
SOX	SRY-box
SSC	Saline Sodium Citrate
SSCTw	SSC-Tween20
TAE	Tris-Acetate-EDTA
TF(s)	Transcription Factor(s)
tlx1	T Cell Leukemia Homeobox
TPO	Thrombopoietin
VE	Vascular Endothelial
VEGF	Vascular Endothelial Growth Factor
WISH	Whole-mount In Situ Hybridization
WT	Wild Type

Appendix A: Supplementary Information

SI.1. Generation of Transgenic Zebrafish

Before I joined the laboratory, in order to label the CHT EC population *in vivo*, stable transgenic zebrafish lines expressing *mrc1a 125 bp*: GFP and *sele 158 bp*: GFP were generated. Briefly, DNA constructs were first built by coupling these enhancer regions to a minimal beta-globin promoter fused to the coding region of GFP using the Tol2 Gateway cloning technology. A solution of each DNA construct, prepared in nuclease-free water (25 ng/μl), was co-injected along with the Tol2 mRNA transposase (Tol2 mRNA; 25 ng/μl) into one-cell stage embryos. Injected embryos were screened for GFP expression, hence germline transmission, at 48-72 hpf. Embryos that showed specific expression of GFP in the CHT region were sorted out and raised to adulthood (3 months). After crossing to WT fish, transgenic founders (F0) were identified and isolated by the presence of GFP expression in the filial 1 (F1) progeny. GFP expression in the F1 fish proved that the DNA constructs were integrated into the zebrafish genome. F1 generation fish that showed GFP positive expression in the CHT were interbred to produce a homozygous F2 generation. In the experiments performed for this thesis work, we generally used founder and F1 zebrafish.
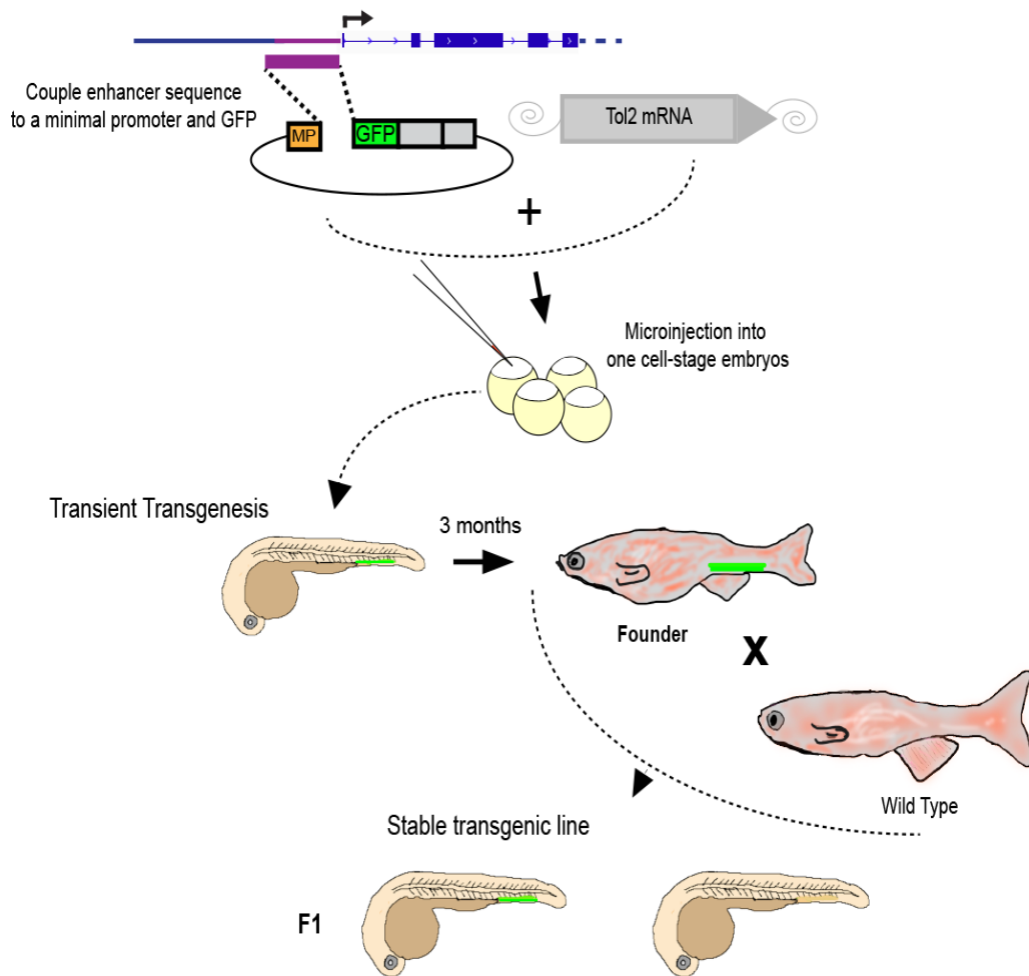
Fig S1. Generation of transgenic zebrafish lines using Tol2 Gateway cloning technology.
Transgenic zebrafish lines expressing *mrc1a 125 bp: GFP* and *sele 158 bp: GFP* were generated. At
the first step, the constructs were created, in which the enhancer region of either *mrc1a* (125 bp) or
sele (158 bp) was cloned downstream to the minimal beta-globin promoter and fused to the coding
region of GFP. The DNA constructs and the mRNA encoding for Tol2 transposase were microinjected
into one cell-stage zebrafish embryos. The founder fish – those that showed GFP expression in the
CHT – were mated with WT fish when they reached the adulthood (from 3 months on). Approximately
half of the progeny derived from these crosses in the F1 presented GFP positive CHT ECs as well
(MP, Minimal Promoter; GFP, Green Fluorescent Protein; F1, Filial 1).

SI.2. FACS Analysis of Whole Zebrafish Embryos
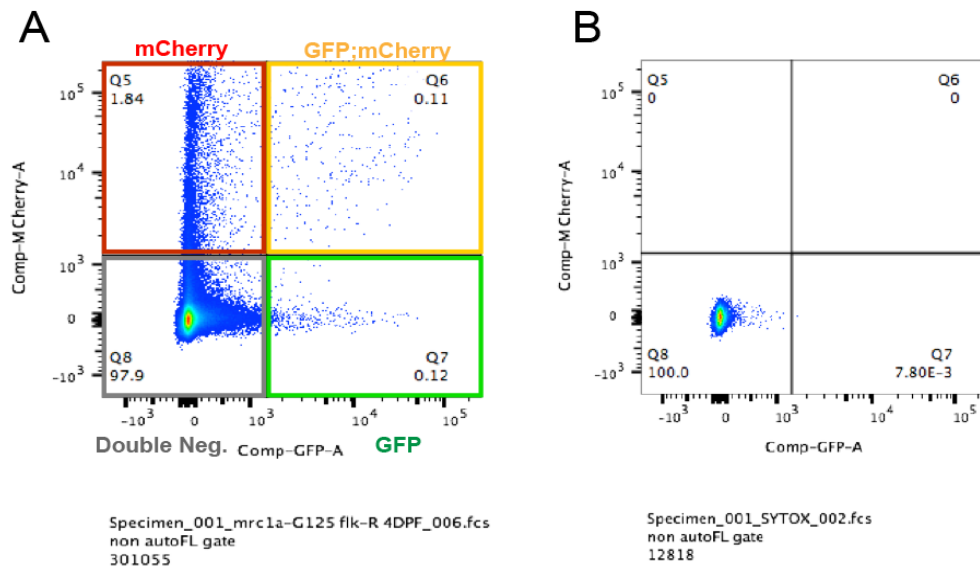
Fig. S2. Graphical representation of FACS profiles of *mrc1a:GFP; flk:mCherry* whole embryos. (A) 4 different cell population were isolated: Double negative cells, mCherry positive cells, GFP positive cells and GFP positive, mCherry positive cells (double positive). (B) Dead cells were identified by Sytox Blue incorporation. Only viable cells were used for RNA-sequencing.

SI.3. Evaluating Quality of a Prepared cDNA Library
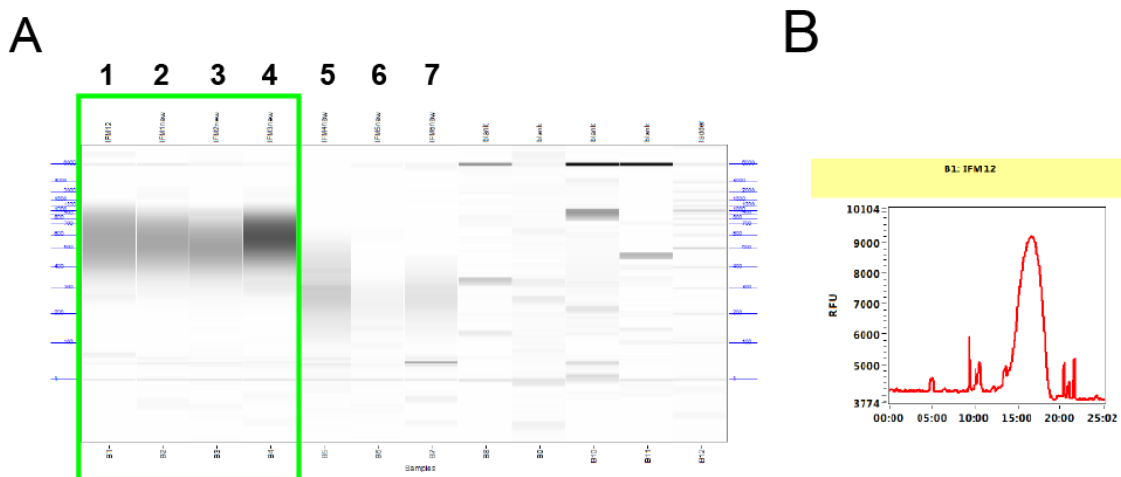
Fig. S3. Assessment of the cDNA library before sequencing using the fragment analyser. (A) Samples 1 to 4 are considered good quality (positive smear analysis). **(B)** Libraries were quantified and qualified using the High Sensitivity fragment analyzer assay. Ideally, one big curve was observed without fragmentation of cDNA. The library shown in B is from sample 1 (A) and was determined to have an average smear size of 524 bp and a concentration of 2.83 ng/ µL.

SI.4. Whole-mount *in situ* hybridization analysis for *ets1* and *nr2f2*
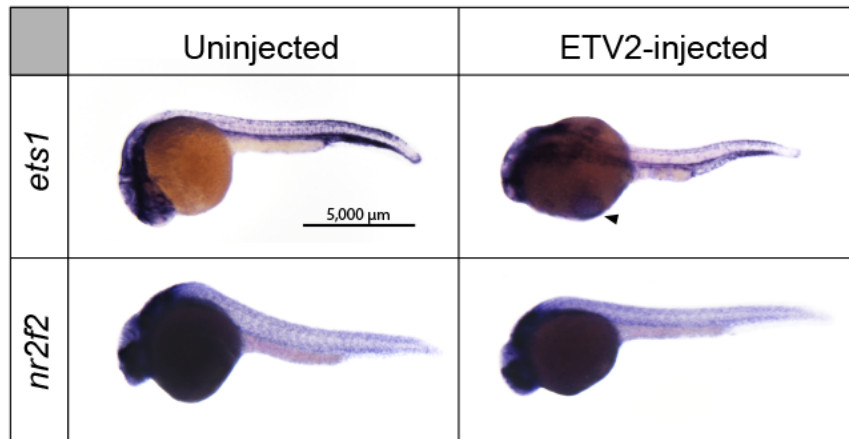
Fig. S4. Whole-mount in situ hybridization for *ets1* and *nr2f2*. WISH for *ets1* showed that this gene is broadly expressed, particularly in dorsal areas of the tail, which made it difficult to identify whether ectopic endothelial expression of this factor was induced. Of note, the black arrowhead indicates a purple staining in the yolk sac of the ETV2-injected embryo, that was considered an artefact of the WISH technique and not a patch of ectopic expression. WISH for *nr2f2* showed that this gene is robustly and widely expressed outside the CHT, especially in areas associated with the notochord, the spinal cord and the head. Since it was difficult to distinguish endothelial from neural expression, this probe was not considered optimal neither.

Appendix B: Materials, Reagents and Equipment

Relevant materials, reagents and equipment listed in order of appearance in the text in the table shown below (see next page). Of note, vectors employed for the Tol2-Gateway cloning are part of our laboratory stock. Vectors for making new p5E or pME are routinely ordered from Invitrogen™; Thermo Fisher Scientific, Waltham, MA, USA.

Material/Reagent/Equipment	Company	Cat. or Product no./Model
Incubator	VWR	102094-516
Round Petri Dishes (145 X 20 mm)	Greiner Bio-one	639102
Ultrapure Agarose Powder	Invitrogen™; Thermo Fisher Scientific	16500500
Petri Dishes (100 X 15 mm)	Falcon®, Corning	351029
Microinjection Plastic Mold With Furrows	Adaptive Science Tools	TU-1
0.5 mm Borosilicate OD Glass Microcapillary Needles With Inner Filament	Sutter Instruments	BF 100-50-10
Needle Puller	Sutter Instruments	P-87
Extra-Long Tips	Eppendorf	5242956003
Micropipettes of Different Types (e.g., p20)	Gilson	-
Micromanipulator	Narishige	MN-151
Pneumatic Microinjector	Harvard Apparatus	PLI-100A
Stereoscope	Nikon	SMZ800
Fine Watchmaker Forceps	Dumont™, Roboz	RS-4955
Micro coverglass slips 18 x 18 mm	vWR	48366205
Paster Disposable Plastic Pipette	Fisher Scientific	13-711-5AM
One Shot™ ; TOP10 Chemically Component Cells	Invitrogen™; Thermo Fisher Scientific	C404003
S.O.C Medium	Invitrogen™; Thermo Fisher Scientific	15544034
Ampicillin	Roche, Sigma-Aldrich	ROAMP
Kanamycin	Sigma-Aldrich	K0254
24-Place Centrifuge	Eppendorf	5424 R; 5404000014
Qiaprep Spin Miniprep Kit	Qiagen	27106
Nanodrop Spectrophotometer	Nanodrop™ ; Thermo Fisher Scientific	Nanodrop ONEC; ND-ONE-W
NotI Enzyme	New England Biolabs	#ROI895
Thermocycler	Applied Biosystems™; Thermo Fisher Scientific	2720; 4359659
10X TAE Buffer	Roche; Sigma-Aldrich	11666690001
Ethidium Bromide, Dropper Bottle	Apex	10-276

Electrophoresis Chambers	Hoefer	HE33-8-1.5
Gel Imager	Protein Simple	AlphaImager HP system
PCR Purification Kit	Qiagen	28104
mMESSAGE mMACHINE SP6 kit	Invitrogen™; Thermo Fisher Scientific	AM1340
DNase I	Roche, Sigma-Aldrich	04716728061
RNase AWAY Decontamination Reagent	Invitrogen™; Thermo Fisher Scientific	10328011
RNAse inhibitor	Invitrogen™; Thermo Fisher Scientific	10777019
0.5% Phenol Red Solution	Sigma-Aldrich	P029
Nuclease-Free Water (not DEPC treated)	Invitrogen™; Thermo Fisher Scientific	AM9939
QIAquick Gel Extraction Kit	Qiagen	28704
NEB	New England Biolabs	M0202S
10X NEB Buffer	New England Biolabs	B7202S
100X BSA	New England Biolabs	B9001S
dNTPs (10nM each)	New England Biolabs	N0447S
1.7 Microcentrifuge Tubes	Denville, Fisher Scientific	C-2172
3M Sodium Acetate, pH 5.2	Corning	43-033-CI
TOPO TA Cloning Kit	Invitrogen™; Thermo Fisher Scientific	451641
LR Clonase Enzyme	Invitrogen™; Thermo Fisher Scientific	11791100
Pronase	Roche, Sigma-Aldrich	11459643001
10XPBS	Sigma-Aldrich	D1408
RNeasy Mini Kit	Qiagen	74104
β-mercaptoethanol	Sigma-Aldrich	M6250
QIAshredder	Qiagen	79654
Superscript III First-Srand Synthesis Super Mix Kit	Invitrogen™; Thermo Fisher Scientific	18080400
Redtaq ReadyMIx PCR reaction mix including DNA Polymerase	Sigma-Aldrich	R2523
T7 RNA Polymerase	Roche, Sigma-Aldrich	10881775001
10X DIG RNA Labeling Mix	Roche, Sigma-Aldrich	11277073910
10X Transcription Buffer	Roche, Sigma-Aldrich	10999644001
Illustra™ Probequant™ G-50 Micro Columns	GE Healthcare; Sigma-Aldrich	28-9034-08
Methanol	Fisher Scientific	AC177150010
KCl	Sigma-Aldrich	P9541

MgSO$_4$	Sigma-Aldrich	M2643
KOH	Sigma-Aldrich	P1767
Formamide Ultra Pure	Carlo Erba	LJ67206AE
Tween20	Sigma-Aldrich	8.22184
Heparin Sodium Salt	Sigma-Aldrich	H3393
tRNA from wheat germ Type IV	Sigma-Aldrich	R7876
H$_2$O$_2$	Sigma-Aldrich	31642
Proteinase K	Roche, Sigma-Aldrich	03115828001
10 % PFA	Polysciences	#04018
25% Glutaraldehyde	Sigma-Aldrich	G5882
Lamb Serum	Gibco^{TM}; Thermo Fisher Scientific	16070096
Anti-Digoxigenin-Ap, Fab Fragments	Roche, Sigma-Aldrich	11093274910
NaCl, 5M	Corning; vWR	45001-125
NBT/BCIP	Promega	53771
Fiber optic illuminator with articulated arms	Schott	170.202
24-Well Plates	Costar®, Corning	3526
Glycerol >99%	Sigma-Aldrich	G5516
Fluorescence Stereomicroscope	Nikon	SMZ18
Pimozide	Sigma-Aldrich	P1793
DMSO	Sigma-Aldrich	D8418
6-Well Plates	Costar®, Corning	3516
Dry Block Incubator (THERMOMIXER)	Eppendorf®; Sigma-Aldrich	T1317-1EA
Glass bottom multi-well plates	Mat Tek	P06G-1.5-10-F
Ultrapure Low Melting Point Agarose	Invitrogen^{TM}; Thermo Fisher Scientific	16520100
Spinning Disk	Yokogawa	CSU-W1
Inverted Microscope	Nikon	Eclipse TI
Liberase	Roche, Sigma-Aldrich	05401119001
Polystere Round-Bottom Tubes With 40 µm Cell Strainer Caps	Falcon®, Corning	352235
Fragment Analyzer	Advanced Analytical	-
FBS	Foundation^{TM}, Gemini	900-108

FACS Machine	BD Biosciences	BD FACSAria^{TM} II Sorter
Sytox Blue	Invitrogen^{TM}; Thermo Fisher Scientific	S34857
Trizol LS	Invitrogen^{TM}; Thermo Fisher Scientific	10296028
Vortex	Scientific Industries, Inc.	Vortex-Genie 2
FlowJo Sotware	FlowJo, LLC	10.5.2
Pure Chloroform	Fisher Scientific	AC383760010
Genelute LPA	Sigma-Aldrich	56575
Isopropanol	Sigma-Aldrich	I9516
DEPC Water	Invitrogen^{TM}; Thermo Fisher Scientific	AM9916
SMART-Seq V4 Ultra Low Input RNA Kit	Takara	634888 (12 Raxns)
Nextera XT DNA Library Preparation Kit	Illumina	FC-131-1024
Agencourt Ampure XP Kit	Beckman Coulter	A63881
Fluorometric Qubit RNA HS Assay	Invitrogen^{TM}; Thermo Fisher Scientific	Q32852
Illumina Hiseq 2500	Illumina	SY-401-2501
FastQC	Babraham Bioinformatics	0.11.17
Cutadapt	MIT-licensed	**-**
Bowtie	Langmead et al., licensee Biomed Central Ldt.	1.2.1
NIS-Elements	Nikon, Laboratory Imaging	4.20.01
Imaris	Bitplane AG	x64 7.6.5
Adobe Photoshop	Adobe Systems Incorporated	CS6. 13.0.1.x64
Microsoft Excel	Microsoft	15.24
Graphpad Prism	GraphPad Software, Inc.	7.03
Adobe Illustrator	Adobe Systems Incorporated	CC. 22.1